

The Effect of Monoethylene Glycol (MEG) on CO₂ Corrosion Mechanisms

A thesis presented to
the faculty of
the Russ College of Engineering and Technology of Ohio University

In partial fulfillment
of the requirements for the degree
Master of Science

Roberto A. Ruiz

December 2017

© 2017 Roberto A. Ruiz. All Rights Reserved.

This thesis titled
The Effect of Monoethylene Glycol (MEG) on CO₂ Corrosion Mechanisms

by
ROBERTO A. RUIZ

has been approved for
the Department of Chemical and Biomolecular Engineering
and the Russ College of Engineering and Technology by

Marc Singer
Assistant Professor of Chemical and Biomolecular Engineering

Dennis Irwin
Dean, Russ College of Engineering and Technology

ABSTRACT

RUIZ, ROBERTO A., M.S., December 2017, Chemical and Biomolecular Engineering

The Effect of Monoethylene Glycol (MEG) on CO₂ Corrosion Mechanisms

Director of Thesis: Marc Singer

The use of monoethylene glycol (MEG) is common in the oil and gas industry as it is injected in subsea flowlines to prevent hydrate formation. Albeit this is one of the main uses for this chemical in this industry, previous studies have indicated that the presence of MEG reduces the extent of corrosion of mild steel in CO₂ and H₂S dominated environments. Furthermore, MEG is reported to serve as a key component of pH-stabilization technique used for corrosion mitigation. Experimental work published over the last few years has provided valuable insight on the possible overall effect of MEG on uniform corrosion rates, however, wide gaps still remain especially related to mechanistic representation of the phenomenon involved. In this work, a systematic electrochemical study was performed on the effect of MEG on CO₂ corrosion mechanisms of mild steel, in particular API 5L X65 (0.16wt. % Carbon). The scope of work covered the influence of temperature from 30 – 80°C, of MEG content from 40 – 85wt. % and of pH 3.5 - 6 at atmospheric pressure for solutions saturated with CO₂ and N₂, respectively. Electrochemical techniques such as linear polarization resistance (LPR), electrochemical impedance spectroscopy (EIS), and potentiodynamic sweeps were used to obtain corrosion rates, mixed potential (*E_{corr}*), current density (*I_{corr}*), Tafel slopes and limiting currents. The experiments were performed in a typical three electrode set-up where a Rotating Cylinder Electrode (RCE) was used to study the effect of flow at rotation speeds of 100,

1000 and 2000RPM (equivalent to 0.2, 1.2 and 2.0m/s, respectively in a 4in pipeline). The completion of these experiments revealed that MEG reduces the corrosion rate by affecting in different ways both anodic and cathodic electrochemical reactions involved in CO₂ corrosion mechanisms. By performing potentiodynamic sweeps, it was noted that the dissolution of iron was retarded with increasing glycol content in solution, inferring that MEG may adsorb on the metal surface and affect the kinetics of the anodic reaction. On the other hand, the effect of MEG on the net cathodic reaction, impacting both charge transfer and limiting current, seemed to be directly related to changes in solution chemistry and properties. Furthermore, it was noted that the electrochemical reactions (Fe dissolution, H⁺ and H₂CO₃ reductions) followed the expected Tafel behavior, and that the respective anodic and cathodic Tafel slopes were unaffected by the presence of MEG. Lastly, literature findings suggested changes in the reduction of water should be expected in the presence of MEG; however, this work found no variations in the reduction of water within the range of MEG content studied. While a mechanistic explanation on the effect of MEG on the anodic reaction remains elusive, all changes in the cathodic lines can be explained by differences in physico-chemical properties of the electrolyte. Upon completion of the experimental trials, a chemical and electrochemical model was developed to simulate CO₂ corrosion in non-ideal solutions and validated using literature and experimental data. This MEG-H₂O-CO₂ corrosion model identified all the necessary changes in physical and electrochemical parameters needed for further implementation to the ICMT flag ship in-house corrosion prediction software FREECORP™.

DEDICATION

This work is dedicated to all my family, specially my siblings and parents Pedro A. Ruiz and Carmen S. Pacheco, my other half Maria, who served as a constant motivation to make this new experience an enjoyable time.

ACKNOWLEDGMENTS

The list of people whom I would like to acknowledge is quite extensive; however, I would like to particularly recognize a set of key individuals who worked closely with me throughout my time at ICMT, and who made this a new great learning experience.

My advisor, Dr. Singer, who not only challenged me to learn a completely new topic in a new field of study, but who also worked closely with me in order to deliver outstanding results.

My project leader, Dr. Brown, who interacted with me throughout the execution of my experiments and provided the necessary help in order for me to complete the tasks related to my research.

To Alexis Barxias and Cody Shafer for providing the help necessary in the laboratory in order to have a robust and clean experimental set-up. Furthermore, they made my experience in Athens, OH a wonderful time.

To Maria for being the backbone that provided support throughout my Master's experience both during the academic and research portion.

To the rest of the ICMT students and staff for providing a great learning environment which I considered my second home during my time in Athens.

To the Corrosion Center JIP and all the board members for providing the financial support during these tough times in the industry in order to make this research topic a successful and completed project.

TABLE OF CONTENTS

	Page
Abstract.....	3
Dedication.....	5
Acknowledgments.....	6
List of Tables	9
List of Figures	11
Glossary	16
Chapter 1 Introduction.....	20
Chapter 2 Literature Review.....	23
2.1 CO ₂ Corrosion.....	23
2.1.1 CO ₂ Corrosion – Chemical and Electrochemical Reactions.....	24
2.1.2 CO ₂ Corrosion – Kinetics of Electrochemical Reactions	26
2.1.3 CO ₂ Corrosion – Effect of Temperature	31
2.1.4 CO ₂ Corrosion – Effect of Partial Pressure of CO ₂	31
2.1.5 CO ₂ Corrosion – Effect of pH.....	32
2.1.6 CO ₂ Corrosion – Effect of Flow	33
2.2 MEG and CO ₂ Corrosion.....	36
2.3 Water/MEG Solution Chemistry.....	48
2.3.1 Proton Activity in Non-Ideal Solutions	49
2.3.2 CO ₂ Solubility in MEG+Water Solutions.....	50
Chapter 3 Motivation, Objectives and Hypotheses	52
3.1 Motivation.....	52
3.2 Proposed Hypotheses	53
3.3 Thesis Objectives and Accompanying Tasks	54
Chapter 4 Methodology.....	56
4.1 Calibration Procedure Required for MEG+Water Solutions	56
4.2 Experimental Procedure.....	58
4.3 Analytical Apparatus and Procedure	59
4.4 Experimental Setup.....	64

4.5	Test Matrix and Experimental Conditions.....	65
Chapter 5	Results.....	69
5.1	Effect of Flow in the Presence of MEG.....	69
5.2	Effect of Temperature in the Presence of MEG.....	73
5.3	Effect of pH in the Presence of MEG.....	78
5.4	Effect of MEG on CO ₂ Corrosion Mechanisms.....	80
5.5	Summary of LPR Data.....	82
5.6	Summary on Experimental Findings.....	88
Chapter 6	Modeling Approach.....	91
6.1	Chemistry of MEG/H ₂ O/CO ₂ Solutions and Calculation of pH (Proton Activity).....	92
6.2	Calculation of the H ⁺ and HCO ₃ ⁻ Limiting Current in the Presence of MEG ..	98
6.3	Modeling the Anodic Reaction in the Presence of MEG.....	104
6.4	MEG-H ₂ O-CO ₂ -NaCl Electrochemical Model Performance.....	109
6.5	MEG Model Validation.....	114
6.5.1	Validation of the Chemistry Model.....	114
6.5.2	Validation of the Electrochemical Model.....	116
6.6	Electrochemical Model Limitations.....	136
6.7	Discussion on Modeling Approach.....	136
Chapter 7	Conclusions.....	140
Chapter 8	Future Work.....	141
	References.....	143
	Appendix A Chemical Composition of Materials [WT. %].....	151
	Appendix B Coefficients Used for Modeling the Electrochemical Reactions.....	152
	Appendix C Changes in Solution pH Due to Increasing Meg Content at 30°C.....	153
	Appendix D Liquid Density and Viscosity Information for Water and Monoethyleneglycol.....	154
	Appendix E Experimental LPR Data.....	155
	Appendix F Validation of Chemistry Model Using Literature Data.....	161
	Appendix G Model Validation – Effect of Flow.....	162

LIST OF TABLES

	Page
Table 1. Chemical reactions related to carbon dioxide/water systems and their respective equilibrium constants. Electro-neutrality, and ionic strength equations used to calculate speciation.	32
Table 2. Measured pH required for a targeted proton activity (pH_{true}) of 4.00 in solution containing MEG at 30°C.	58
Table 3. Proposed test matrix used to complete the objectives and validate the hypotheses. The x marks in the highlighted cells represent the experimental tests to be completed at different alkalinity levels.	65
Table 4. Experimental parameters used for preliminary electrochemical results for solutions purged with N_2 and CO_2 gas, respectively.	67
Table 5. Equivalent water velocities in a single-phase pipeline using Silverman's mass transfer correlation for rotating cylinders. ⁵⁴	67
Table 6. pKa values for water-MEG as a function of temperature in Kelvin, K.	94
Table 7. Coefficients used for the calculation of MEG dependence on activity coefficients for components. Discussion of the results are presented by Sandengen et al. ³⁴	96
Table 8. Calculations of the pH for a solution saturated with 0.5bar CO_2 , at 30°C and 1wt. % NaCl.	97
Table 9. Table of reference diffusion coefficients of species in water used in the model. ²⁹	100
Table 10. Comparison between literature and FREECORP™'s values for anodic Tafel slope for iron dissolution.	106
Table 11. Values for the anodic exchange current density coefficients used in this research.	107
Table 12. Chemical Composition of API 5L X65 steel (wt. %). ⁵⁸	151
Table 13. Coefficients proposed in the literature ^{21, 22} for the expression of the exchange current densities of electrochemical reactions.	152
Table 14. Changes in solution pH due to increasing MEG content at 30°C for a desired solution pH_{true} of 5.00.	153
Table 15. Changes in solution pH due to increasing MEG content at 30°C for a desired solution pH_{true} of 6.00.	153
Table 16. Liquid properties for MEG and H_2O as a function of temperature and pressure.	154
Table 17. Comparison between experimental LPR Data and FREECORP™ (FC) predictions for a solution at 30°C, pH 4.00, 5.00 and 6.00 at 0.5bar CO_2 , 1wt. % NaCl and 0wt. % MEG.	155
Table 18. Comparison between experimental LPR Data and FREECORP™ (FC) predictions for a solution at 30°C, pH 3.91,4.91,5.91 at 0.5bar CO_2 , 1wt. % NaCl and 40wt. % MEG.	156

Table 19. Comparison between experimental LPR Data and FREECORP™ (FC) predictions for a solution at 30°C, pH 3.77, 4.77, 5.77 at 0.5bar CO ₂ , 1wt. % NaCl and 55wt. % MEG.	157
Table 20. Comparison between experimental LPR Data and FREECORP™ (FC) predictions for a solution at 30°C, pH 3.66, 4.66, 5.66 at 0.5bar CO ₂ , 1wt. % NaCl and 70wt. % MEG.	158
Table 21. Comparison between experimental LPR Data and FREECORP™ (FC) predictions for a solution at 30°C, pH 3.54,4.54, 5.54 at 0.5bar CO ₂ , 1wt. % NaCl and 85wt. % MEG.	159
Table 22. Comparison between experimental LPR Data and FREECORP™ (FC) predictions for a solution at 60°C, pH 3.44, 0.5bar CO ₂ , 1wt. % NaCl and 70wt. % MEG.	160
Table 23. Comparison between experimental LPR Data and FREECORP™ (FC) predictions for a solution at 80°C, pH 3.52, 4.52, 5.52 at 0.5bar CO ₂ , 1wt. % NaCl and 70wt. % MEG.	160

LIST OF FIGURES

	Page
Figure 1. Half reactions for each component plotted against a potential and current density frame. The mixed potential is where the iron oxidation happens at the same rate as the reduction of protons. JONES, DENNY A., <i>PRINCIPLES AND PREVENTION OF CORROSION</i> , 2nd, © 1996. Reprinted by permission of Pearson Education Inc., New York, New York. ²⁴	29
Figure 2. Evans diagrams showing: a). Effect of velocity on limiting current. b). Effect of velocity on corrosion current. JONES, DENNY A., <i>PRINCIPLES AND PREVENTION OF CORROSION</i> , 2nd, © 1996. Reprinted by permission of Pearson Education Inc., New York, New York. ²⁴	36
Figure 3. Potentiodynamic sweeps obtained for 0wt. % and for 70wt. % MEG-Water-CO ₂ -NaCl systems. Reproduced with permission from NACE International, Houston, TX. All rights reserved. Gulbrandsen E and Morad J, Paper 221 presented at Corrosion/1998, San Diego California. © NACE International 1998. ¹³	39
Figure 4. CO ₂ diffusivity (left axis) and solubility viscosity (right axis) as a function of glycol content at 25°C. Reproduced with permission from NACE International, Houston, TX. All rights reserved. Gulbrandsen E and Morad J, Paper 221 presented at Corrosion/1998, San Diego California. © NACE International 1998. ¹³	40
Figure 5. Effect of MEG content on CO ₂ and solubility for a solution at 25°C, and 1atm CO ₂ pressure. Reproduced with permission from NACE International, Houston, TX. All rights reserved. Gulbrandsen E and Morad J, Paper 221 presented at Corrosion/1998, San Diego California. © NACE International 1998. ¹³	40
Figure 6. Evans diagram showing the effect of 0, 30, 50, 70 and 90wt. % MEG in solution, respectively for a solution at 50°C, 1bar CO ₂ and 1wt. % NaCl. Javidi, M., & Khodaparast, M. (2015). Inhibitive Performance of Monoethylene Glycol on CO ₂ Corrosion of API 5L X52 Steel. <i>Journal of Materials Engineering and Performance</i> , 24(4), 1417-1425. With Permission of Springer. ¹⁶	45
Figure 7. Nyquist plot showing the imaginary (y-axis) and real (x-axis) impedances at a frequency range between 1,000,000 – 0.01 Hz for X52 steel in a CO ₂ saturated solution with 1wt. % NaCl, different MEG contents and at a temperature of 50°C. Javidi, M., & Khodaparast, M. (2015). Inhibitive Performance of Monoethylene Glycol on CO ₂ Corrosion of API 5L X52 Steel. <i>Journal of Materials Engineering and Performance</i> , 24(4), 1417-1425. With permission of Springer. ¹⁶	46
Figure 8. Reprinted with permission from Kan, A. T., Lu, H., & Tomson, M. B. (2010). Effects of Monoethylene Glycol on Carbon Dioxide Partitioning in Gas/Monoethylene Glycol/Water/Salt Mixed Systems. <i>Industrial & Engineering Chemistry Research</i> , 49(12), 5884-5890. Copyright 2003 American Chemical Society. Effect of temperature on the behavior of the activity coefficient of aqueous CO ₂ in non-ideal solutions at constant electrolyte concentrations ³⁰	50

Figure 9. FREECORP™ 2.0 estimating uniform corrosion rates for a set of inputs. Accompanying potentiodynamic sweeps are provided for the predicted results demonstrating the overall, and individual electrochemical reactions.	55
Figure 10. Top Nyquist plot shows the effect of 0, 40, 55, 70, 85vol. % MEG in solution resistance at 30°C, pH~4.00 and 100RPM. Bottom plot shows a close-up version.	61
Figure 11. Polarization curve using FREECORP™ for a CO ₂ saturated solution with an electrolyte content of 1wt. % NaCl, at 30°C, water velocity of 1.2m/s ($V_{RCE} = 1000RPM$) and pH of 4.00.....	63
Figure 12. Three electrode rotating cylinder electrode (RCE) setup, consisting of a working, a counter and a reference electrode inserted in a 2L glass cell, on top of a hot plate. Setup is connected to a rotameter used to control the gas flowrate into the system. (Image courtesy of Cody Shafer, ICMT).....	64
Figure 13. Comparison between experimental LPR results (dotted points) and FREECORP™'s predictions (solid continuous lines) of corrosion rates obtained at 30°C for 100, 1000 and 2000RPM, at pH 4.00, 5.00 and 6.00, respectively, for a solution saturated with 0.5bar CO ₂ , and 1wt. % NaCl, 0% MEG.	70
Figure 14. Comparisons between experimental results (70vol. %, pH 3.66) and FREECORP™ predictions (0vol. % MEG, pH 3.66) for solutions purged with 0.5bar CO ₂ at 30°C, 1wt. % NaCl.	71
Figure 15. Comparisons between experimental results (70vol. %, pH 3.66) and FREECORP™ predictions (0vol. % MEG, pH 3.66) for solutions purged with ~1bar N ₂ at 30°C, and 1wt. % NaCl.	72
Figure 16. Polarization curves at 1000RPM for solutions at pH 4.00 and 0vol. % MEG purged with 0.5bar CO ₂	74
Figure 17. Polarization curves at 1000RPM for solutions at pH 4.00 and 0vol. % MEG purged with ~ 1bar N ₂	75
Figure 18. Potentiodynamic curves at 1000RPM for solutions at pH ~ 4.00 with 70vol. % MEG and purged with 0.5bar CO ₂ and 1wt. % NaCl.	76
Figure 19. Potentiodynamic curves at 1000RPM for solutions at pH ~ 4.00 with 70vol. % MEG and purged with ~1bar N ₂ and 1wt. % NaCl.....	77
Figure 20. Comparison between experimental results (70vol. % MEG) and FREECORP™'s prediction (0vol. % MEG) for a solution at 30°C, 0.5bar CO ₂ , 1wt. % NaCl and $V_{RCE} = 1000$ RPM.	78
Figure 21. Comparison between experimental results (70vol. % MEG) and FREECORP™'s prediction (0vol. % MEG) for a solution at 30°C, ~1bar N ₂ , 1wt. % NaCl and $V_{RCE} = 1000$ RPM.....	79
Figure 22. Evans diagram showing the effect of 0, 45, 50, 70 and 85vol. % MEG in solution for an RCE rotation of 1000 RPM [$V_{eq} = 1.2m/s$], at 30°C saturated with 0.5bar CO ₂ and 1wt. % NaCl at pH ~ 6.00 (top) and pH ~ 4.00 (bottom).....	81
Figure 23. LPR measurements obtained for a solution with 0, 40, 55, 70 and 85vol. % MEG, at 30°C and pH ~ 4.00 purged with 0.5bar CO ₂ and 1wt. % NaCl.	83
Figure 24. LPR measurements obtained for a solution purged with 0.5bar CO ₂ and with 0, 40, 55, 70 and 85vol. % MEG, at 30°C and pH ~ 5.00 and 1wt. % NaCl.	85

Figure 25. LPR measurements obtained for a solution purged with 0.5bar CO ₂ and with 0, 40, 55, 70 and 85vol. % MEG, at 30°C and pH ~ 6.00 and 1wt. % NaCl.	86
Figure 26. LPR data for 30, 60 and 80°C, at pH ~ 4.00 for a solution containing 70vol. % MEG saturated with 0.5bar CO ₂ , and 1wt. % NaCl.....	87
Figure 27. Activation energy schematic for iron dissolution into water and MEG-Water solutions. Reproduced with permission from NACE International, Houston, TX. All rights reserved. Gulbrandsen E and Morad J, Paper 221 presented at Corrosion/1998, San Diego California. © NACE International 1998. ¹³	89
Figure 28. Reference diffusivity for CO ₂ in MEG-Water solutions at 25°C.	101
Figure 29. Reference diffusivity for H ⁺ in MEG-Water solutions at 25°C.....	102
Figure 30. MEG Factor, η_{MEG} calculated from experimental E_{corr} values at various pH ranges for solutions at 30°C saturated with 0.5bar CO ₂ and 1wt. % NaCl.	108
Figure 31. Changes in MEG factor with alterations in temperatures for a solution saturated with 1wt. % NaCl, 0.5bar CO ₂ and 70vol. % MEG in solution.	109
Figure 32. Model predictions - Potentiodynamic sweeps for a solution saturated with 0.5bar CO ₂ , 1wt. % NaCl and with a MEG content of 70vol. % MEG at 30°C, 60°C and 80°C and pH 4.00.	110
Figure 33. Model predictions - Potentiodynamic sweeps for a solution at 30°C saturated with 0.5bar CO ₂ , 1wt. % NaCl and with a MEG content of 70vol. % MEG and pH 4.00, 5.00 and 6.00.....	111
Figure 34. Model predictions - Potentiodynamic sweeps for a solution at 30°C and pH 4.00 saturated with 0.5bar CO ₂ , 1wt. % NaCl and a MEG content of 70vol. % MEG for RCE rotation of 100, 1000 and 2000RPM.....	112
Figure 35. Model predictions - Potentiodynamic sweeps for an RCE velocity of 1000RPM for a solution at 30°C and pH 4.00 saturated with 0.5bar CO ₂ , 1wt. % NaCl and with a MEG content of 0, 40, 55, 70 and 85vol. % MEG.....	113
Figure 36. MEG model prediction of solution pH for a system saturated with 0.5bar CO ₂ , 1wt. % NaCl and at 30°C.	115
Figure 37. Comparison between model prediction (blue solid line) and Gulbrandsen's results (red dots) for of carbon dioxide's solubility as a function of glycol content for a solution at 30°C, 1bar CO ₂ and 1wt. % NaCl.	116
Figure 38. Comparison between model predictions (black continuous line) and experimental results (blue dotted line) for a solution saturated with 0.5bar CO ₂ , 1wt. % NaCl, 0% MEG at pH 4.00, 30°C and for a $V_{\text{RCE}} = 1000\text{RPM}$	117
Figure 39. Comparison between model predictions (black continuous line) and experimental results (blue dotted line) for a solution saturated with 0.5bar CO ₂ , 1wt. % NaCl, 40vol. % MEG at pH 3.91, 30°C and for a $V_{\text{RCE}} = 1000\text{RPM}$	118
Figure 40. Comparison between model predictions (black continuous line) and experimental results (red dotted line) for a solution saturated with 0.5bar CO ₂ , 1wt. % NaCl, 55vol. % MEG at pH 3.77, 30°C and for a $V_{\text{RCE}} = 1000\text{RPM}$	120
Figure 41. Comparison between model predictions (black continuous line) and experimental results (green dotted line) for a solution saturated with 0.5bar CO ₂ , 1wt. % NaCl, 70vol. % MEG at pH 3.66, 30°C and for a $V_{\text{RCE}} = 1000\text{RPM}$	121

Figure 42. Comparison between model predictions (black continuous line) and experimental results (purple dotted line) for a solution saturated with 0.5bar CO ₂ , 1wt. % NaCl, 85vol. % MEG at pH 3.54, 30°C and for a V _{RCE} = 1000RPM.	122
Figure 43. Comparisons between model predictions (solid continuous lines) and experimental results (dotted lines) for a solution at 30°C and pH 3.66 saturated with 0.5bar CO ₂ , 70vol. % MEG and 1wt. % NaCl.....	123
Figure 44. Comparisons between the model predictions (solid continuous lines) and experimental results (dotted lines) for solutions saturated with 0.5bar CO ₂ , 70vol. % MEG, 1wt. % NaCl, 1000RPM and pH 3.66 (30°C), 3.44 (60°C) and 3.52 (80°C).	125
Figure 45. Comparison between model predictions (black continuous line) and experimental results (blue dotted line) for a solution saturated with 0.5bar CO ₂ , 1wt. % NaCl, 0vol. % MEG at pH 6.00, 30°C and for a V _{RCE} = 1000RPM.	126
Figure 46. Comparison between model predictions (black continuous line) and experimental results (blue dotted line) for a solution saturated with 0.5bar CO ₂ , 1wt. % NaCl, 40vol. % MEG at pH 5.91, 30°C and V _{RCE} = 1000RPM.	127
Figure 47. Comparison between model predictions (black continuous line) and experimental results (red dotted line) for a solution saturated with 0.5bar CO ₂ , 1wt. % NaCl, 55vol. % MEG at pH 5.77, 30°C and V _{RCE} = 1000RPM.	128
Figure 48. Comparison between model predictions (black continuous line) and experimental results (green dotted line) for a solution saturated with 0.5bar CO ₂ , 1wt. % NaCl, 70vol. % MEG at pH 5.66, 30°C and for a V _{RCE} = 1000RPM.	129
Figure 49. Comparison between model predictions (black continuous line) and experimental results (purple dotted line) for a solution saturated with 0.5bar CO ₂ , 1wt. % NaCl, 85vol. % MEG at pH 5.54, 30°C and V _{RCE} = 1000RPM.	130
Figure 50. Comparison between model predictions (black continuous line) and experimental results (blue dotted line) for a solution saturated with 0.5bar CO ₂ , 1wt. % NaCl, 0% MEG at pH 5.00, 30°C and for a V _{RCE} = 1000RPM.	131
Figure 51. Comparison between model predictions (black continuous line) and experimental results (blue dotted line) for a solution saturated with 0.5bar CO ₂ , 1wt. % NaCl, 40vol. % MEG at pH 4.91, 30°C and V _{RCE} = 1000RPM.	132
Figure 52. Comparison between model predictions (black continuous line) and experimental results (red dotted line) for a solution saturated with 0.5bar CO ₂ , 1wt. % NaCl, 55vol. % MEG at pH 4.77, 30°C and V _{RCE} = 1000RPM.	133
Figure 53. Comparison between model predictions (black continuous line) and experimental results (green dotted line) for a solution saturated with 0.5bar CO ₂ , 1wt. % NaCl, 70vol. % MEG at pH 4.66, 30°C and for a V _{RCE} = 1000RPM.	134
Figure 54. Comparison between model predictions (black continuous line) and experimental results (purple dotted line) for a solution saturated with 0.5bar CO ₂ , 1wt. % NaCl, 85vol. % MEG at pH 4.54, 30°C and V _{RCE} = 1000RPM.	135
Figure 55. Comparison between model prediction (solid continuous lines) and literature data (dotted points in graph) for the activity coefficient of aqueous carbon dioxide as a function of ethylene glycol at different temperatures.	161

Figure 56. Comparisons between model predictions (solid continuous lines) and experimental results (dotted lines) for a solution at 30°C and pH 3.91 saturated with 0.5bar CO ₂ , 40vol. % MEG and 1wt. % NaCl.....	162
Figure 57. Comparisons between model predictions (solid continuous lines) and experimental results (dotted lines) for a solution at 30°C and pH 4.91 saturated with 0.5bar CO ₂ , 40vol. % MEG and 1wt. % NaCl.....	163
Figure 58. Comparisons between model predictions (solid continuous lines) and experimental results (dotted lines) for a solution at 30°C and pH 5.91 saturated with 0.5bar CO ₂ , 40vol. % MEG and 1wt. % NaCl.....	164
Figure 59. Comparisons between model predictions (solid continuous lines) and experimental results (dotted lines) for a solution at 30°C and pH 4.66 saturated with 0.5bar CO ₂ , 70vol. % MEG and 1wt. % NaCl.....	165
Figure 60. Comparisons between model predictions (solid continuous lines) and experimental results (dotted lines) for a solution at 30°C and pH 5.66 saturated with 0.5bar CO ₂ , 70vol. % MEG and 1wt. % NaCl.....	166

GLOSSARY

T, unless otherwise specified, temperature in Kelvin, [K]

T_{ref} , reference temperature, [K]

p_{CO_2} , partial pressure of carbon dioxide, [bar]

$p_{\text{H}_2\text{O}}$, partial pressure of water vapor, [bar]

p_{MEG} , partial pressure of MEG vapor, [bar]

f_{CO_2} , fugacity of carbon dioxide, [bar]

ρ_{MEG} , density of MEG, [kg/m^3]

$\rho_{\text{MEG_ref}}$, reference density of MEG, [kg/m^3]

$\text{mass_H}_2\text{O}$, mass of water in solution, [kg]

mass_MEG , mass of MEG in solution, [kg]

mass_total , total mass of solution, [kg]

$\rho_{\text{H}_2\text{O}}$, density of water, [kg/m^3]

μ_{MEG} , viscosity of MEG, [$\text{kg}/(\text{m}^*\text{s})$]

$\mu_{\text{MEG_ref}}$, viscosity of MEG, [$\text{kg}/(\text{m}^*\text{s})$]

$\mu_{\text{H}_2\text{O}}$, viscosity of water, [$\text{kg}/(\text{m}^*\text{s})$]

$\mu_{\text{H}_2\text{O_ref}}$, reference of viscosity of water, [$\text{kg}/(\text{m}^*\text{s})$]

VBI_{MEG} , viscosity blending index for MEG

$\text{VBI}_{\text{H}_2\text{O}}$, viscosity blending index for water

$\text{VBI}_{\text{MIXTURE}}$, viscosity blending index for mixture

Cs_MEG , viscosity of MEG in centiStokes, [Cs]

$\text{Cs_H}_2\text{O}$, viscosity of water in centiStokes, [Cs]

$C_{S_MIXTURE}$, viscosity of mixture in centiStokes, [Cs]

V , volume, [L]

$[CO_2]_b$, concentration of carbon dioxide in the bulk, [mol/L_{water}]

$[H^+]_b$, concentration of H^+ in the bulk, [mol/L_{water}]

γ_{H^+} , activity coefficient for H^+ in solution based on L_{water}

$\gamma_{CO_2, aq}$, activity coefficient for CO_2 in solution

$\gamma_{CO_2, g}$, activity coefficient for CO_2 in the gas phase for the system

$\gamma_{HCO_3^-}$, activity coefficient for CO_2 in solution

γ_{OH^-} , activity coefficient for CO_2 in solution

D_{H^+} , diffusivity of H^+ in solution, [m^2/s]

$D_{H^+_ref}$, reference diffusivity of H^+ in solution, [m^2/s]

D_{CO_2} , carbon dioxide in MEG-Water solution, [m^2/s]

$D_{H_2CO_3}$, carbonic acid diffusivity in solution, [m^2/s]

$D_{H_2CO_3_ref}$, reference diffusivity of carbonic acid in solution, [m^2/s]

D_{AB} , diffusivity of species A into B, [m^2/s]

x_{H_2O} , mole fraction of water in solution

U_{pipe} , velocity in pipe, [m/s]

d_{pipe} , diameter of pipe, [m]

d_{cyl} , diameter of rotating cylinder, [m]

U_{cyl} , rotating cylinder velocity, [RPM]

K_{hy} , hydration constant

$K_{hy,f}$ hydration constant, [1/s]

K_{sol} , solubility constant, Henry's constant, [Molar/bar]

K_{ca} , carbonic acid constant, [Molar]

K_{bi} , bicarbonate constant, [Molar]

K_{wa} , dissociation constant, [Molar²]

w_{MEG} , mass fraction of MEG in solution

I , ionic strength, [Molar]

I_{molal} , ionic strength, [molal]

MW , molecular weight of working electrode, [g/mol]

A , area of working electrode, [cm²]

i_o , exchange current density, [A/m²]

i_a , anodic current density, [A/m²]

i_c , cathodic current density, [A/m²]

$i_{lim_H^+}$, limiting current for H⁺, [A/m²]

$i_{lim_H_2CO_3}$, limiting current for H₂CO₃, [A/m²]

$i_{\alpha_charge\ transfer_H^+}$, [A/m²]

$i_{\alpha_charge\ transfer_H_2CO_3}$, [A/m²]

R , universal gas constant, [J/K* mol]

F , Faraday's constant, [C/mol]

E , potential for working electrode, [V]

E_{rev} , reversible potential, [V]

Re , Reynolds number

Sc , Schmidt's number

Sh, Sherwood number

$k_m_{H^+}$, mass transfer coefficient, [m/s]

$k_m_{H_2CO_3}$, mass transfer coefficient in solution, [m/s]

CR, corrosion rate, [mm/y]

R_p , polarization resistance, [ohms]

β_a , anodic Tafel slope, [mV/decade]

β_c , cathodic Tafel slope, [mV/decade]

B, B value, [mV]

α_c , apparent transfer coefficient

n, number of electrons transferred in reactions

f, flow coefficient for H_2CO_3 in solution

δ_m , mass transfer thickness, [m]

δ_r , reaction layer thickness, [m]

CHAPTER 1 INTRODUCTION

The spontaneous phenomenon of corrosion has notoriously become a multibillion-dollar industry that affects every industrialized country in almost every field. Previous studies have estimated the direct economic impact related to corrosion damages in the United States to be about 3-5% of the nation's gross domestic product (GDP)¹. While these figures are staggering, they do not reflect indirect costs that corrosion presents on a yearly basis. A new research validated the previous estimates presented by NACE International in 1998¹, and included factors such as safety hazards and economic inflation in their evaluations putting the costs associated with corrosion damages in the United States above the trillion-dollar mark². One particular sector that gets heavily affected by the presence of corrosive environments is the oil and gas industry. It has been estimated that only in this field, the economic impact associated to the damages on yearly basis surpasses the billion-dollar mark³. While it could be beneficial to enforce systematic measures to reduce corrosion related damages in this field (such as using corrosion resistant alloys), the economic investment associated to such effort makes it an extremely difficult task. Therefore, the oil and gas industry has used corrosion prediction models that consider various assumptions in order to estimate how and what type of corrosion will occur during the extraction and production of hydrocarbons⁴.

As the demand for energy increases with an ever-growing worldwide population, so does the need for extraction of hydrocarbons from fields that are far from common shore areas. The extraction and transportation of hydrocarbons from these fields to onshore refineries is an economical and technical challenge; floating platforms are often needed in

order to perform preliminary separation steps before transportation to onshore facilities for further refining. During this multiphase flow process, many challenges related to the transport of hydrocarbons to processing units exist, some of them due to diverse types of corrosion attacks.

One of these challenges is due to the potential development of hydrates, which if formed, can fully block the passage of processed fluids and compromise production. Hydrates are solid crystalline structures, very similar to ice, that form due the natural presence of water coming from oil wells, light molecular weight gases, high operating pressures and low subsea temperatures – which are natural forming conditions during subsea exploration. Hydrate formation is prevented by the injection of certain types of alcohols that act as thermodynamic inhibitors, essentially decreasing the water content in the gas phase. This, in turn, prevents further process flow interruption. One chemical that has been very effective in the prevention of hydrates is monoethylene glycol (MEG). Although hydrate prevention has been its main use, several studies have also demonstrated that the presence of MEG reduces the average corrosion rate of mild steel, as well as the likelihood of localized corrosion⁵.

Extensive publications have been presented to demonstrate that MEG can be used as an indirect corrosion mitigation technique^{6,7}. More specific studies focusing directly on its effect on uniform corrosion have also been presented⁸⁻¹². However, MEG does not qualify as a corrosion inhibitor per se, since its effective concentration is above 70vol% of the aqueous phase. Several authors have extended these analyses by applying electrochemical techniques in order to understand the underlying mechanisms occurring in

corrosion processes. Among these authors, Gulbrandsen, et al.¹³, Ehsani et al.¹⁵, Javidi et al.¹⁶ and Pojtanabuntoeng, et al.¹⁸ have produced the most significant contributions to this effort. While these results were useful in understanding this complex topic, the range of experimental conditions tested therein was fairly limited, and much of the observed corrosion behavior at times, was left unexplained. Thus, it is essential that a thorough parametric study of the effect of MEG on corrosion mechanisms for sweet (CO₂ saturated) environments is completed, in order to expand the understanding from a mechanistic perspective.

The Institute for Corrosion and Multiphase Technology (ICMT) at Ohio University has developed FREECORP™, an electrochemical model used to predict corrosion rates based on given operating conditions for CO₂, H₂S and HAc containing environments. Compared to other models such as deWaard-Milliams¹⁸ or NORSOK⁴, which are essentially empirical or semi-empirical models, FREECORP™ is built on the mechanistic understanding of how electrochemical reactions are affected during corrosion processes. The main objective of the proposed work is to develop MEG corrosion prediction capabilities, following a similar electrochemical approach developed with FREECORP™.

CHAPTER 2 LITERATURE REVIEW

The purpose of this study is to investigate how MEG affects corrosion mechanisms of carbon steel in environments containing carbon dioxide. Before introducing previous literature related to corrosion in the presence of MEG, a thorough description of the chemical and electrochemical reactions involved in the overall corrosion mechanism is presented. This is intended to highlight the importance of key parameters in CO₂ corrosion such as partial pressure of corrosive gases, temperature, solution pH and flowing conditions. Such parameters are seen to affect kinetically and thermodynamically the reactions involved in the corrosion processes. An effort is also made to show how some of these aspects are modelled.

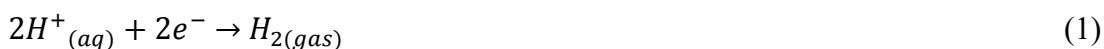
2.1 CO₂ Corrosion

The topic of carbon dioxide corrosion, or sweet corrosion, has been extensively studied in the past^{4, 18, 21}. Semi-empirical or mechanistic models have been developed based on different starting assumptions; however, all models share a common goal of predicting uniform corrosion in a single or multiphase flow environment.

During exploration and extraction of hydrocarbons from oil wells, gaseous carbon dioxide will react with water available in the system increasing the corrosivity of the transported water in the fluid. This corrosive fluid then interacts with the exposed surface of the pipeline in an electrochemical process that leads to material loss. The main reactions involved in this process are outlined below.

2.1.1 CO₂ Corrosion – Chemical and Electrochemical Reactions

Corrosion is an electrochemical process that involves half reactions; reduction and oxidation reactions. Protons from the aqueous solution are reduced on the exposed material as can be shown by Equation (1). The corresponding oxidation reaction is the dissolution of iron shown in Equation (2) that provides the electrons used for proton reduction. The combination of the oxidation of iron and the reduction of protons in solution represents the overall corrosion reaction seen in strong acid solutions, as shown by Equation (3)



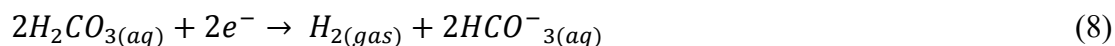
The presence of CO₂ gas in a solution increases the corrosiveness of the environment by acting as a source of protons, as described by Nordsveen et al.,²¹ and it is shown as follows:



Carbon dioxide gas dissolves into solution and hydrolyzes to form carbonic acid as shown by Equation (4) and (5), respectively. Carbonic acid which is a weak acid is susceptible to donating protons while forming bicarbonate ions, as presented by Equation (6).



The dissociation of bicarbonate ions leads to the formation of additional protons and carbonate ions as shown in Equation (7). However, this reaction is not favored at low pH values. It can be seen that the presence of carbon dioxide adds an additional source of proton to the overall corrosion process; this in turn generates a higher acidity and corrosion rate. A certain level of controversy exists when considering the role carbonic acid plays in increasing the corrosion rate. Nordsveen et al.,²¹ among others authors proposed two ways carbonic acid can affect the overall corrosion process. First, carbonic acid can be directly reduced at the metal surface, as shown in Equation (8)



Additionally, it has been proposed that the purpose of carbonic acid in corrosion mechanisms is to act a buffer, providing an extra source of protons that can be further reduced according to Equation (3). Moreover, Nordsveen's research indicated that even bicarbonate ions may provide its own direct reduction step at pH of 5.00 and above; however, this reaction step is not relevant at low pH and is not considered any further. While the scope of this work is not to prove, or disprove the role of carbonic acid in solution, it is important to note that consideration of the products formed by the presence of the acid gas in solution is still a topic that is debated today. FREECORP™ currently implements the direct reduction of carbonic acid in the prediction of the uniform corrosion rate, and since this work intends to emulate the modeling approach applied in that software, the direct reduction of carbonic acid and its contribution to the corrosion mechanisms are considered.

Lastly, the reduction of water, presented in Equation (9), is also naturally considered in this study:



Studies have demonstrated that the presence of glycol in solution should affect this reaction by reducing the activity of water in the system¹³.

2.1.2 *CO₂ Corrosion – Kinetics of Electrochemical Reactions*

The rate at which electrons are transferred during corrosion processes is crucial in defining the basis of corrosion reactions. This section gives a brief summary of the approach selected to determine these reaction rates, and defines the physical meaning of some key parameters that will be of interest in the study.

When iron is placed in an acidic aqueous environment, it naturally acquires a certain electrical potential, called the corrosion or mixed potential. At this potential, the anodic and cathodic reactions rates are equal and define the rate of corrosion, also expressed as the corrosion current. It is not possible to measure this current directly on the metal surface, and this is why electrochemical processes are often studied experimentally using a three electrodes system made of a working, a counter and a reference electrode. Typically, corrosion rates are measured using methods that essentially disturb the system away from electrochemical equilibrium and measure its response. The disturbance away from electrochemical equilibrium, or polarization, occurs by applying a difference of voltage between the working and counter electrode using a potentiostat. The response of the system is measured in terms of the current density. When an anodic polarization is applied, the working electrode surface is deprived of electrons leading to an acceleration

of the anodic reaction, in this case the oxidation of iron. A cathodic polarization provides extra electrons at the metal surface, accelerating the rate of the reduction reaction, in this case the proton and the carbonic acid reductions.

The rate of the cathodic reaction $M^{n+} + ne^- \rightarrow M$ can be expressed in terms of current density, considering a charge transfer control mechanism where there is no limitation with regards to transport of corrosive species to the metal surface (a.k.a. Tafel approximation) as shown by Equation (10):

$$i_c = i_o * \exp\left(-\frac{nF\eta\alpha_c}{RT}\right) \quad (10)$$

where i_o which is the exchange current density, i_c is the cathodic current density obtained from the applied overpotential, η , n is the equivalent number of electrons transferred by each component, F is Faraday's constant, R is the universal gas constant, T the temperature of the system and α_c is the apparent transfer coefficient.

This is analogous to writing

$$\ln\left(\frac{i_c}{i_o}\right) = -\frac{\alpha_c\eta Fn}{RT} \text{ and } \log\left(\frac{i_c}{i_o}\right) = -\frac{\alpha_c n F \eta}{2.3RT} \quad (11)$$

where Equation (11) considers the following parameters:

$$\beta_c = \frac{2.3 * R * T}{\alpha_c * F} \quad (12)$$

and

$$\eta = E - E_{rev} \quad (13)$$

where E is the potential applied to the system, and E_{rev} is the reversible potential of the reaction of interest. The Tafel relationship is obtained, considering $n=1$ for the proton reduction:

$$\eta = -\beta_c * \log\left(\frac{i_c}{i_o}\right) \quad (14)$$

or

$$i_c = i_o * 10^{\left(\frac{-\eta}{\beta_c}\right)} \quad (15)$$

Similarly, the rate of the anodic reaction $M \rightarrow M^{n+} + ne^-$ can be expressed as follows:

$$i_a = i_o * \exp\left(\frac{\alpha_a n F \eta}{RT}\right) \quad (16)$$

which can be similarly rewritten as follows:

$$\ln\left(\frac{i_a}{i_o}\right) = \frac{\alpha_a n F \eta}{RT} \quad (17)$$

with

$$\eta = E - E_{rev} \quad (18)$$

where the Tafel relationship, considering $n=2$ for iron dissolution, is shown as

$$\eta = \beta_a * \log\left(\frac{i_a}{i_o}\right) \quad (19)$$

with

$$\beta_a = \frac{2.303 * R * T}{2 * \alpha_a * F} \quad (20)$$

and

$$i_a = i_o * 10^{\left(\frac{\eta}{\beta_a}\right)} \quad (21)$$

where η is the over-potential applied; and the β_a and β_c values are known as the Tafel constants for each half reaction involved during corrosion process. The values of β_a and β_c for each reaction can be determined theoretically as long as the proper mechanism is known. However, in practice it is determined experimentally.

Plots representing the over-potential and current density for electrochemical reactions are created in a logarithmic scale in order to linearly represent how the reductions reactions happen simultaneously with metal oxidation at the electrode surface. Figure 1 illustrates how graphs known as Evans diagrams are commonly used in corrosion analyses.

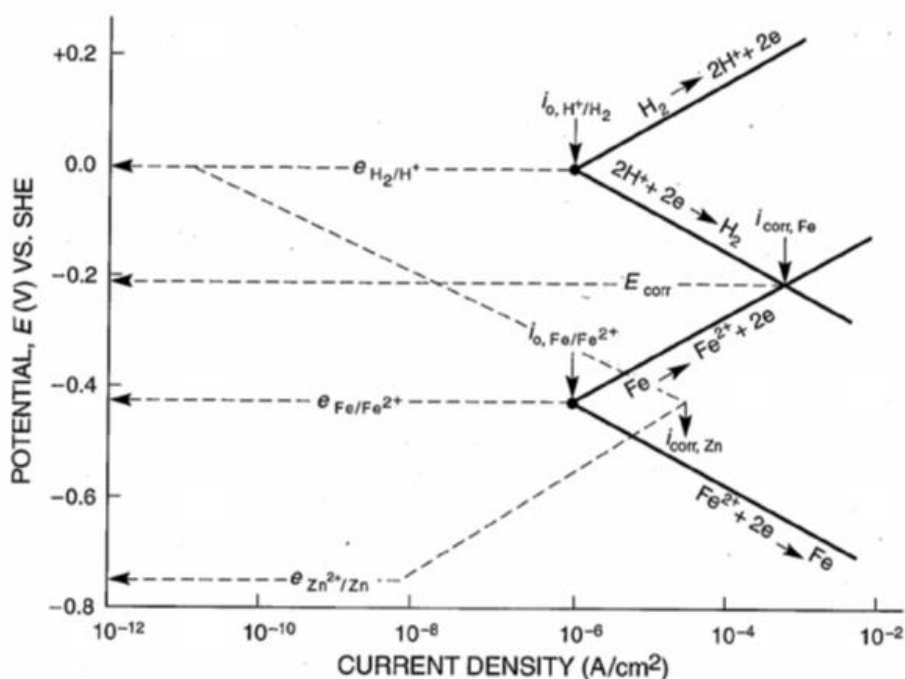


Figure 1. Half reactions for each component plotted against a potential and current density frame. The mixed potential is where the iron oxidation happens at the same rate as the reduction of protons. JONES, DENNY A., *PRINCIPLES AND PREVENTION OF CORROSION*, 2nd, © 1996. Reprinted by permission of Pearson Education Inc., New York, New York. ²⁴

As it can be seen from Figure 1, the lines representing the reduction of protons and the oxidation of iron – given by Equations (1) and Equation (2) – intersect at a point. This point corresponds to the mixed (or corrosion) potential, E_{corr} , and the corrosion current

density I_{corr} . This in turn is used to calculate the corrosion rate as it is shown in Equation (22).

$$CR = \frac{I_{corr}(MW)}{\rho nF} \quad (22)$$

where I_{corr} is the corrosion current density, n is the number of electrons involved in the reaction, F is Faraday's constant, MW and ρ are the molecular weight and density of the alloy, respectively and CR is the corrosion rate often expressed in MPY or mm/year. Experimentally speaking, corrosion currents are often measured using a technique called Linear Polarization Resistance (LPR). This technique assumes that the current density is a linear function of the applied potential near the corrosion potential. Small over-potentials are applied and the slope of the current density vs. applied potential line is defined as the resistance of polarization as shown by Equation (23)

$$R_p = \frac{\beta_a \beta_c}{2.3(\beta_a + \beta_c) i_{corr}} = \frac{B}{i_{corr}} \quad (23)$$

with

$$B = \frac{\beta_a \beta_c}{2.3 * (\beta_a + \beta_c)} \quad (24)$$

According to data obtained from deWaard's research, a B value of 13 and 26 mV can be assumed for solutions sparged with nitrogen and carbon dioxide, respectively^{13, 18}. There is no data regarding the effect of MEG on the B value. Determining possible changes of this value in the presence of MEG is one focus of the present study. Lastly, it is important to highlight that Nordsveen et al.²¹ developed an expression for the exchange current density of each electrochemical reaction based on a given set of conditions as shown by Equation (25):

$$i_i = i_{i_ref} * \left(\frac{C_{H^+}}{C_{H^+_ref}}\right)^{a1} * \left(\frac{C_{CO_2}}{C_{CO_2_ref}}\right)^{a2} * \left(\frac{C_{H_2CO_3}}{C_{H_2CO_3_ref}}\right)^{a3} * e^{\frac{-\Delta H}{R} * \left(\frac{1}{T} - \frac{1}{T_{ref}}\right)} \quad (25)$$

where the coefficients for each reaction, i , are shown in Table 13 in APPENDIX B COEFFICIENTS USED FOR MODELING THE ELECTROCHEMICAL REACTIONS. The next section focuses on expanding on the parametric and mechanistic analysis provided by Nesic et al.,²⁰ and Nordsveen et al.,²¹ for CO₂ corrosion reactions.

2.1.3 CO₂ Corrosion – Effect of Temperature

As shown in the previous section, corrosion involves electrochemical reactions that are governed by the direct exchange of electrons in a system. As with all chemical reactions, there is a direct relationship between the temperature and the rate of the reaction.

For corrosion mechanisms, an increase in temperature will cause an increase in rate of the anodic and cathodic reactions, thus increasing the corrosion rate. Corrosion product formation is also accelerated at high temperature, which may lead to some level of protection against corrosion. However, the formation of corrosion products is not considered in the present study.

2.1.4 CO₂ Corrosion – Effect of Partial Pressure of CO₂

The partial pressure of CO₂, together with the pH and the temperature, determines the concentration of dissolved carbonic species in solution as shown in Table 1. At constant pH and temperature, a decrease in partial pressure of carbon dioxide results in a decrease in the concentration of carbonic acid which in turn leads to lower corrosion rate. This statement holds where carbonic acid is considered as a reducible species or solely as a buffering agent. Similarly, an increase in CO₂ partial pressure will result in an increase in corrosion rate; however, it may also promote formation of corrosion products through the

increase in carbonate ions concentration. A more detailed description has been provided by Nestic et al.,^{20,21} and has served as the basis and starting point for several electrochemical models, one of which is FREECORP™. The values of the equilibrium constants and other relevant parameters are provided elsewhere²¹.

Table 1. Chemical reactions related to carbon dioxide/water systems and their respective equilibrium constants. Electro-neutrality, and ionic strength equations used to calculate speciation.

	Reaction	Equilibrium Constant
Dissolution of Carbon Dioxide	$CO_2 (g) \rightleftharpoons CO_2(aq)$	$K_{sol} = [CO_2]/pCO_2$
Water Dissociation	$H_2O (liq) \rightleftharpoons H^+ (aq) + OH^- (aq)$	$K_{wa} = [H^+] [OH^-]$
Carbon Dioxide Hydration	$CO_2 (aq) + H_2O (liq) \rightleftharpoons H_2CO_3(aq)$	$K_{hyd} = [H_2CO_3]/ [CO_2]$
Carbonic Acid Dissociation	$H_2CO_3(aq) \rightleftharpoons H^+ (aq) + HCO_3^- (aq)$	$K_{ca} = [H^+] [HCO_3^-]/[H_2CO_3]$
Bicarbonate Anion Dissociation	$HCO_3^- (aq) \rightleftharpoons H^+ (aq) + CO_3^{2-} (aq)$	$K_{bi} = [H^+] [CO_3^{2-}]/ [HCO_3^-]$
Electro-neutrality Equation	$[Na^+] + [H^+] = [OH^-] + [Cl^-] + [HCO_3^-] + 2*[CO_3^{2-}]$	**All species are in the aqueous phase (aq)
Ionic Strength	$I = 0.5 * \sum_1^N c_i * z_i^2$	N is the total number of species

2.1.5 CO₂ Corrosion – Effect of pH

The pH of the solution plays a major role in corrosion processes since the main cathodic reaction is the proton reduction²¹. For the same solution pH, the presence of a weak acid (carbonic acid for example) will lead to higher corrosion rate compared to a

strong acid environment. This is attributed to the buffering effect, providing extra protons through the dissociation of the weak acid, and/or the weak acid direct reduction at the metal surface, in addition to the proton reduction.

2.1.6 *CO₂ Corrosion – Effect of Flow*

Flowing conditions have a strong impact on corrosion mechanisms^{4, 24}. The main part of the corrosion process that gets affected by changes in flowing conditions (for solutions with low pH values) is the reduction of protons since the oxidation of iron is not flow dependent as demonstrated by Nescic's investigation²⁰.

The rate of proton reduction is controlled either by the rate of mass transfer of H⁺ to the metal surface or by the electron transfer rate of the reduction reaction. Typically, a higher mass transfer rate increases the flux of protons towards the metal surface, which can accelerate the reduction reaction rate. However, this is true as long as the electron transfer rate can keep up with the flux of H⁺ to the surface. Beyond this point, the H⁺ reduction rate is not anymore flow dependent as the slowest step in the process switches from mass transfer to charge transfer. It should be stressed that the corrosion process is always controlled by its slowest step, which can either be related to charge transfer, mass transfer (flow dependent), or chemical reaction, as it is explained later on.

In the previous section, the expression of the current density of the cathodic reaction was expressed considering a system under charge transfer control. In a system where mass transfer (or chemical reaction) can be a limitation (which is true for most corrosion systems), these expressions are not valid anymore and need to be corrected as follows:

$$\frac{1}{i(H^+)} = \frac{1}{i_{\infty}(H^+)} + \frac{1}{i_{lim}^d(H^+)} \quad (26)$$

Equation (26) shows how the current density is comprised of two important parameters $i_{\infty}(H^+)$, which is known as the charge transfer current density (this was presented in the previous section) and is independent of flow. And the other parameter, $i_{lim}^d(H^+)$, which is defined as the diffusion limiting current density, and it is dependent on the mass transfer properties of the system. The limiting current for proton reduction can be calculated using Equation (59).

$$i_{lim}^d(H^+) = k_m * F * [H^+]_b \quad (27)$$

where k_m is the mass transfer coefficient that can be calculated from Equation (28)²⁵

$$Sh = \frac{k_m * d}{D_{AB}} = 0.0791 * Re^a * Sc^b \quad (28)$$

where a, and b are 0.7 and 0.356, respectively for the rotating cylinder electrode setup used in this research²⁰. Re and Sc are the commonly known Reynolds and Schmidt number, respectively, and each parameter represents fluid properties which are calculated as follows:

$$Re = \frac{\vartheta * d_{cyl}}{\nu} \text{ and } Sc = \frac{\nu}{D} \quad (29)$$

where ϑ = the rotational velocity in the rotating cylinder, d_{cyl} is the diameter of the sample (in this case the rotating cylinder), and ν is the kinematic viscosity. As it can be seen from Equation (28), an increase in flow will result in an increase in the Sherwood number, which in turn causes a higher mass transfer coefficient for the system.

The limiting current corresponding to the reduction of carbonic acid is expressed in Equation (30). This limiting current is only weakly flow dependent, and mostly

controlled by the slow carbon dioxide hydration step (chemically controlled instead of mass transfer controlled).

$$i_{lim}(H_2CO_3) = F * [CO_2]_b * f * \sqrt{(D_{H_2CO_3} * k_{f,Hyd} * K_{Hyd})} \quad (30)$$

Additional parameters can be added to take into account the formation of corrosion products but they are ignored in this study. Furthermore, f is called the flow factor and it is within this parameter that the integration of the mass transfer coefficient, k_m for a system with carbonic acid is involved as shown by Equation (31).²⁸

$$f = \frac{1 + e^{-2 * \frac{\delta_m}{\delta_r}}}{1 - e^{-2 * \frac{\delta_m}{\delta_r}}} \quad (31)$$

where,

$$\delta_m = \frac{D_{H_2CO_3}}{K_{m,H_2CO_3}} \quad (32)$$

and,

$$\delta_r = \sqrt{\frac{D_{H_2CO_3} * K_{Hyd}}{k_{Hyd,f}}} \quad (33)$$

In practice, Equation (26) can be plotted in the Evans diagram shown clearly in Figure 2, when the system is under mass transfer – points A, B or C – or charge transfer control – point D.

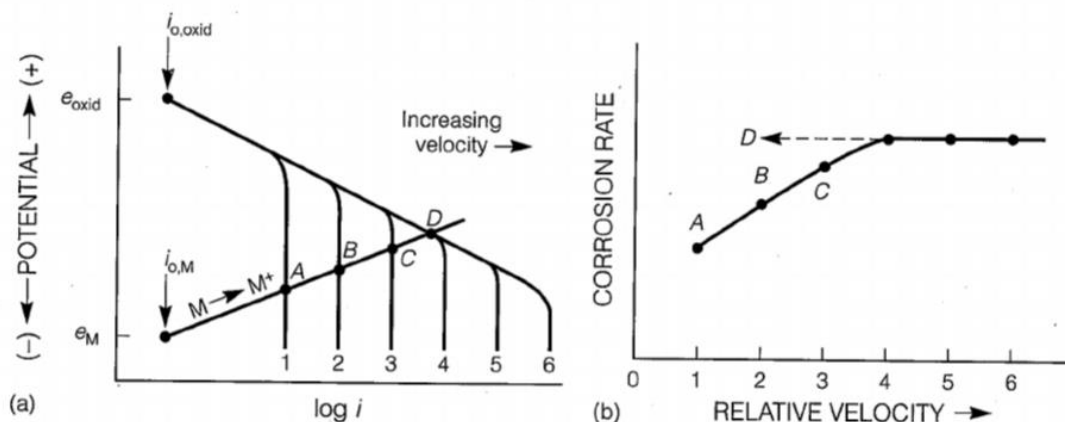


Figure 2. Evans diagrams showing: a). Effect of velocity on limiting current. b). Effect of velocity on corrosion current. JONES, DENNY A., *PRINCIPLES AND PREVENTION OF CORROSION, 2nd*, © 1996. Reprinted by permission of Pearson Education Inc., New York, New York.²⁴

2.2 MEG and CO₂ Corrosion

There have been many publications related to how MEG decreases the corrosion rate^{4,8-12,18,29-30}. Although these publications have provided reasonable explanations related to the effects of MEG on corrosion, a wide gap still remains in the mechanistic understanding. Work from deWaard et al.,¹⁸ has been deemed as groundbreaking in the corrosion community due to the early contribution of a conservative corrosion predictive model. The authors' semi-empirical model accounted for worse case scenarios of corrosion rates obtained from a given temperature and partial pressure of CO₂ as shown by Equation (34).

$$\text{Log}V = 5.8 - \frac{1710}{T} + 0.67 * \log(p\text{CO}_2) \quad (34)$$

where, V = corrosion rate in mm/y, pCO₂ in bar, and T in Kelvin.

Although this model was initially based on parametric analyses, deWaard decided to expand on it by adding factors – one of which was a MEG factor – obtained experimentally as demonstrated in Equation (35).

$$\text{Log}F_{glycol} = 1.6 * \log(\text{wt}\%) - 3.2 \quad (35)$$

where $\text{wt}\%$ = weight % of water in MEG/Water mixture, F_{glycol} is the glycol factor.

This factor is still used today as a method of prediction from what the corrosion rate should be in the presence of MEG, however recent publications have demonstrated that predicted values at temperatures above 50°C underestimate the expected corrosion rate¹⁶.

In a study presented by vanBodegom et al.⁸ on glycolic and methanol containing solutions, the corrosion rates obtained from weight loss and LPR measurements were in accordance with those predicted by deWaard's glycol factor. Technical and analytical grades of alcohol were used in his experiment, and variations in temperatures and partial pressures of carbon dioxide were tested. Results from this work demonstrated that at temperatures of 20 and 80°C, and 1bar partial pressure of CO₂, solutions containing mono and tri-ethylene glycol showed decreases in the corrosion rates, but no further systematic analyses were shown.

In 1993, Crolet et al.⁹ found that it could be suitable to inject MEG as part of a “technical package” in conjunction with other chemicals in order to act as a pH stabilizer in gas-condensate lines, and thus serve as a primary CO₂ corrosion mitigation method. The authors highlighted that this method favored the formation of protective corrosion products

and had been successfully used in different oil fields around the world. However, no effort was made towards developing a mechanistic explanation for the observed results.

In a 1994, Dugstad et al.⁴ published a review on how to control CO₂ corrosion in multiphase pipelines, and discussed the importance of approaching this issue from a mechanistic perspective. The authors highlighted that considering the application of hydrate inhibitors as corrosion prevention methods during the pipeline design phase can be beneficial in the longevity of the project. Unfortunately, the authors essentially referred to the results from the study presented by Crolet et al.⁹ but did not perform their own experimental study.

In 1998, the first mechanistic analysis on CO₂ corrosion in the presence of MEG was presented by Gudbrandsen et al.¹³ This paper is of great relevance due to the focus on better understanding of the corrosion process, as well as the electrochemical measurement techniques used therein. Evans diagrams were obtained as shown in Figure 3 considering the effect of MEG for a given concentration.

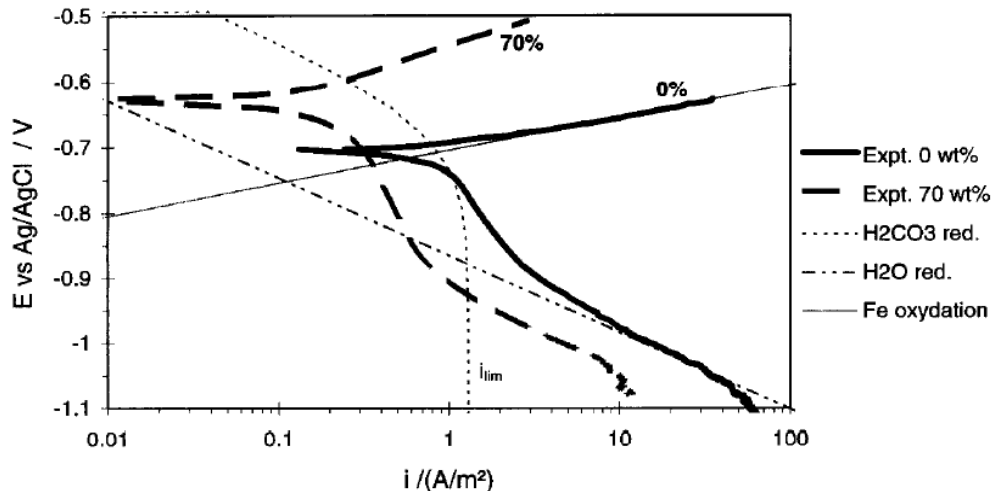


Figure 3. Potentiodynamic sweeps obtained for 0wt. % and for 70wt. % MEG-Water-CO₂-NaCl systems. Reproduced with permission from NACE International, Houston, TX. All rights reserved. Gulbrandsen E and Morad J, Paper 221 presented at Corrosion/1998, San Diego California. © NACE International 1998.¹³

This study has been the subject of reference for various corrosion and chemistry related publications due to its excellent description of the changes in physico-chemical properties of CO₂-H₂O-NaCl reactions in the presence of MEG. Figure 4 and Figure 5 demonstrate the findings presented in Gulbrandsen's research where these results reflect how the solubility and diffusivity of CO₂ in a H₂O-MEG-NaCl solution were affected by the presence of ethylene glycol.

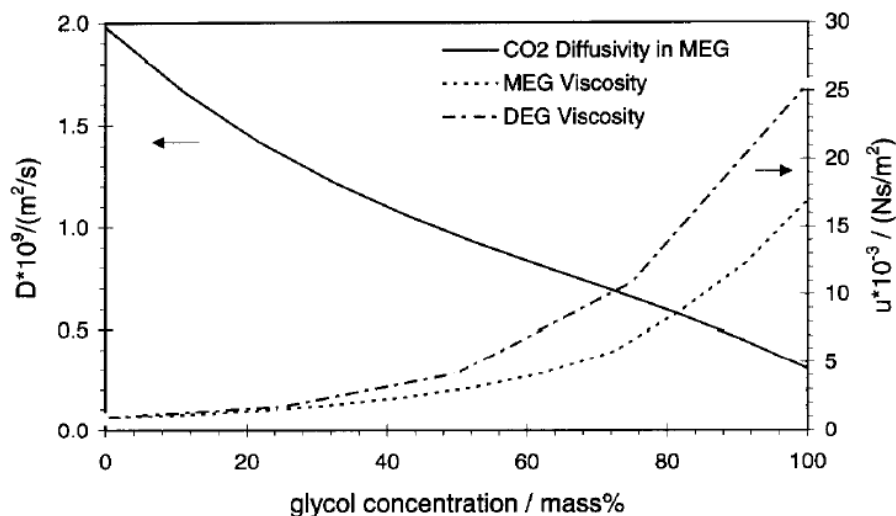


Figure 4. CO₂ diffusivity (left axis) and solubility viscosity (right axis) as a function of glycol content at 25°C. Reproduced with permission from NACE International, Houston, TX. All rights reserved. Gulbrandsen E and Morad J, Paper 221 presented at Corrosion/1998, San Diego California. © NACE International 1998.¹³

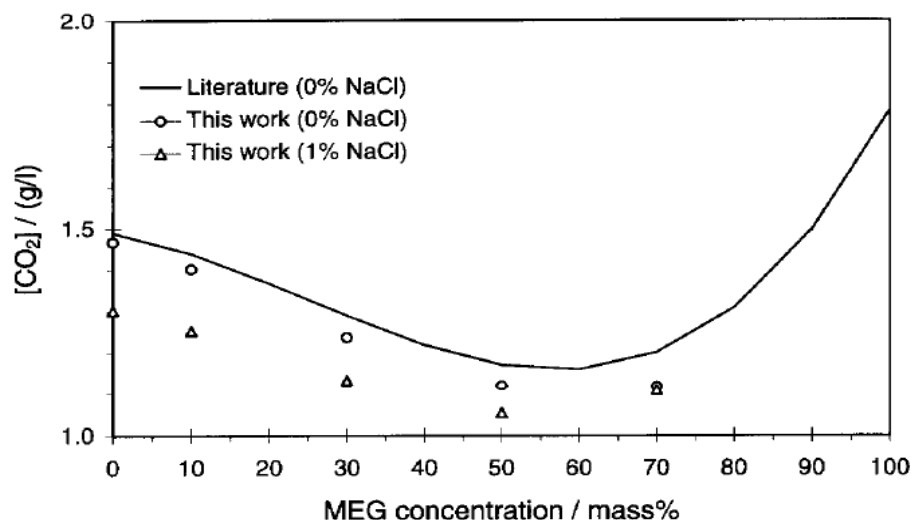


Figure 5. Effect of MEG content on CO₂ and solubility for a solution at 25°C, and 1atm CO₂ pressure. Reproduced with permission from NACE International, Houston, TX. All rights reserved. Gulbrandsen E and Morad J, Paper 221 presented at Corrosion/1998, San Diego California. © NACE International 1998.¹³

Additional observations were presented regarding the increases in solution viscosity, as well as decreases in solution polarity (with increases in glycol content in

solution), and linked to the decrease of the overall corrosivity of mixture. While these were new and reasonable explanations to the effect of MEG on corrosion mechanisms, these results could only associate the decreases in corrosion rates to the cathodic reactions. However, the authors then proposed that changes in solution properties and MEG adsorption on the metal surface also affected the dissolution of iron in solution. Furthermore, they also acknowledge that this aspect was not clearly understood. Finally, the focus of that paper shifted to investigating the effect of glycol purity, as well as the effect of various concentrations of NaCl in MEG-H₂O-CO₂ solutions. The year after, Dugstad et al.,⁶ and Olsen et al.,⁷ cited Gulbrandsen's findings¹³ to discuss the inclusion of MEG as part of the pH-stabilization-technique for field applications.

In 2000, Gonzalez, et al.¹⁰ studied the use of MEG as a corrosion prevention method in a natural gas dehydration plant that was experiencing corrosion attacks. This work demonstrated that the corrosion problems were substantially diminished by the use of MEG. The authors used electrochemical techniques similar to those applied in this research; however, the author omitted key details in the experimental procedure and results, leading to confusing information regarding the amount of MEG used during experiments. One of the key findings in this work was that the presence of rich MEG (glycolic solutions high in water content) at low pH and high temperatures (>60°C) seemed to increase the corrosion rate, and endanger the integrity of the materials. To address this issue, studies with pH neutralizers were performed, which allowed for better control of the acidity in the environment and hence lower corrosion rates.

A few years later in 2005, Kvarekval et al.¹¹ were the first to investigate a combined CO₂-H₂S-H₂O environment in the presence of glycols. The focus of that study was to determine the likelihood of pitting corrosion for such corrosive environments by altering different parameters including different types of material. Even though results interestingly showed that the likelihood for localized and pitting corrosion was decreased in the presence of MEG for this combined environment, no systematic investigation was presented.

In a publication made by Ehsani et al.¹⁵ in 2011, an excellent study was done from a mechanistic view with regards to the effects of MEG on CO₂ corrosion. The authors in that work, applied LPR and potentiodynamic measurements similar to those used in the present study for solutions containing up to 50vol. % MEG in solution. It was found that MEG exhibited inhibitive effects on the dissolution of iron into solution, and that this was the main contribution to the reduction in corrosion rates in the presence of MEG. Furthermore, these authors also found that the Tafel slopes were minimally affected in the presence of MEG. Ehsani's research also used SEM analyses of exposed steel surfaces for both water based and water-MEG based solutions. These SEM images demonstrated that corrosion samples in MEG-free environments were uniformly covered with corrosion products, whereas those subjected to MEG "contaminated" solutions showed a clearer and smoother exposed surface. Even though this work is highly relevant based on the electrochemical techniques used, as well as the experimental execution, the authors only investigated low MEG content, and only one temperature of 60°C was reported leaving room for a more thorough investigation to be performed.

A few years later in 2013, a study by Ivonye et al.¹² investigated CO₂ corrosion in the presence of MEG, as well as tests involving commercially available corrosion inhibitors. Electrochemical results showing the decrease in corrosion rate by the presence of MEG were obtained by using LPR and EIS measurements. This work applied a parametric approach to the study of corrosion mechanisms in glycolic solutions and the authors found similar results to those from Gulbransen's investigation¹³. Additionally, just like other authors, only a few conditions were tested in that work without expanding on mechanistic related reasoning from their findings.

In 2013, Kvarekval et al.⁵ expanded on his previous study from 2005¹¹. This time, the focus lied on understanding the effect of increased salinity and alkalinity in solution, and determining if these changes had any effect on corrosion mechanisms under sour (H₂S) glycolic systems. Although the authors in that work performed full potentiodynamic sweeps (anodic and cathodic), only the anodic sweeps were shown in order to determine the effect of glycol on inhibitor efficiency. These anodic potentiodynamic curves demonstrated that increasing the NaCl content in solution by about an order of magnitude (0, 0.82g/L, 8.2g/L, 82g/L) at low pH (4.1) resulted in decreased corrosion potentials and an increased in the anodic rate of reaction (a right displacement of the anodic reaction in the Evans diagram). Although there was an increase in current density due to the positive shift of the anodic reaction, the authors did not find any localized corrosion in their samples. For the same conditions but at high pH (5.1) the same trend in increased anodic rate was obtained; however, some localized corrosion attacks were generated in the presence of NaCl containing solution. While this was a comprehensive electrochemical

study with interesting results regarding the understanding of the effects of alkalinity and salinity, no thorough analysis was done to understand mechanistic effects of MEG in the system.

In 2014, a publication presented by Pojtanabuntoeng et al.,¹⁸ a thorough mechanistic analysis at temperatures and pressures that resembled those found in MEG regeneration units. The authors expanded on what had been proposed by Gulbrandsen et al.¹³ with regards to changes in the cathodic reaction being related to the properties of the fluid. Moreover, Pojtanabuntoeng's research investigated the effect of MEG on the oxidation of the iron. This was of particular interest since no thorough investigation for the effect of MEG on the oxidation of iron had been presented, outside of that one presented by Ehsani et al.¹⁵ relating the decreases in corrosion potential with increasing glycol content in solution. The authors first mentioned that at temperatures of 80°C to 120°C, the iron dissolution seemed to be independent of MEG content, and that no change in Tafel slopes was observed. Furthermore, the authors postulated that intermediate reactions in the dissolution of iron were slowed down by the presence of MEG. Overall, the results from this research still found that at elevated temperatures and pressures, the corrosion rate was also decreased in the presence of MEG. Additionally, this work demonstrated that the corrosion rate predicted with deWaard's conservative predictive glycol factor underestimated experimental values at temperatures above 80°C.¹⁸

A year after, Javidi et al.¹⁶ in 2015 applied similar electrochemical techniques in an effort to provide a robust understanding regarding corrosion in MEG-CO₂-H₂O systems. From the LPR and potentiodynamic measurements, the author found the common trend in

decreasing corrosion rate with increasing MEG presence (up to 90wt. %) for brine solutions, as well as similar “inhibition” effects on the anodic reaction as shown in the Figure 6 below.

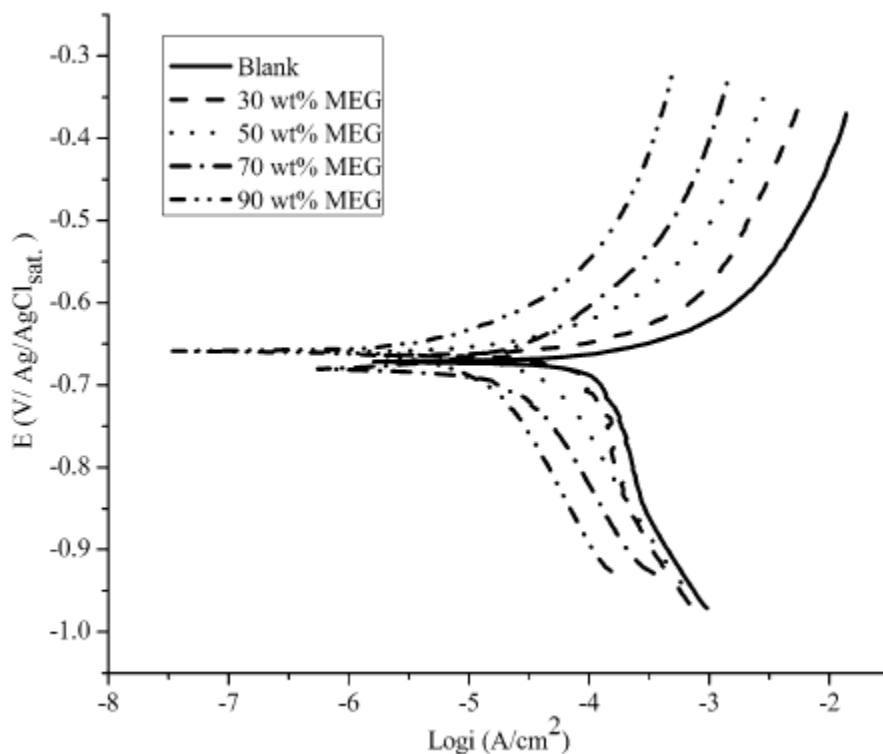


Figure 6. Evans diagram showing the effect of 0, 30, 50, 70 and 90wt. % MEG in solution, respectively for a solution at 50°C, 1bar CO₂ and 1wt. % NaCl. Javidi, M., & Khodaparast, M. (2015). Inhibitive Performance of Monoethylene Glycol on CO₂ Corrosion of API 5L X52 Steel. *Journal of Materials Engineering and Performance*, 24(4), 1417-1425. With Permission of Springer.¹⁶

From the EIS results, the authors performed an extensive analysis following Gulbrandsen's¹³ findings regarding the increase in solution resistance with increasing MEG content. Figure 7 illustrates the electrochemical impedance spectroscopy results in the presence of MEG, which corroborate Gulbrandsen's results.

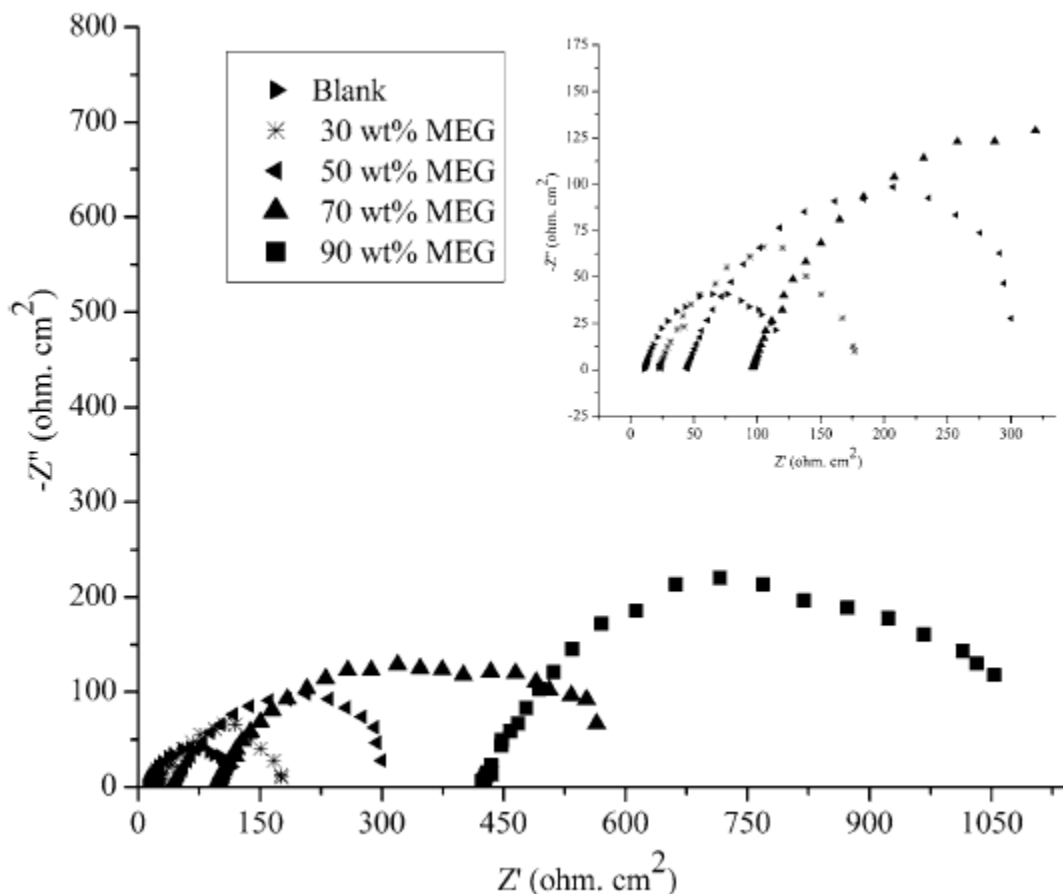


Figure 7. Nyquist plot showing the imaginary (y-axis) and real (x-axis) impedances at a frequency range between 1,000,000 – 0.01 Hz for X52 steel in a CO₂ saturated solution with 1wt. % NaCl, different MEG contents and at a temperature of 50°C. Javidi, M., & Khodaparast, M. (2015). Inhibitive Performance of Monoethylene Glycol on CO₂ Corrosion of API 5L X52 Steel. *Journal of Materials Engineering and Performance*, 24(4), 1417-1425. With permission of Springer. ¹⁶

According to the EIS measurements, Figure 7 shows a clear increase in both solution and polarization resistances with increasing MEG content. Additionally, Javidi's research postulated that the decreases in corrosion rate were due to the plausible site blocking effect due to MEG adsorption on the metal surface. Lastly, and equally as important, these authors found that the deWaard glycol factor¹⁸ underestimates the predicted corrosion rate at temperatures of 50°C by 30%. Due to this finding, an adjusted

glycol factor value was proposed to be applied to deWaard's original model in order to account for temperatures above 50°C. Although this extensive publication provides an in-depth explanation on LPR, potentiodynamic and specially EIS grounds, there were gaps left unexplained in that paper, as well as key experimental conditions that were not well defined. For example, the pH of the solution was not mentioned in the experimental procedure. Additionally, only one temperature was used to perform their research, again leaving room to perform this type of analysis on a wider temperature range. Lastly, the authors decided to focus their efforts in trying to understand the effects of ionic strength in MEG-Water solutions.

In 2017, the most recent findings were published by Ekawati et al.¹⁷. While the goals and objectives of that work were to determine the likelihood of iron carbonate formation, as well as the effect of bicarbonate ions under various levels of alkalinity in the presence of MEG, potentiodynamic sweeps therein demonstrated common trends observed in the literature regarding the anodic-inhibitive effects that MEG presents for CO₂ corrosion mechanisms. Solutions containing up to 50wt. % of MEG in solution were tested utilizing X65 and St52 at different temperatures, where each material demonstrated the same behavior in retardation of the anodic reactions. Additionally, these authors found that there were no effects on the Tafel slopes for solutions containing up to 50wt. % MEG in solution at low alkalinity. An anodic Tafel slope value of 40mV/decade fitted their experiments appropriately, however, it was seen that the slope changed slightly to 60 – 70 mV/decade for solutions at high at pH of 5 and 6, respectively.

2.3 Water/MEG Solution Chemistry

MEG+water solutions are defined as non-ideal because they exhibit deviations from the commonly accepted ideal behavior. Ideal conditions are based on the assumption of non-interaction between molecules. Whether it is a multiphase environment or a single-phase system (gas, liquid or solid), intensive and extensive properties of non-ideal solutions deviate from expected behaviors (ideal systems), and more complex, often semi empirical methods have to be used in order to accurately predict non-ideal conditions. The next sections expand on how thermodynamic parameters such as species fugacity and activity coefficients are affected by temperature and pressure, and how they are used to simulate non-ideal solutions. The complete description of the MEG-Water-NaCl-CO₂ system requires the implementation of proper equation of state and activity model. The gaseous phase is not expected to deviate from ideality in the experimental conditions tested. However, in an effort to be consistent, the Peng-Robinson equation of state is used in order to model the non-ideal behavior in the gas phase as shown by Equation (36)

$$P = \frac{RT}{(V-b)} - \frac{a(T)}{V(V+b)+b(V-b)} \quad (36)$$

where a and b are constants that depend on the critical temperature and pressure of the compound, V is the molar volume of the gas, T is the temperature of the gas and P is the calculated pressure of the corresponding gas, in this case CO₂.

Lastly, the changes exhibited in solution by increasing the concentration of MEG are also a key consideration in this context, as they will affect concentrations of species involved in the hydration and dissociation of carbonic acid. The next sections discuss the

derivations used to calculate the solution pH and the activity of dissolved CO₂ in the liquid phase. More details on the modeling approach are shown in Chapter 6.

2.3.1 Proton Activity in Non-Ideal Solutions

A number of studies have been published demonstrating the non-ideal behavior of MEG+Water solutions^{26, 27, 34, 49}. Compared to ideal solutions where the concentration of protons determines directly the pH of a system, non-ideal mixtures require taking into account the activity of proton, and of each component in general. Taking H⁺ proton as an example, the representation of non-ideality is expressed by Equation (37)

$$a_{H^+} = m_{H^+} * \gamma_{H^+} \quad (37)$$

where a denotes the activity, m and γ represent the concentration and activity coefficient of the species, respectively. The activity coefficient is what will demonstrate how the solution deviates from ideality and the solution pH can then be calculated using Equation (38)

$$pH = -\log[a_{H^+}] = -\log[m_{H^+} * \gamma_{H^+}] \quad (38)$$

For geochemical systems, solutions often contain large concentrations of salts, further contributing to the non-ideality of the aqueous phase. Furthermore, the presence of carbonate species adds to the complexity in predicting the pH of the mixture. This determination of activity coefficients for each component in the presence of MEG is a crucial part in this research for the development of the chemistry model, and a thorough explanation is provided in Chapter 6.

2.3.2 CO₂ Solubility in MEG+Water Solutions

Carbon dioxide solubility in water in combination with other solvents has been a topic that has been extensively studied^{13,38-46}. More specifically, the study of the solubility of CO₂ in non-ideal solutions has gained strong momentum in recent years due to the interest in prevention of hydrates during wet gas transport processes. Additionally, solubility data for CO₂ in MEG-Water-NaCl systems also aids in the planning and design of pipelines and processing units due to the likelihood of scaling effects for such solutions.^{29,34} Work done by Lu et al.,²⁹ Kan et al.,³⁰ and Serpa et al.,^{45,46} provided empirical data demonstrating the decrease in solubility of CO₂ in MEG-Brine solutions, for a constant ionic strength, as shown in Figure 8.

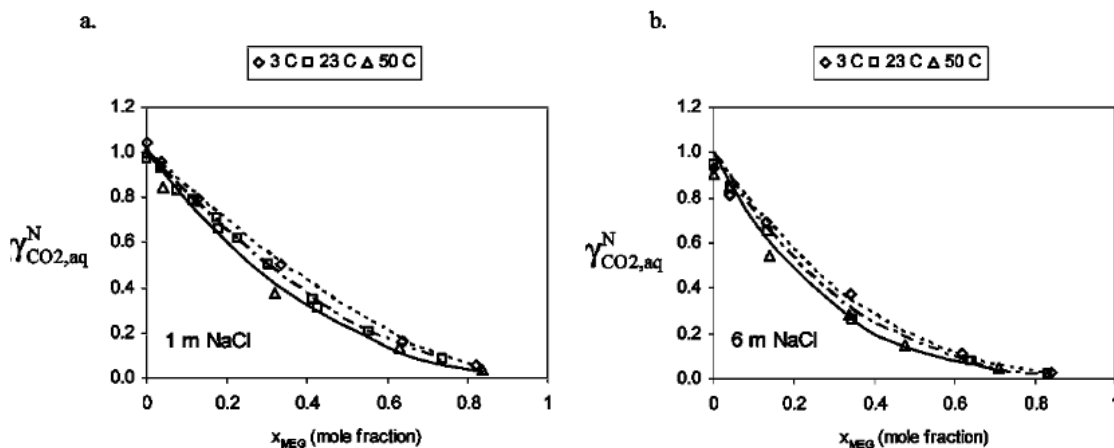


Figure 8. Reprinted with permission from Kan, A. T., Lu, H., & Tomson, M. B. (2010). Effects of Monoethylene Glycol on Carbon Dioxide Partitioning in Gas/Monoethylene Glycol/Water/Salt Mixed Systems. *Industrial & Engineering Chemistry Research*, 49(12), 5884-5890. Copyright 2003 American Chemical Society. Effect of temperature on the behavior of the activity coefficient of aqueous CO₂ in non-ideal solutions at constant electrolyte concentrations³⁰.

Also, both increasing ionic strength and the MEG content in solution seemed to decrease the solubility of CO₂ in the system. As demonstrated by Kan et al.³⁰, the expressions of the equilibrium constants shown in Table 1 should be modified to represent non-ideal conditions. For the dissolution of carbon dioxide in a non-ideal mixture, the following can be proposed:

$$K_{sol} = \frac{a_{CO_2(aq)}}{f_{CO_2(g)}} \quad (39)$$

where $a_{CO_2(aq)}$ is the activity of the carbon dioxide in the aqueous phase and $f_{CO_2(g)}$ denotes the pressure of the gas, which is now represented by its fugacity.

The thermodynamic Henry's constant used in Equation (39) can be obtained as follows from Equation (40):

$$K_{sol} = \frac{a_{CO_2(aq)}}{f_{CO_2(gas)}} = \frac{[CO_2(aq)] \cdot \gamma_{CO_2(aq)}^S \cdot \gamma_{CO_2(aq)}^M}{P_{CO_2} \cdot \gamma_{CO_2}^g} \quad (40)$$

where $\gamma_{CO_2}^g$, $\gamma_{CO_2}^S(aq)$ and $\gamma_{CO_2}^M(aq)$ are the CO₂ activity coefficients of the gas and liquid phases, respectively and a more detailed explanation is provided in Chapter 6. Furthermore, definition of units used in this work is provided in the Glossary section. Additional data related to the viscosity and diffusivity of CO₂ in non-ideal solutions found in literature^{38-44, 50} are used in order to model the chemistry of the solution. It is of high importance to accurately model and understand the solubility of CO₂ in the non-ideal solution, in order to more accurately model corrosion mechanisms. Such understanding can lead to better and improved prediction models that account not only for corrosion mitigation techniques, but also for scaling^{31, 32, 33, 35} prediction capabilities.

CHAPTER 3 MOTIVATION, OBJECTIVES AND HYPOTHESES

3.1 Motivation

Although extensive efforts have been made to study CO₂ corrosion and the factors influencing it, several knowledge gaps still exist, which warrants continuous research efforts. This is especially true as it relates to the mechanistic understanding of CO₂ corrosion in the presence of MEG. Literature findings clearly show a reduction of the corrosion rate of mild steel in CO₂/H₂O/MEG systems. Although no firm conclusions can be taken yet, several common key observations accepted by most researchers and regarded as highly relevant to the present study can be extracted from the literature review:

- Increasing glycol content alters the physico-chemical properties of the non-ideal solution.
- MEG seems to reduce considerably the rate of dissolution of iron into solution, while the corresponding Tafel slope seems to be relatively unaffected, especially at a pH of 4.
- While cathodic reaction rates are also reduced in the presence of MEG, the corresponding Tafel slopes do not seem to change.
- Water reduction rate seems to be altered in MEG-Water mixtures due to the decrease in water activity.
- MEG can be included in a chemical package to help stabilize the acidity of the solution and control corrosion formation.

However, although several researchers¹³⁻¹⁶ have shown a common interest in the understanding of corrosion behaviors, no systematic and comprehensive parametric study

has been performed over a wide range of operating conditions. Conflicting information is presented about the mechanisms leading to the observed decreases in reaction rates. In addition, no comprehensive effort has been made to model the overserved behavior and confront the predictions with experimental data.

It is imperative to adopt a parametric approach in studying this complex phenomenon in order to isolate the effect of each controlling parameters. Only then can a robust understanding on the mechanisms be developed. A thorough effort to model the results, considering both the changes in fluid properties and the potential effects on the electrochemical reactions, should be undertaken and compared to existing experimental data.

3.2 Proposed Hypotheses

Based on the gaps found in the literature with regards to this topic, the following hypotheses are proposed to guide the research work.

1. The addition of MEG to a CO₂-H₂O system does not change the commonly accepted corrosion behaviors of mild steel with respect to temperature, pH and flow changes.
2. MEG is not an electroactive species and therefore, is not expected to affect the Tafel slopes of the anodic or cathodic reactions. Any changes observed in the presence of MEG can be explained by the physico-chemical characteristics of the fluid such as proton activity, viscosity, density, CO₂ solubility, etc.

3.3 Thesis Objectives and Accompanying Tasks

The purpose of this study is to improve the understanding of corrosion mechanisms in the presence of MEG.

The following specific objectives have been identified:

- **Task#1 – Systematic study of parameters impacting CO₂ Corrosion**

Perform a parametric electrochemical study on the effect of MEG on CO₂ corrosion mechanisms. The parameters of interest are temperature, solution pH, rate of mass transfer and MEG content in solution.

- **Task#2 – Development of MEG-CO₂ Chemistry Model**

Develop and validate a chemistry model that simulates speciation in CO₂-MEG-Water systems.

- **Task#3 – Development of MEG Capabilities for FREECORP™**

Determine relevant thermodynamic and kinetic parameters in order to simulate the corrosion mechanisms and update FREECORP™ to account for the presence of MEG.

FREECORP™ is an open source software, developed by ICMT that currently estimates uniform corrosion rates for a given set of initial values in H₂O/CO₂/H₂S/O₂ environments. Figure 9 shows the user interface of this in-house electrochemical model.

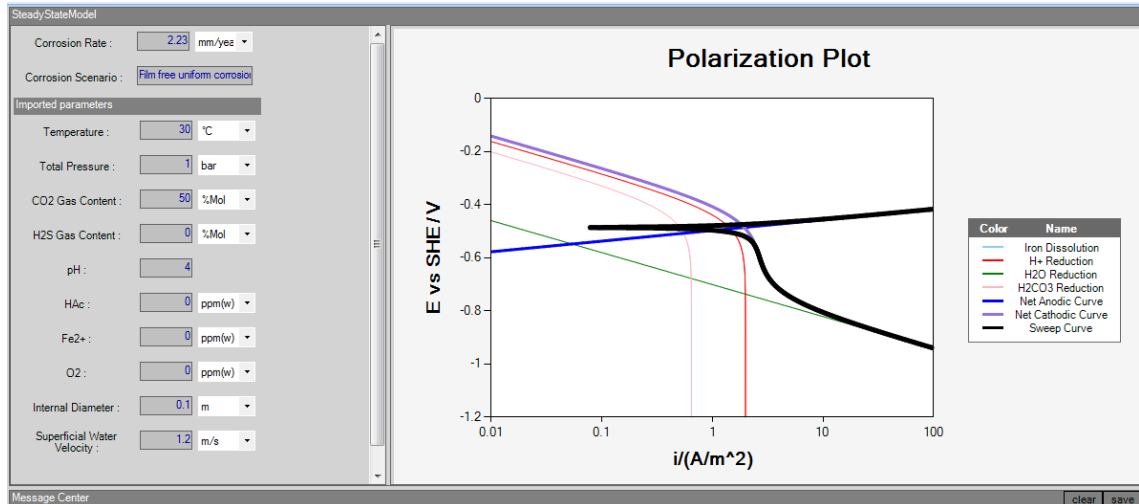


Figure 9. FREECORP™ 2.0 estimating uniform corrosion rates for a set of inputs. Accompanying potentiodynamic sweeps are provided for the predicted results demonstrating the overall, and individual electrochemical reactions.

Upon completion of Task #2, relevant thermodynamic and kinetic parameters will be identified in order to update the code of FREECORP™ to account for the presence of MEG.

CHAPTER 4 METHODOLOGY

The first section presents the methodology used for the execution of all experiments. Then, the subsequent section outlines the procedure used to obtain all of the experimental results, since they were obtained using a unique set of experimental methods and setups.

4.1 Calibration Procedure Required for MEG+Water Solutions

This section discusses the calibration procedure that was used to adjust the pH of the solution, and to measure the accurate value of the H^+ proton activity in the presence of MEG.

Modeling the non-ideal behavior exhibited by the mixture of water and MEG is a complex procedure. Similarly, measuring the true solution pH for MEG+Water mixtures during experimental studies is not as trivial as in pure water systems. Using the readings of a standard pH probe will lead to a deviation from the true activity of the protons^{26,49}. Sandengen et al.⁴⁹ proposed a calibration procedure that enables the determination of pH in MEG/water systems, and accounts for any deviations that may occur during experimental execution in the presence of MEG. The pH meter used throughout this work was an ACORN Series pH 6 meter, and probe by Oaklon Instruments. 500 grams of potassium hydrogen phthalate (KHP) with 99.99% purity was purchased from Fisher Scientific for use during the preliminary calibration procedure.

For the experimental temperature of 30°C (same was done at 60°C and 80°C):

1. The pH probe is calibrated in standard 4.00 and 7.00 buffer solutions

2. A 0.05m KHP buffer solution is created to measure the effect of increasing MEG content on MEG+Water solutions. This pH value is denoted as “ pH_{buffer} ”.
3. Using an empirical formula proposed by Sandengen, et al,⁴⁹ theoretical changes in solution pH from increasing MEG wt. % in solution are calculated. This theoretical change is denoted as “ pH_{RVS} ” and is calculated using Equation (41):

$$pH_{RVS} = 4.00249 + 1.0907w_{MEG} + 0.9679w_{MEG}^2 + 0.3430z + 0.03166w_{MEG}z - 0.8978w_{MEG}^2 z + 7.7821 \left\{ \ln \left(\frac{T}{\theta} \right) - z \right\} + 9.8795w_{MEG}^3 \left\{ \ln \left(\frac{T}{\theta} \right) - z \right\} \quad (41)$$

where $\theta = 298.15$ K; $z = \frac{(T-\theta)}{T}$; $w_{MEG} = \text{MEG wt. \%}$

4. The theoretical and experimental changes from increasing MEG (wt. %) content in solution are then combined, and denoted as “ ΔpH_{MEG} ” in Equation (42):

$$\Delta pH_{MEG} = pH_{RVS} - pH_{buffer} \quad (42)$$

5. Lastly, the true pH of solution (proton activity) can be calculated by adding the pH measurement during the CO₂-MEG-H₂O experiment, denoted as “ $pH_{measured}$ ”, to the empirically determined MEG changes, denoted as “ ΔpH_{MEG} ”, as shown in Equation (43):

$$pH_{true} = pH_{measured} + \Delta pH_{MEG} \quad (43)$$

Table 2 shows the adjusted values seen from increasing concentrations of MEG in solution. Although these could be considered minor changes, such deviations are crucial to accurately model the solution chemistry.

Table 2. Measured pH required for a targeted proton activity (pH_{true}) of 4.00 in solution containing MEG at 30°C.

MEG [wt. %]	pH_{rvs}	$\text{pH}_{\text{buffer}}$	$\Delta\text{pH}_{\text{MEG}}$	$\text{pH}_{\text{measured}}$
0	4.01	4.01	0.00	4.00
10	4.13	4.01	0.03	3.99
20	4.27	4.19	0.08	3.96
30	4.42	4.32	0.10	3.94
40	4.60	4.45	0.15	3.91
50	4.79	4.61	0.18	3.82
60	5.01	4.78	0.23	3.72
70	5.24	4.91	0.33	3.66
80	5.49	5.07	0.42	3.58
90	5.76	5.23	0.54	3.46

4.2 Experimental Procedure

Ethylene Glycol was purchased from ACROS Organics a subsidiary of Fisher Scientific and used for analysis with a purity of 99.95%. This glycol was also used during the calibration procedure described in the previous section. Sodium chloride was obtained from Fisher Scientific with a purity range of 99-100%. A 5 stage EVOQUA filtering system provided deionized water during experimental trials. Carbon dioxide with purity range of 99.9 – 99.9995% was purchased from Airgas® with an oxygen content less than 20 ppb.

A 2L glass cell was used to hold the prepared solution and to perform the corrosion experiments. A solution of MEG and water by volume was prepared for each desired MEG content. 1wt. % NaCl was measured and added to this solution. The temperature of the system was controlled using an isolated jacket, and set to the desired value using a Fisher Scientific Isotemp® hot plate and stirrer device. After adjusting the temperature, a magnetic stir bar was inserted in the cell, and was set to 400RPM to aid in the mixing of

the electrolyte with the solution for the first 30 minutes. After assuring that no air was coming into the cell, either CO₂ or N₂ was bubbled into the cell and the system was purged for at least 2 hours. The addition of CO₂ or N₂ helped in the purging of oxygen in the system, and allowed for the system to be equilibrated and prepared for electrochemical analysis. The pH of the solution was then recorded, and adjusted with 0.1M HCl or with 0.1M NaHCO₃ solutions depending on the desired value from Table 2. After reaching the targeted pH value, the sample was prepared to be mounted on the rotating shaft. Physical measurements of the sample were taken to calculate the exposed area in solution. Then, the X65 sample was polished with silicon carbide (SiC) paper grits 150, 400 and 600 subsequently. Water was used as a lubricant for 150 and 400 grits, and for the 600 grit paper, and isopropyl alcohol was used instead to complete the polishing of the sample. The sample was then ultrasonically dried for 1 minute, and then dried with hot air for half a minute. The sample was then carefully mounted onto the rotating shaft - avoiding any contact with the prepared sample - and immediately inserted into the glass cell. RCE rotations of 1000, 2000, and 100RPM were used sequentially to test the effect of various flowing conditions in the presence of MEG.

4.3 Analytical Apparatus and Procedure

After verification of positive pressure in the system, a Gamry Reference 600 Potentiostat/Galvanostat/ZRA was connected to the set-up and used for electrochemical measurements. In order to accomplish the presented objectives, LPR, EIS and potentiodynamic sweeps were taken in order for each RCE rotation speed. LPR measurements were completed by polarizing the working electrode with ± 5 mV versus the

open circuit potential, E_{oc} at a scan rate of 0.125 mV/s. By collecting the measured polarization resistance, R_p Equation (22) was then used to obtain the equivalent i_{corr} to calculate the corrosion rate for a given rotation and MEG content. For solutions saturated with CO_2 , the Tafel slopes used for the calculation of the B-value were 120mV for the anodic and cathodic reactions. For solutions without CO_2 , the Tafel slopes changed to 120mV for the cathodic reaction, and 40mV for the anodic reaction. These values are purely experimental and have been identified as the base for calculation of the corrosion rate in experiments with CO_2 and N_2 .²¹ Calculation of the corrosion rate was done by using a modified version of Equation (22) in order to obtain mm/y units, as shown by Equation (44) below:

$$CR = 3272 * \frac{i_{corr} * (MW)}{\rho * A} \quad (44)$$

where A is the area of the exposed surface of the working electrode in solution in [cm^2], ρ in [g/cm^3] and MW in [g/mol] are the density and the molecular weight of the working electrode, respectively. i_{corr} [A] is the corrosion current obtained from the polarization resistance. The electrochemical impedance spectroscopy, EIS, was done at an initial and final frequency of 5000 to 0.5 Hz, respectively for a signal amplitude of ± 5 mV. This measurement was done in order to capture the solution resistance in the presence of MEG. Figure 10 demonstrates the results obtained by using EIS in the presence of glycol concentrations proposed.

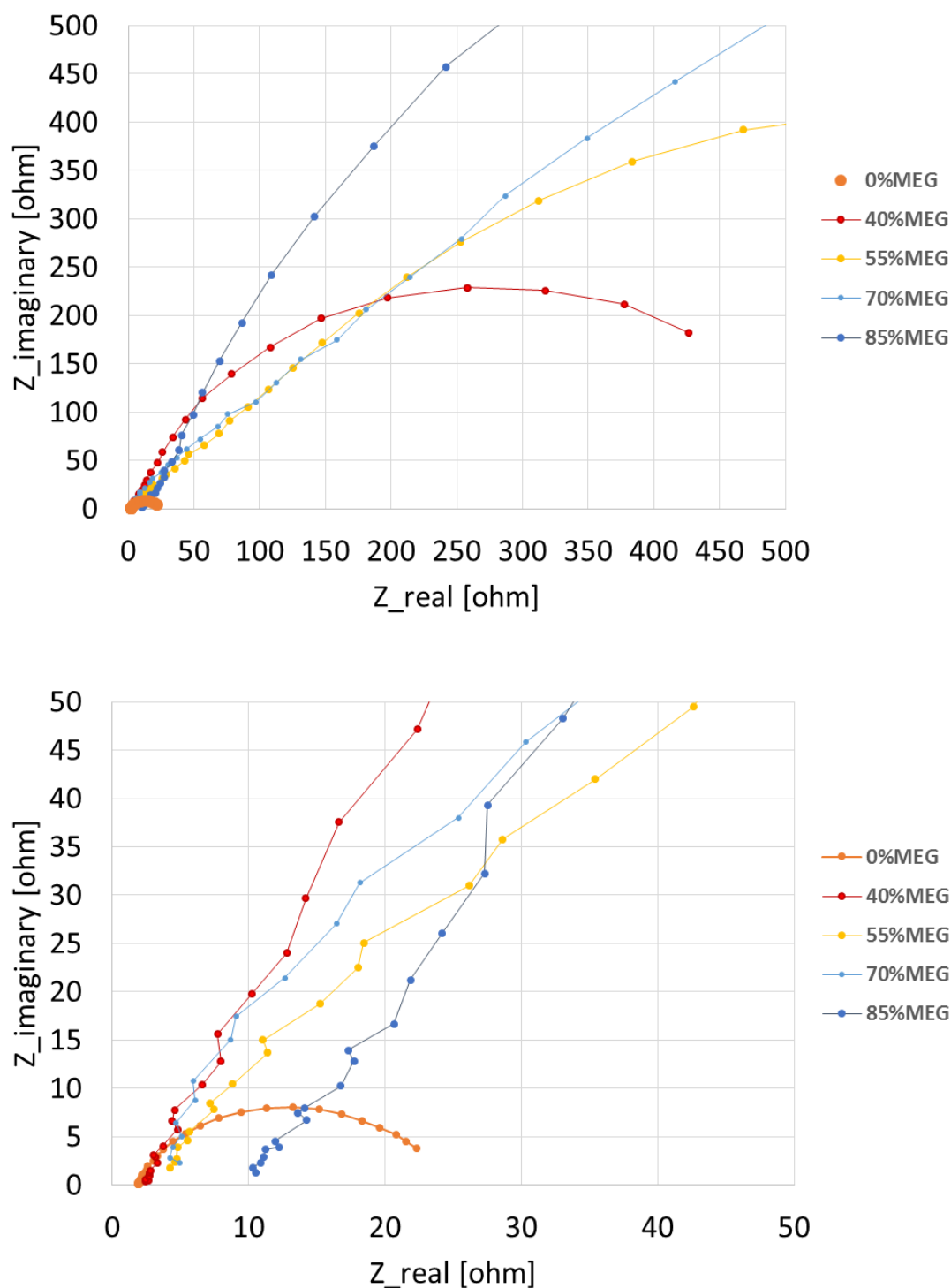


Figure 10. Top Nyquist plot shows the effect of 0, 40, 55, 70, 85vol. % MEG in solution resistance at 30°C, pH~4.00 and 100RPM. Bottom plot shows a close-up version.

As can be seen from the Nyquist plot above, the solution resistance - which is measured by obtaining the lowest value of the real impedance, Z_{real} - gathered for each MEG concentration falls mostly within the single digit range, which demonstrates that no major changes in solution resistance are obtained in the presence of MEG. The cathodic potentiodynamic sweeps were done first for each rotation speed at a scan rate of 0.125mV/s for -0.6V versus the open circuit potential. After completion of each cathodic sweep, the new rotation was adjusted and the system was allowed to equilibrate for at least 30 minutes. Lastly, two anodic potentiodynamic sweeps were completed at a scan rate of 0.125mV/s for a 0.02V applied voltage versus the open circuit potential for the 100 and 2000 rotational speed. The last anodic polarization curve was completed for the 1000RPM speed and done for an overpotential of 0.1V versus the open circuit potential, at the same scanning rate of 0.125mV/s. The above experimental procedure was conducted over approximately 10 hours depending on stabilization time for each open circuit potential.

Figure 11 presents an example of how the current densities measurements are translated into total polarization curves. It also presents a useful explanation on how the total current density curves are built.

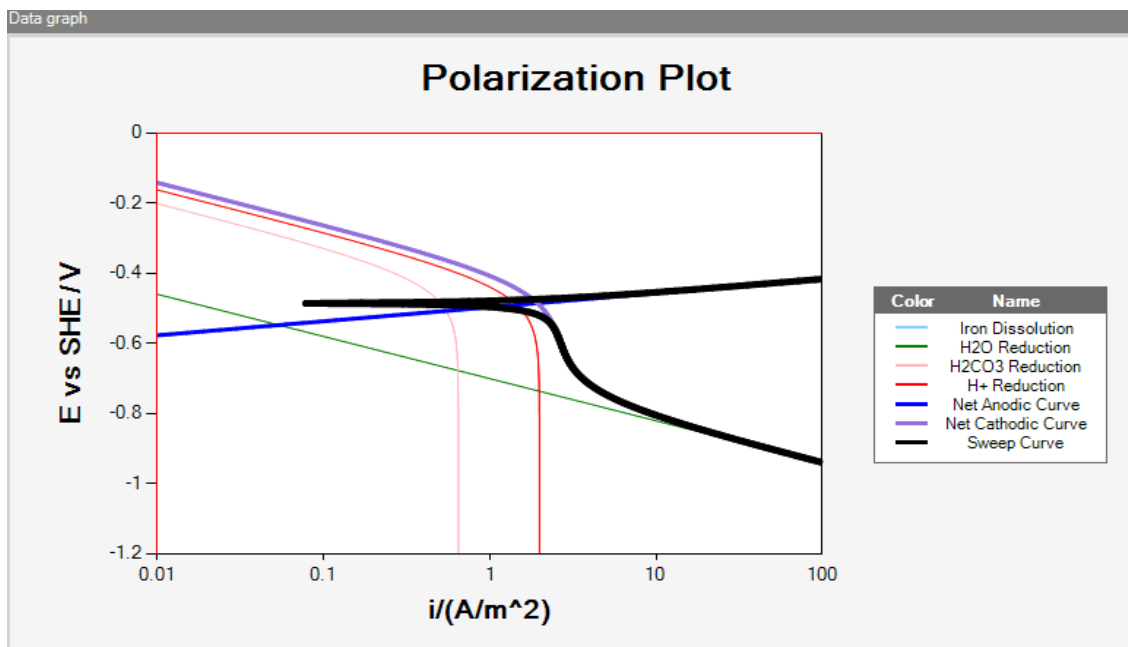


Figure 11. Polarization curve using FREECORP™ for a CO₂ saturated solution with an electrolyte content of 1 wt. % NaCl, at 30°C, water velocity of 1.2m/s ($V_{RCE} = 1000\text{RPM}$) and pH of 4.00.

It is important to highlight how polarization curves are modeled as more emphasis will be given to each section in the upcoming chapters.

From the cathodic section, four curves are plotted in the diagram: the water reduction (green), the H⁺ reduction (red), the H₂CO₃ reduction (pink) and the net cathodic current (purple). The H⁺ and H₂CO₃ reduction lines display a limiting current portion, due to mass transfer and chemical reaction limitations, respectively. The net cathodic curve is obtained by adding all cathodic reactions together.

For the anodic section, the only reaction to be considered in the iron dissolution. The oxidation of iron (light blue) and the net anodic curve (blue) are the same curve and consequently overlap on the graph. The net anodic and net cathodic curves intersect at the corrosion potential, E_{corr} and the corrosion current i_{corr} , which is in turn used to calculate

the corrosion rate. Experimental values of the corrosion rate obtained via LPR measurements are usually compared to their polarization curves counterpart to validate the results. Finally, the potentiodynamic sweep (black) is the compilation of the net anodic and cathodic curves and can be generally compared to experimental results.

4.4 Experimental Setup

Figure 12 illustrates the configuration used to execute each experimental trial.

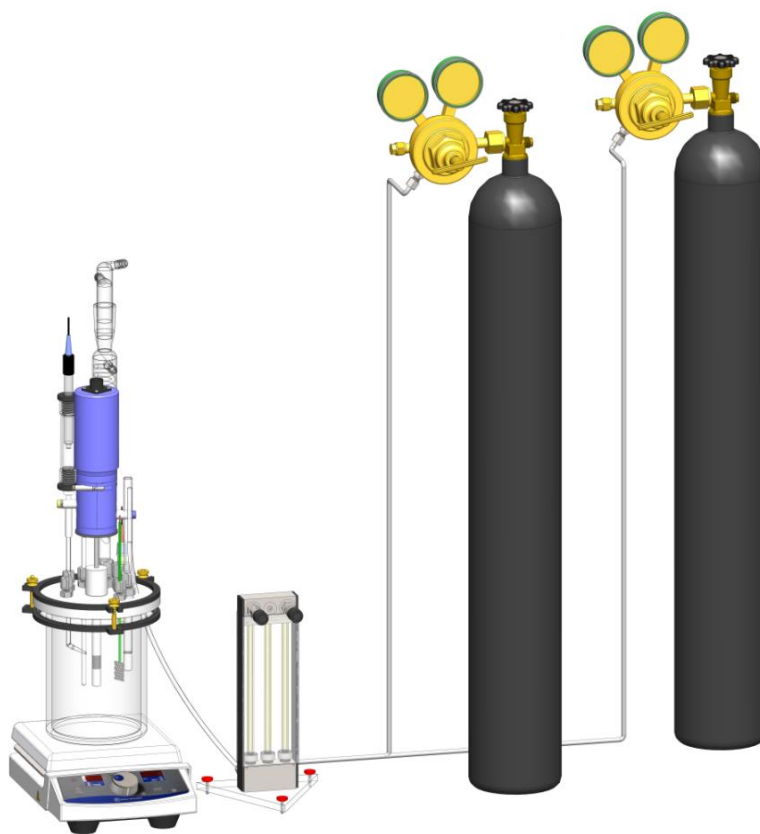


Figure 12. Three electrode rotating cylinder electrode (RCE) setup, consisting of a working, a counter and a reference electrode inserted in a 2L glass cell, on top of a hot plate. Setup is connected to a rotameter used to control the gas flowrate into the system. (Image courtesy of Cody Shafer, ICMT)

A 2L glass cell comprised of a three-electrode set-up defined as: a platinum covered mesh, which acted as the counter electrode, the cylinder electrode mounted on a rotating shaft, which acted as the working electrode, and a saturated silver silver-chloride (Ag | AgCl), which acted as the reference electrode. A porous luggin capillary was used to transfer concentrated potassium chloride (KCl) solution, maintaining electrical contact with the reference electrode. A thermocouple was used to help control the desired temperature of solution, and the pH meter was inserted to measure the chemistry of the mixture at equilibrium. CO₂ in conjunction with N₂ gas was bubbled into the cell via polytetrafluoroethylene (PTFE) tubes in order to establish the desired partial pressure of the acid gas discussed in the next section.

4.5 Test Matrix and Experimental Conditions

The following test matrix was developed for the parametric study. It is geared towards MEG injection and regeneration conditions common subsea exploration and processing units in the oil and gas industry.

Table 3. Proposed test matrix used to complete the objectives and validate the hypotheses. The x marks in the highlighted cells represent the experimental tests to be completed at different alkalinity levels.

MEG [vol. %]	T [°C]		
	30	60	80
40	x		
55	x		
70	x	x	x
85	x		

Upon injection in the wellhead, MEG is considered lean MEG due to the cleanness of the chemical with a concentration of about 90wt. %. Once mixing with water and other components in the hydrocarbon extraction process has occurred, the concentration MEG drops rapidly and can reach about 40wt. % by the end of the flow line where it is considered rich MEG, due to the rich water/hydrocarbon component. Therefore, the proposed concentration of MEG, highlighted in Table 3, ranges between 40 and 85vol. % (42 and 85.4wt. %, respectively). Furthermore, the temperatures encountered during the injection and regeneration process are close to those resembling subsea temperatures as well those in the regeneration process units. This range of temperatures can be quantified between 0 and 90°C. Performing the investigation at temperature below 30°C is not relevant as corrosion rates, even in the absence of MEG, should be already very low. Experiments were performed at a fixed CO₂ partial pressure of 0.5bar, for all sweet corrosion tests. Table 4 shows all of the conditions that were tested in this study.

Table 4. Experimental parameters used for preliminary electrochemical results for solutions purged with N₂ and CO₂ gas, respectively.

<i>Parameters</i>	<i>Conditions</i>
Material	X65 (0.16wt. % C)
pH	4.00, 5.00, 6.00 ± 0.05
Partial pressure of CO₂ [bar]	0.5 ± 0.05*
Total Pressure [bar]	1
RCE Flow [RPM]	100, 1000, 2000
Temperature [°C]	30, 60, 80
MEG Content in Solution [vol. %]	0, 40, 55, 70, 85
NaCl Content in Solution [wt. %]	1
<i>Electrochemical Measurements</i>	
LPR	± 5mV Polarization Scan Rate: 0.125 mV/s
EIS	5000 – 0.5Hz
Potentiodynamic Sweeps	Scan Rate: 0.125 mV/s
-Cathodic	E_{oc} to $E_{oc} - 0.6V$
-Anodic	E_{oc} to $E_{oc} + 0.1V$

*Some experiments were completed in N₂ only environments.

As specified in Table 4, the tested velocities are given in RPM as a rotating cylinder electrode was used. These RPM values are only relevant to the specific setup used in this study, but a conversion can be done to determine the equivalent fluid velocity in a 4" ID pipe in single phase flow, considering the same mass transfer coefficient as shown in Table 5. A more in-depth representation of the calculation for the equivalent fluid velocities is explained in the modeling approach section Chapter 6, and only the main results are shown here.

Table 5. Equivalent water velocities in a single-phase pipeline using Silverman's mass transfer correlation for rotating cylinders.⁵⁴

RCE Velocity [RPM]	Water Velocity in 4in Pipeline [m/s]
100	0.2
1000	1.2
2000	2.0

Furthermore, an error in the calculation for the preliminary pH calibration provided in the methodology section was noticed and this changed the true activity measured during the solution. This error was found after the experimental trials had been completed, which resulted in a tested pH range different from the one initially planned. Instead of alkalinities of 4, 5 and 6 in the presence of MEG, the pH ranged from 3.5 – 5.9. Similar to Table 2, additional results can be found in APPENDIX C CHANGES IN SOLUTION PH DUE TO INCREASING MEG CONTENT AT 30°C at different pH ranges. This does not invalidate any of the findings, but renders the plotting of the results cumbersome as pH values slightly differ from the targeted pH. Following this explanation, the next chapter highlights the obtained experimental results.

CHAPTER 5 RESULTS

This section highlights the execution and completion of the tasks presented in the objectives section. A comprehensive review of the effect of each controlling parameter (pH, Temperature, MEG content, flow) is first presented before exploring the experimental results in more depth in a subsequent section. The experimental results are displayed in form of potentiodynamic sweeps; the cathodic sweeps present an average of three trials while the anodic sweeps were not repeated. The error bars illustrate minimum and maximum current densities obtained for a given potential. An effort is made to compare the results obtained in the presence of MEG with MEG-free data in equivalent environments. FREECORP™ simulation results are used when experimental data are not available. Finally, a summary of the findings is given at the end of this chapter.

5.1 Effect of Flow in the Presence of MEG

As presented in the literature review section, changes in flow can alter the expected corrosion rate in a system. The flow effect and its contribution to the overall cathodic current is shown through changes in limiting current, i_{lim} for the H^+ reduction and, to a much lesser degree, for the H_2CO_3 reduction, which involve the mass transfer coefficients in solution, k_m . This mass transfer coefficient is related to the Sherwood correlation used for the RCE set-up, which in turn dependent on the fluid properties. In order to illustrate the major changes expected with alterations in flow, FREECORP™ simulation results are shown in conjunction with the experimental results to reflect the effect of flow on the corrosion rate in the presence and absence of MEG (Figure 13). As mentioned before, FREECORP™ uses an electrochemical and mechanistic approach to predict the behavior

of electrochemical reactions involved in corrosion processes for strong and weak acids. A uniform corrosion rate estimate can be obtained in conjunction with a description of how every anodic and cathodic reaction responds. As expected, flow effects on corrosion rate are strong at low pH, where the rate limiting step is often the transport of protons, while they are relatively weak (with regards to corrosion rate values) at higher pH in sweet environments, where the main cathodic reaction is the H_2CO_3 reduction, which limiting current is controlled by the rate of the CO_2 hydration reaction, which is not flow dependent.

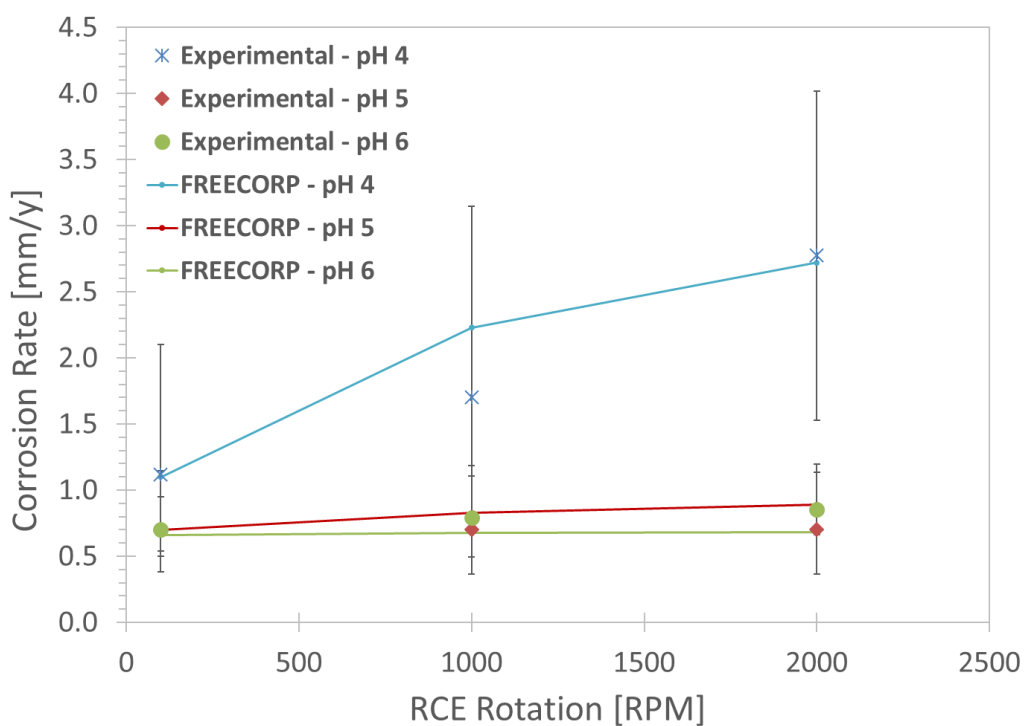


Figure 13. Comparison between experimental LPR results (dotted points) and FREECORP™'s predictions (solid continuous lines) of corrosion rates obtained at 30°C for 100, 1000 and 2000RPM, at pH 4.00, 5.00 and 6.00, respectively, for a solution saturated with 0.5bar CO_2 , and 1wt. % NaCl, 0% MEG.

It can be seen that in the presence of CO_2 , major changes in corrosion rate occur for solutions with pH of 4.00. Also, the comparison in LPR values obtained experimentally and those with the electrochemical model are well in accordance. A more in-depth explanation of this phenomenon is provided in the next section.

Using FREECORP™, three polarization curves are displayed for each rotation speed investigated, for a solution saturated with carbon dioxide and nitrogen, respectively. For clarity reasons, only the data obtained at pH 4.00, at 30°C and with either 0 or 70vol.% MEG are shown in this section while more results are presented in APPENDIX G MODEL VALIDATION – EFFECT OF FLOW.

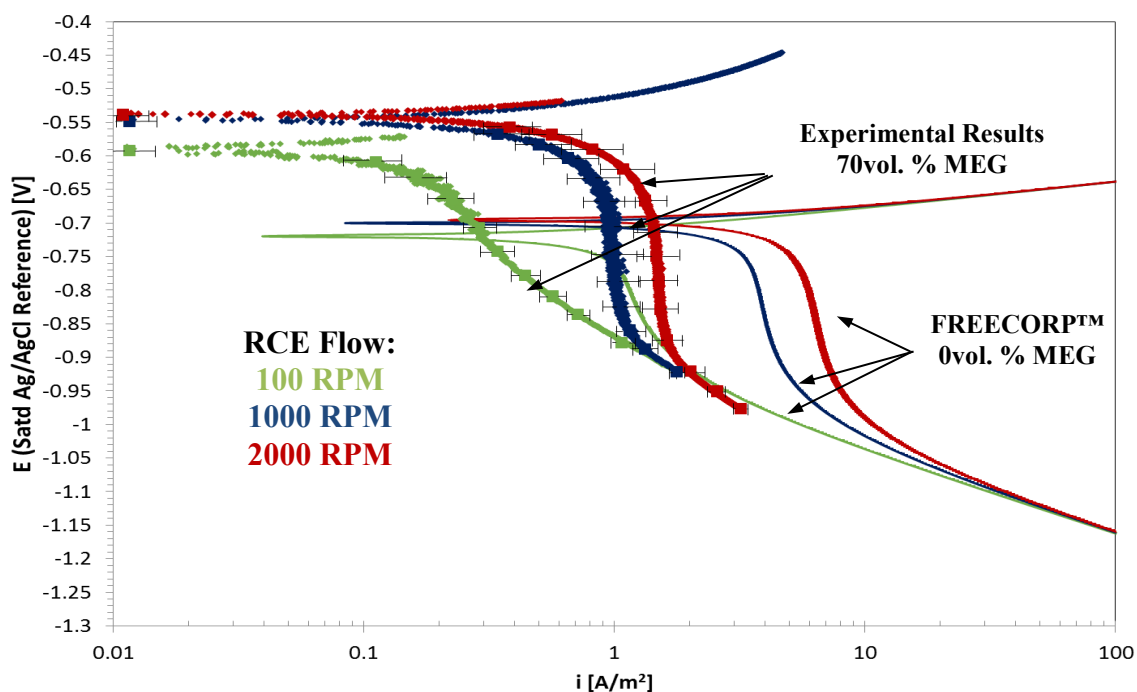


Figure 14. Comparisons between experimental results (70vol. %, pH 3.66) and FREECORP™ predictions (0vol. % MEG, pH 3.66) for solutions purged with 0.5bar CO_2 at 30°C, 1wt. % NaCl.

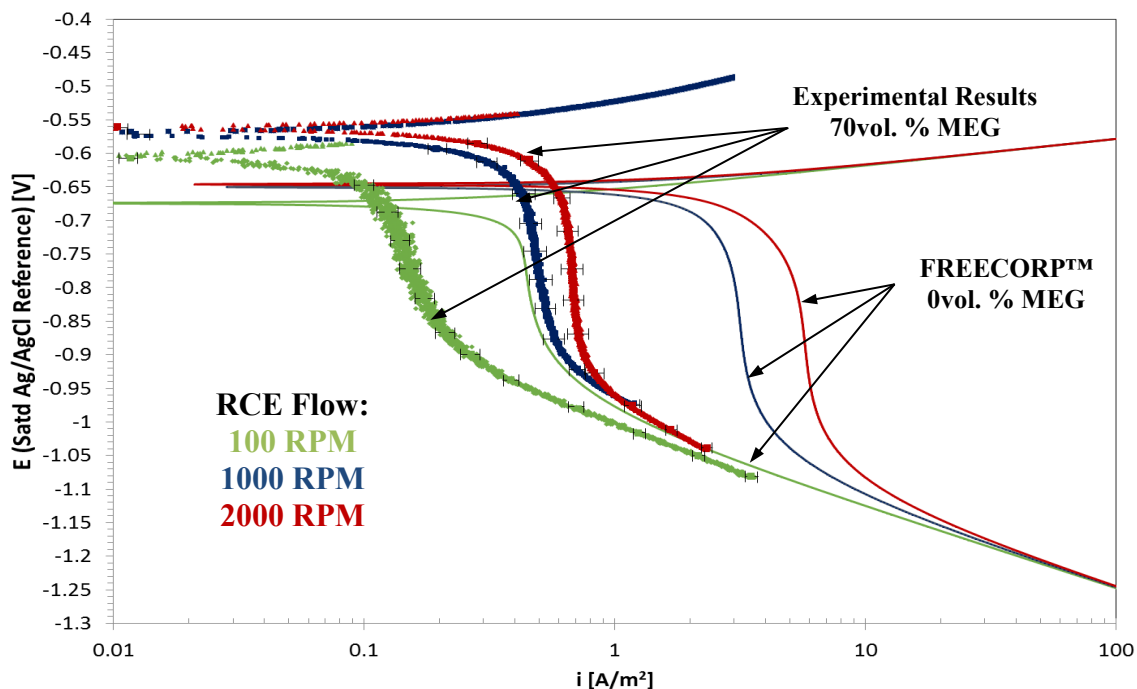


Figure 15. Comparisons between experimental results (70vol. %, pH 3.66) and FREECORP™ predictions (0vol. % MEG, pH 3.66) for solutions purged with ~1bar N₂ at 30°C, and 1wt. % NaCl.

As can be seen Figure 14 and Figure 15, the effect of flow for CO₂ and N₂ saturated solutions for pure water and for solutions with 70vol. % MEG demonstrate that increases in rotation speed generate a bigger cathodic current, which in turn, lead to a higher corrosion rate. At pH 4.00 and with 0.5 bar of CO₂, it is fully expected that the dominant cathodic reaction is H⁺ reduction and that the process is under mass transfer control. When MEG is present, the corrosion rate is decreased, however, it is interesting to observe that this decrease in corrosion rate is not only caused by the clear reduction in the limiting current, but also by the retardation of the anodic reaction, which is given by a more positive open circuit potential. Furthermore, when compared to a MEG free environment, it is also important to note that the same expected flow behavior is obtained even when 70vol. %

MEG is added to the solution. Lastly, the behavior of the water reduction line (linear section of each cathodic line for lower applied potential) is also quite relevant as it appears that neither flow nor the presence of MEG have any effect. While it is known the water reduction does not depend on flow, it is expected from literature data that the addition of MEG in solution should cause a retardation of the water line due to the decreases in water activity.¹³ However, this behavior is not observed at all in this test series as the water reduction line appears independent of MEG content.

In summary, this work demonstrates that, in the presence of MEG, changes in flow follow similar behavior (and trends in corrosion rate) as those in MEG-free solutions. This is an improvement to the current understanding as other researchers have tested the effect of MEG on corrosion mechanisms only for a fixed fluid velocity¹³⁻¹⁷. Additional results demonstrating the effect of flow for various MEG content, and at a different pH are presented in APPENDIX G MODEL VALIDATION – EFFECT OF FLOW. The changes in flow and hence alterations in mass transfer coefficients are less drastic as the alkalinity in solution is increased.

5.2 Effect of Temperature in the Presence of MEG

As with purely chemical reactions, there is a direct relationship between temperature and the rate of reaction. Increases or decreases in temperature will cause an increase or decrease in the rate at which reactions occur in a given system. In this section, in order to avoid a high quantity of data to be clustered in one single Evans diagram, the effect of temperature is shown only at pH 4.00, 1000 RPM, and with either 0 or 70vol.%

MEG. The results for a solution without MEG and saturated with carbon dioxide are shown in Figure 16.

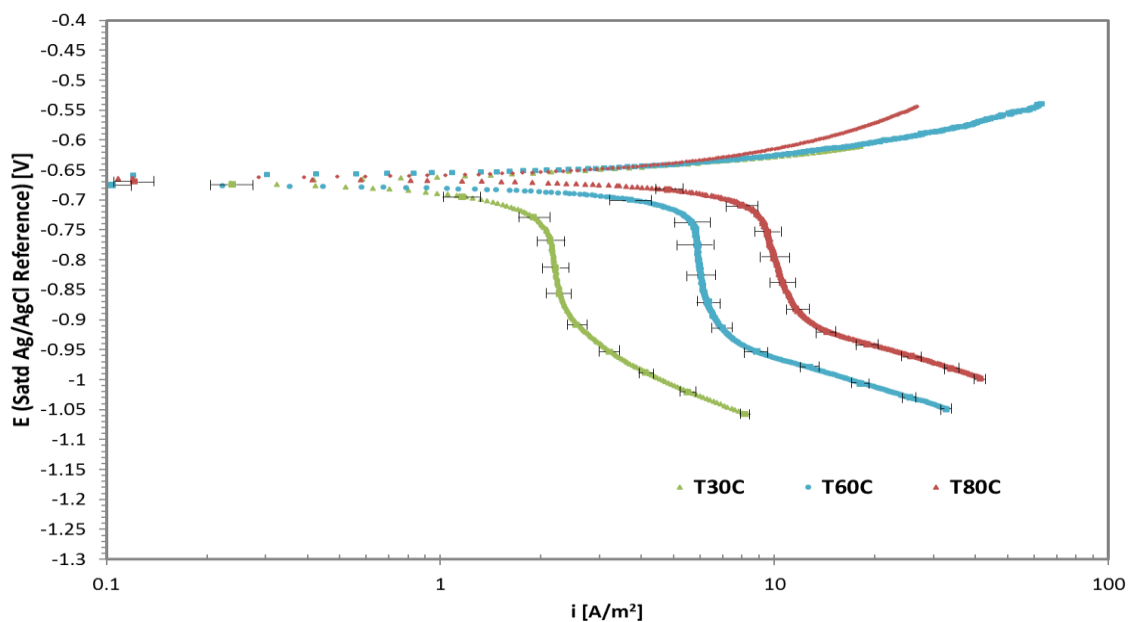


Figure 16. Polarization curves at 1000RPM for solutions at pH 4.00 and 0vol. % MEG purged with 0.5bar CO₂.

The results for a system saturated with nitrogen are shown below in Figure 17.

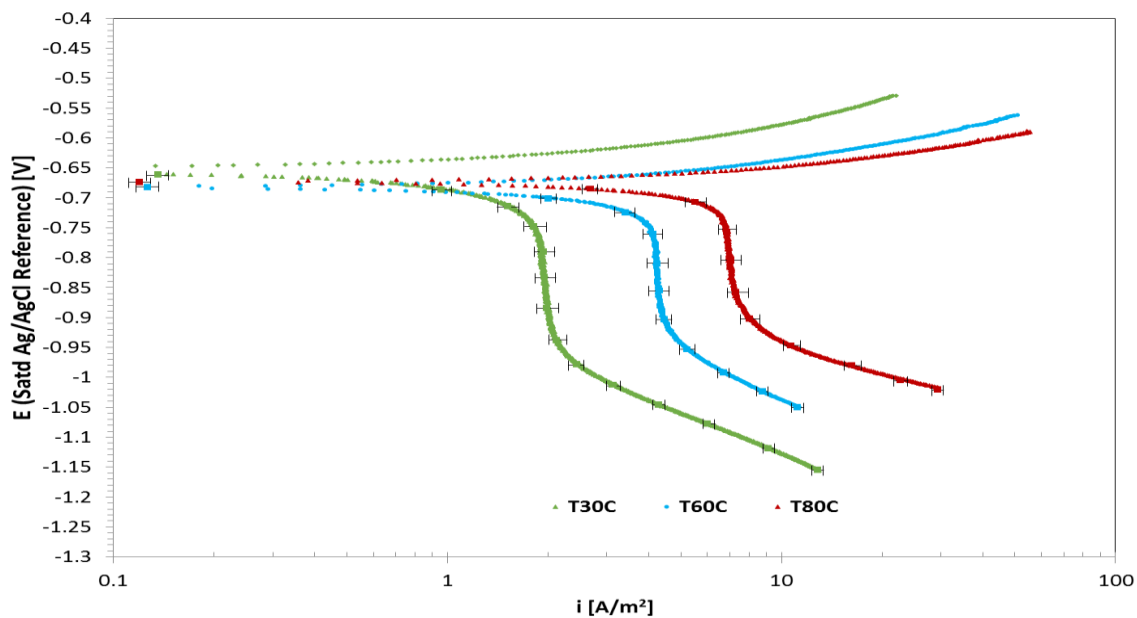


Figure 17. Polarization curves at 1000RPM for solutions at pH 4.00 and 0vol. % MEG purged with ~ 1 bar N_2 .

As it can be seen, the effect of temperature for MEG-free solutions sparged with CO_2 or N_2 showed increases in corrosion rates, which is given by the simultaneous acceleration of both anodic and cathodic reactions. The more drastic effect of temperature can be noted in the cathodic side of the diagram, where regardless of the saturating gas (presence or absence of CO_2), an increase in charge transfer and limiting currents is obtained with increases in temperature. On the other hand, changes on the anodic side are not as dramatic; a positive shift is seen on the anodic reactions for solutions saturated with N_2 , whereas those with CO_2 , this shift is almost negligible. Additionally, the presence of CO_2 in solution logically leads to an increase in the corrosion rate due to the added H_2CO_3 reduction reaction/buffering effect.

Now, Figure 8 presents the experimental results obtained for a CO_2 saturated system and for the same operating conditions but considering 70vol. % MEG in solution.

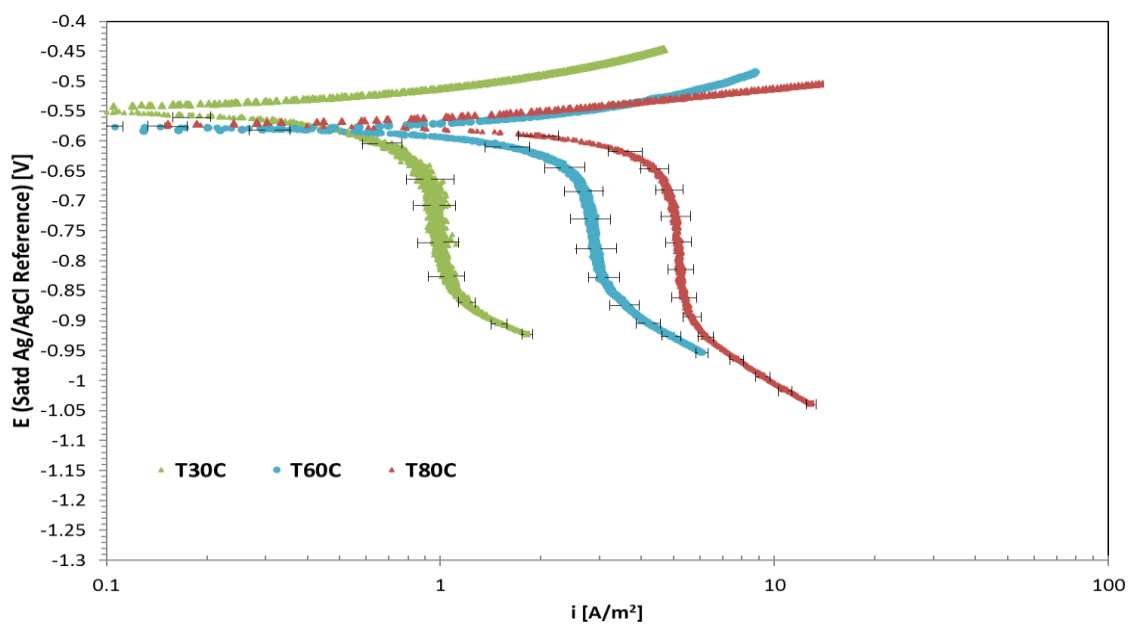


Figure 18. Potentiodynamic curves at 1000RPM for solutions at pH \sim 4.00 with 70vol. % MEG and purged with 0.5bar CO₂ and 1wt. % NaCl.

And the results for a solution sparged with nitrogen are shown in Figure 19 as follows:

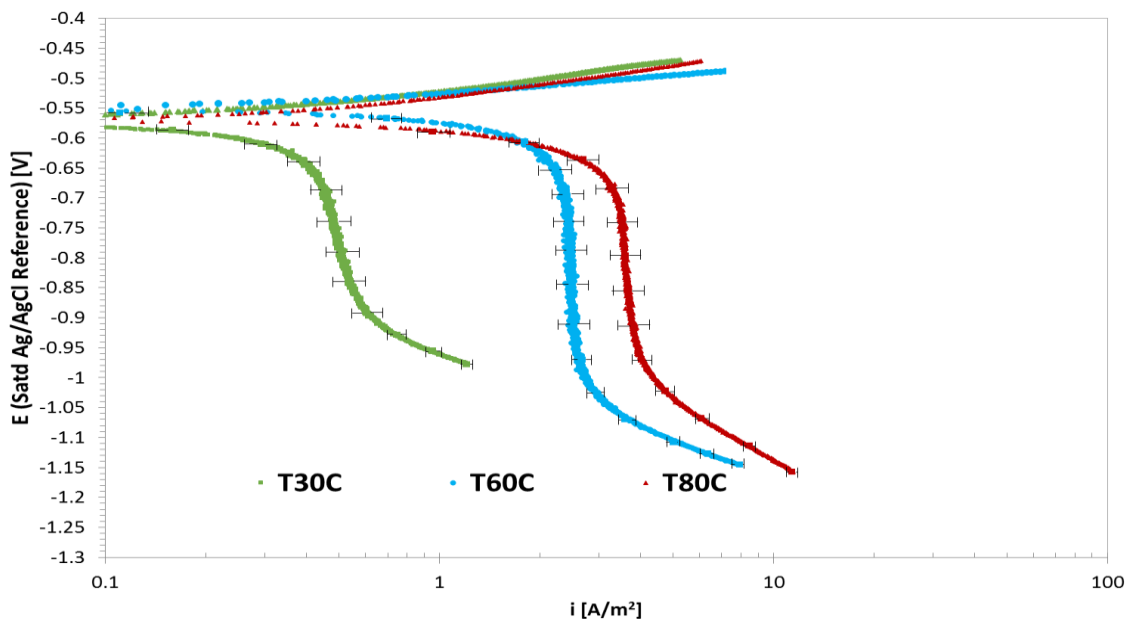


Figure 19. Potentiodynamic curves at 1000RPM for solutions at pH \sim 4.00 with 70vol. % MEG and purged with \sim 1bar N_2 and 1wt. % NaCl.

Figure 18 and Figure 19 show that for a solution containing 70vol. % MEG, an increase in corrosion rate is still obtained with increases in temperature, as it is expected. These rates are naturally lower than those obtained for pure water solutions. Furthermore, the changes in both anodic and cathodic reactions are also seen with increases in temperatures in the presence of MEG, and also show similar behavior to those for pure water solutions. For the net cathodic curve, both an increase in the limiting current and an acceleration of the charge transfer rate are observed, irrespective of the presence or absence of CO_2 . This is explained by the change in kinetic parameters and in species diffusivities and overall mass transfer. For the anodic reaction, however, the changes with alterations in temperature are not as significant as those observed in the cathodic reaction but follow the same trend. Environments with CO_2 always lead to higher corrosion rates than environments without, irrespective of the presence or absence of MEG.

5.3 Effect of pH in the Presence of MEG

Similarly to the previous section, the results comparison is given by showing the experimental results in conjunction with FREECORP™'s prediction. The results in this section are limited to 30°C, 1000 RPM, and with either 0vol. % (FREECORP™) or 70vol. % MEG. The results for a solution saturated with carbon dioxide and with 70vol% MEG are shown below in Figure 20.

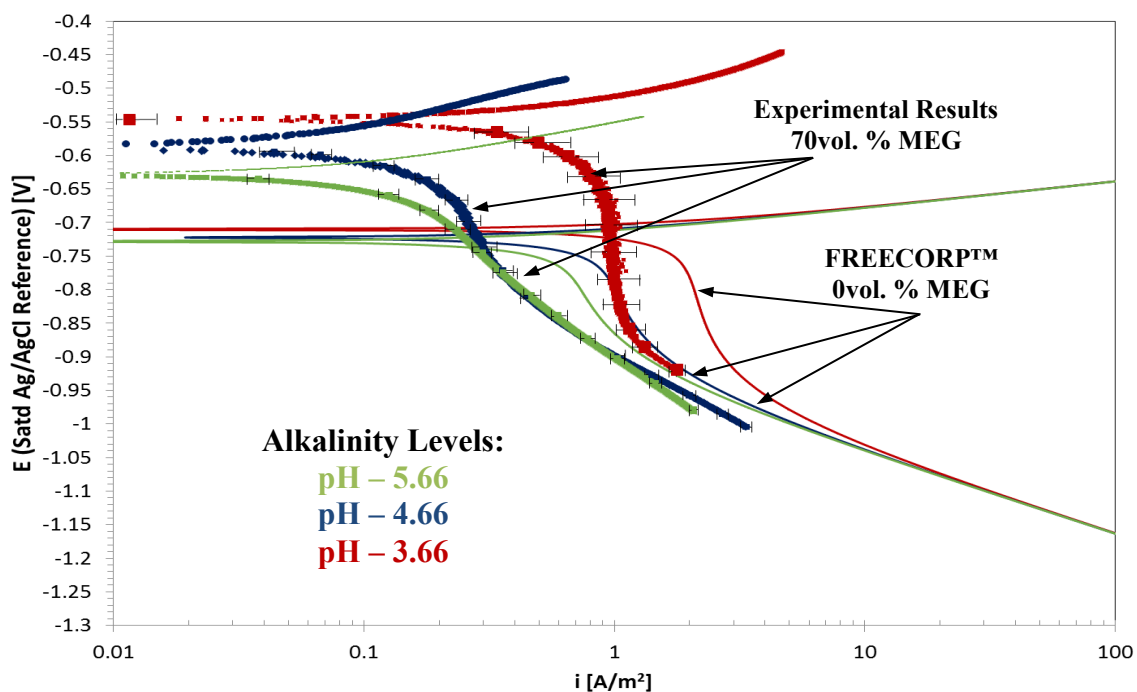


Figure 20. Comparison between experimental results (70vol. % MEG) and FREECORP™'s prediction (0vol. % MEG) for a solution at 30°C, 0.5bar CO₂, 1wt. % NaCl and $V_{RCE} = 1000$ RPM.

And the results obtained with a solution sparged with nitrogen are shown below in Figure 21.

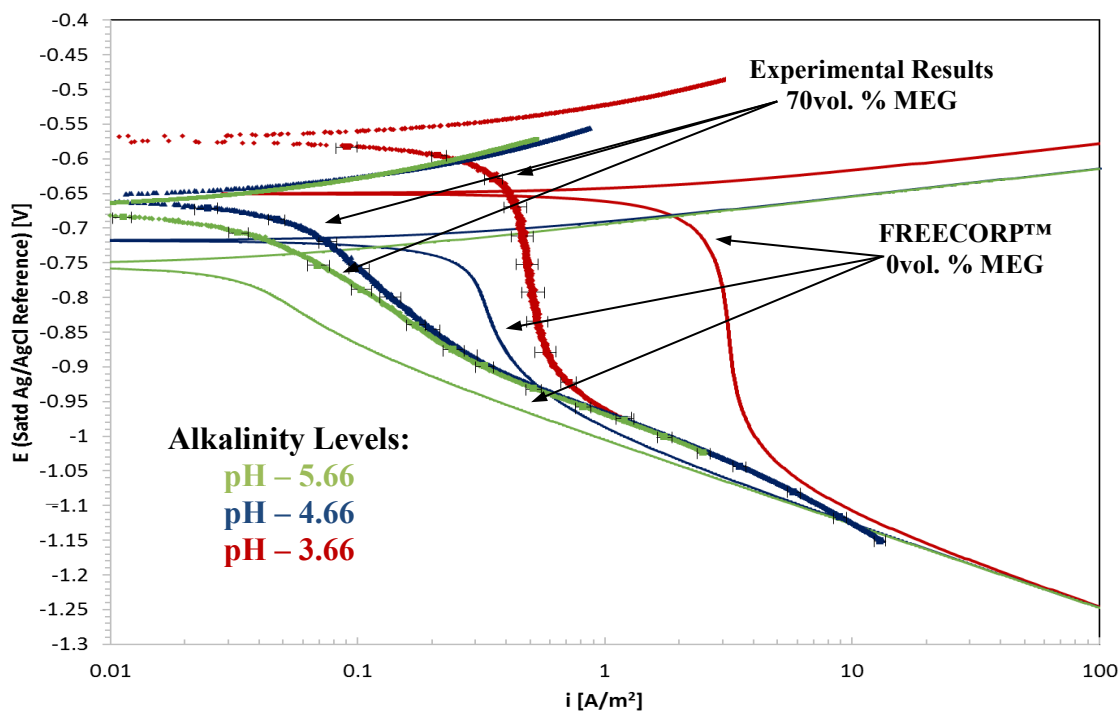


Figure 21. Comparison between experimental results (70vol. % MEG) and FREECORP™'s prediction (0vol. % MEG) for a solution at 30°C, ~1bar N₂, 1wt. % NaCl and V_{RCE} = 1000 RPM.

A few observations can be made from Figure 20 and Figure 21. Typically, as the pH in solution is increased, the corrosion rate decreases. Second, the effect of CO₂ in solution is clearly seen as higher currents are obtained. Additionally, the representation provided by FREECORP™ shows that the limiting current is greater at pH of 4.00 in nitrogen or carbon dioxide environments; this is simply due to the concentration of H⁺ in solution. Moreover, it is important to note that FREECORP™ presents the total limiting current, which combines the $i_{lim_H^+}$ and $i_{lim_H_2CO_3}$. By plotting the expected behavior in corrosion mechanisms at various levels of alkalinity, a distinction between mass transfer control (low pH), and chemical reaction control (high pH) can be seen. This is because for a pH of 6.00 and above, the limiting current is mainly due to the slow chemical reaction of

CO₂ hydration. Adding 70vol. % MEG in the system shows that the effect of pH, in the presence of glycol, resulted in similar trends compared to those observed in water-only solutions. From an anodic point of view, there is a retardation of the anodic reaction due to the presence of MEG regardless of the pH evaluated. This can be noted by the E_{corr} (open circuit potential) obtained with and without MEG. On the cathodic side, a lower limiting current is obtained for a given pH due to the changes in physico-chemical properties of the solution induced by the presence of MEG. Lastly the presence of CO₂ in solution increases the limiting current (and hence corrosion rate) for the same pH compared to those solutions purged with N₂ in the presence of 70vol. % MEG.

5.4 Effect of MEG on CO₂ Corrosion Mechanisms

Up to this point, experimental results were focused on the effects of operating parameters (flow, pH, temperature) on the corrosion behavior of steel in aqueous solutions containing either 0 or 70vol. % MEG.

In this section, the effect of MEG is explored over a wide range of concentrations. The main objective is to investigate how the addition of MEG to a H₂O-CO₂-NaCl system affects the corrosion mechanisms.

The experimental results seen in Figure 22 illustrate the effect of MEG on CO₂ corrosion mechanisms for targeted pH 6.00 and 4.00.

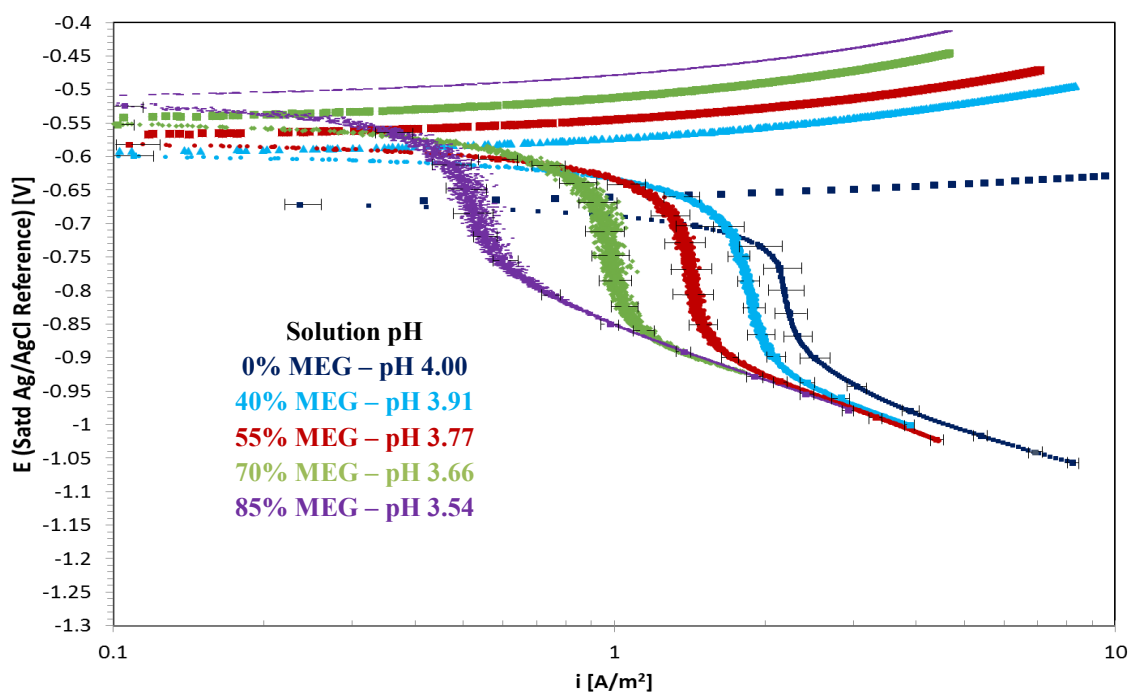
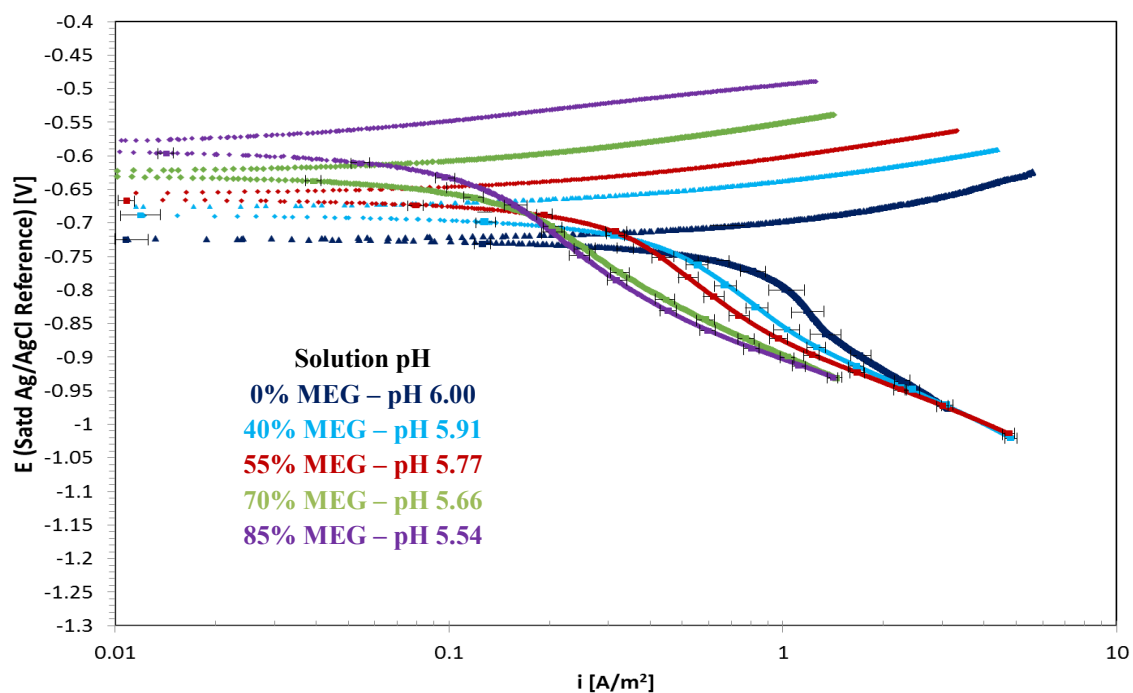


Figure 22. Evans diagram showing the effect of 0, 45, 50, 70 and 85 vol. % MEG in solution for an RCE rotation of 1000 RPM [$V_{eq} = 1.2\text{m/s}$], at 30°C saturated with 0.5bar CO₂ and 1wt. % NaCl at pH ~ 6.00 (top) and pH ~ 4.00 (bottom).

Several very clear and interesting effects occur with the electrochemical reactions with the increase in MEG content in the system. First, there is a retardation of the anodic reaction, which can be seen by the more positive open circuit potential obtained with each concentration of MEG. Additionally, no obvious changes in anodic Tafel slope are observed for each of the anodic sweeps done at 1000RPM. This was one particular finding in literature¹⁵⁻¹⁷ that was validated by studying the effect of increasing MEG concentration in solution. On the cathodic side, there is no visible change with the cathodic Tafel slopes of the H^+ reduction (observed at pH 4.00), the H_2CO_3 (observed at pH 6.00), or the water reduction reactions by adding MEG in solution. The limiting current of the net cathodic curve is also strongly decreased, especially at low pH. Lastly, the reduction of water does not seem to be affected at all by the non-ideal MEG/ H_2O solution. This is somehow unexpected as literature¹³ suggested a possible shift in the reduction of water due to the decrease in water activity from the presence of MEG in solution. However, this result is consistent throughout the entire series of test completed.

5.5 Summary of LPR Data

LPR measurements were also completed co-currently with the potentiodynamic sweeps and the results also validate the decrease in corrosion rate seen with increasing MEG content in solution. As stated earlier, FREECORP™ is currently unable to predict the effect of MEG on the corrosion rate. However, by applying deWaard's glycol factor¹⁸ to FREECORP™ predictions, corrosion rates in the presence of MEG can be calculated. In this section, a parity plot is created comparing the experimental corrosion rates obtained

for each pH with the model predictions provided by FREECORP™ in conjunction with deWaard's glycol factor.

Figure 23 shows the LPR results for a solution at 30°C and pH ~ 4.00.

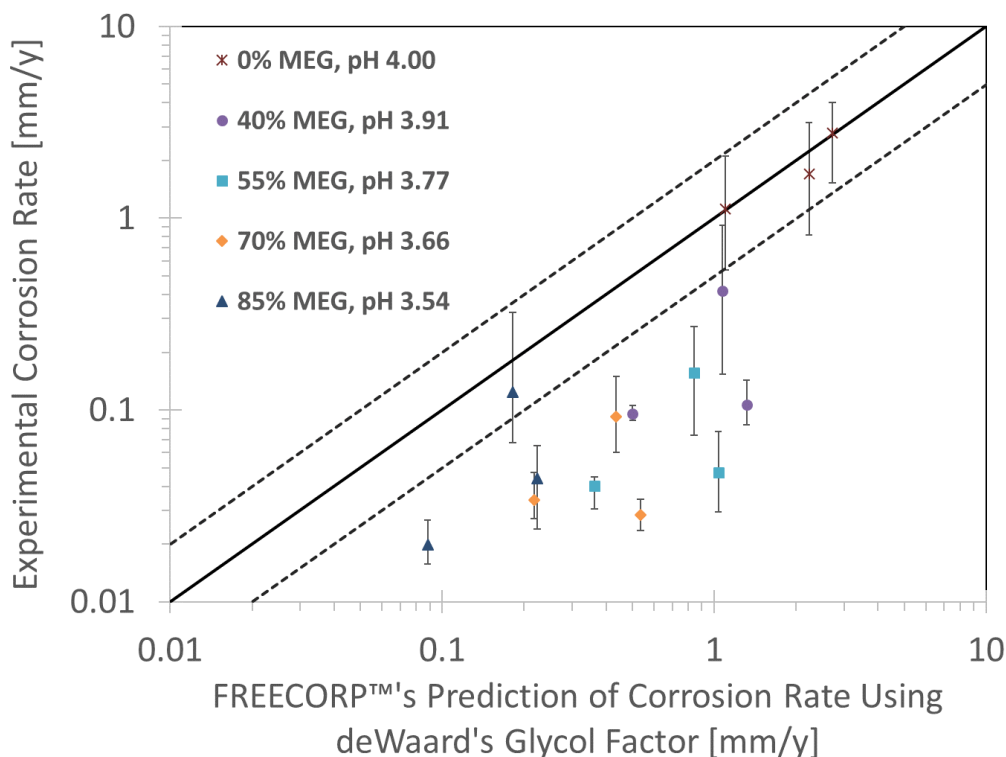


Figure 23. LPR measurements obtained for a solution with 0, 40, 55, 70 and 85vol. % MEG, at 30°C and pH ~ 4.00 purged with 0.5bar CO₂ and 1wt. % NaCl.

A few observations could be made regarding from the results shown in Figure 23. The expected trend in decreases in corrosion rate with increasing glycol content is clearly shown. Three data points are shown for each MEG content and correspond to the three rotation speeds tested: 100, 1000 and 2000 RPM, matching the data points from further left to further right. The error bars reflect the number of repeat experiments, and the dashed lines top and bottom of the graph represent a deviation by a factor of 2. The most important

point is that FREECORP™ predictions associated with deWaard's glycol factor over predict the corrosion rate at 30°C and pH 4.00, for most glycol concentrations. Other authors^{18,16} have shown similar discrepancies between experimental and predicted results for temperatures above 50°C. Some inconsistencies with LPR measurements were also noted with respect to rotation speed, with corrosion rates being unexpectedly lower at 2000 RPM compared to 1000 RPM. This behavior is not reflected in the potentiodynamic sweeps presented in the previous section and is only present in the LPR data. The reason behind this inconsistency is not clear but could be due to the low pH values tested and the uncertainty around the B values. However, this is not believed that these results invalidate the trends observed in Figure 23.

Figure 24 presents the next set of data obtained at pH ~ 5.00 and 30°C.

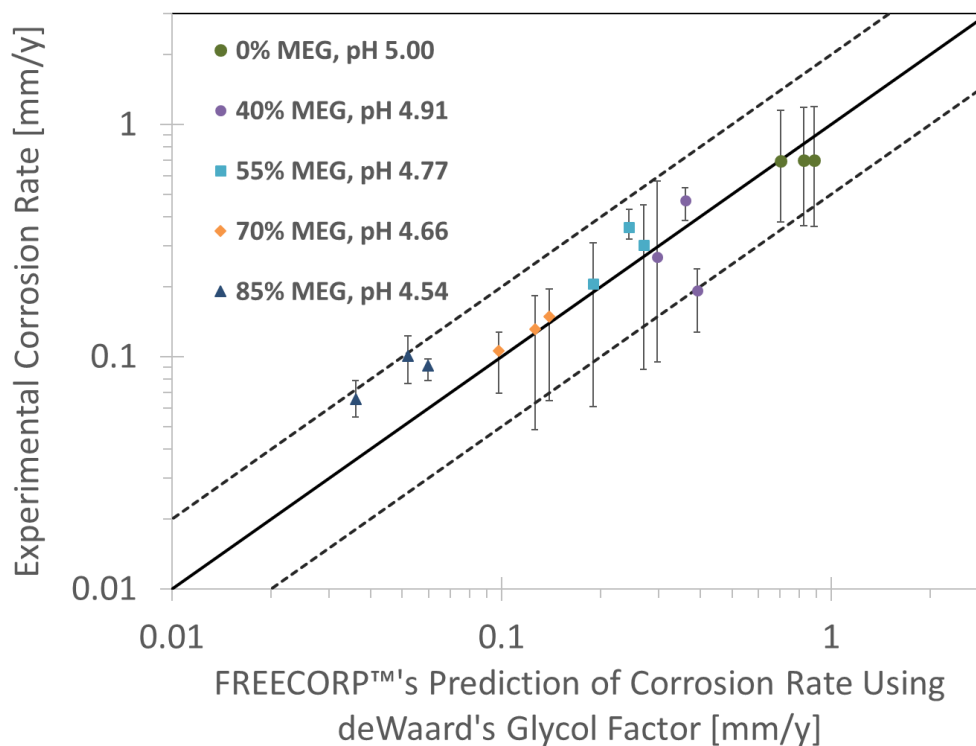


Figure 24. LPR measurements obtained for a solution purged with 0.5bar CO₂ and with 0, 40, 55, 70 and 85vol. % MEG, at 30°C and pH ~ 5.00 and 1wt. % NaCl.

As it can be observed in Figure 24, the parity plot illustrates that the corrosion rates obtained by using deWaard's glycol factor with FREECORP™ results in better agreement for a solution at pH of 5.00 as all the results fall within a factor of 2.

Finally, Figure 25 presents the next set of data obtained at pH ~ 6.00 and 30°C.

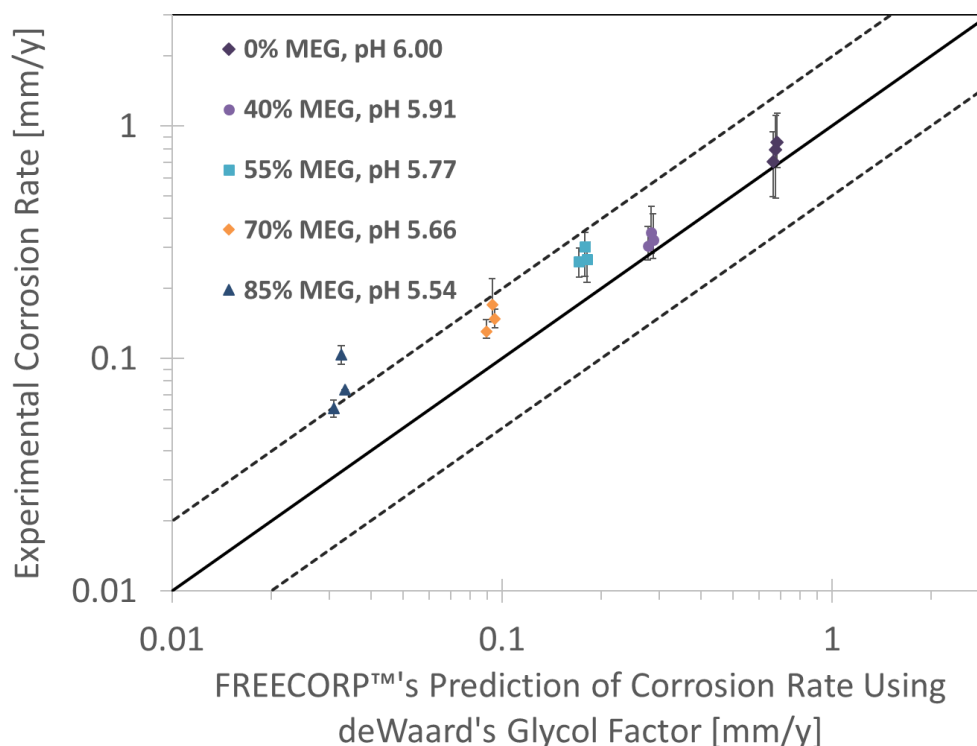


Figure 25. LPR measurements obtained for a solution purged with 0.5bar CO₂ and with 0, 40, 55, 70 and 85vol. % MEG, at 30°C and pH ~ 6.00 and 1wt. % NaCl.

At pH of 6.00, experimental results and model predictions, using deWaard's glycol factor with FREECORP™, are also in good agreement. A decrease in corrosion rate is seen with each given glycol concentration, and for all rotations obtained. Furthermore, the results demonstrate that at high pH and as the glycol content is increased, the predicted data become less and less conservative. For high glycol content and for low solution acidity, the deWaard factor+FREECORP™ predictions tend to under-estimate the corrosion rates.

Lastly, a comparison using this same approach for a fixed ethylene glycol content at various temperatures is shown in Figure 26.

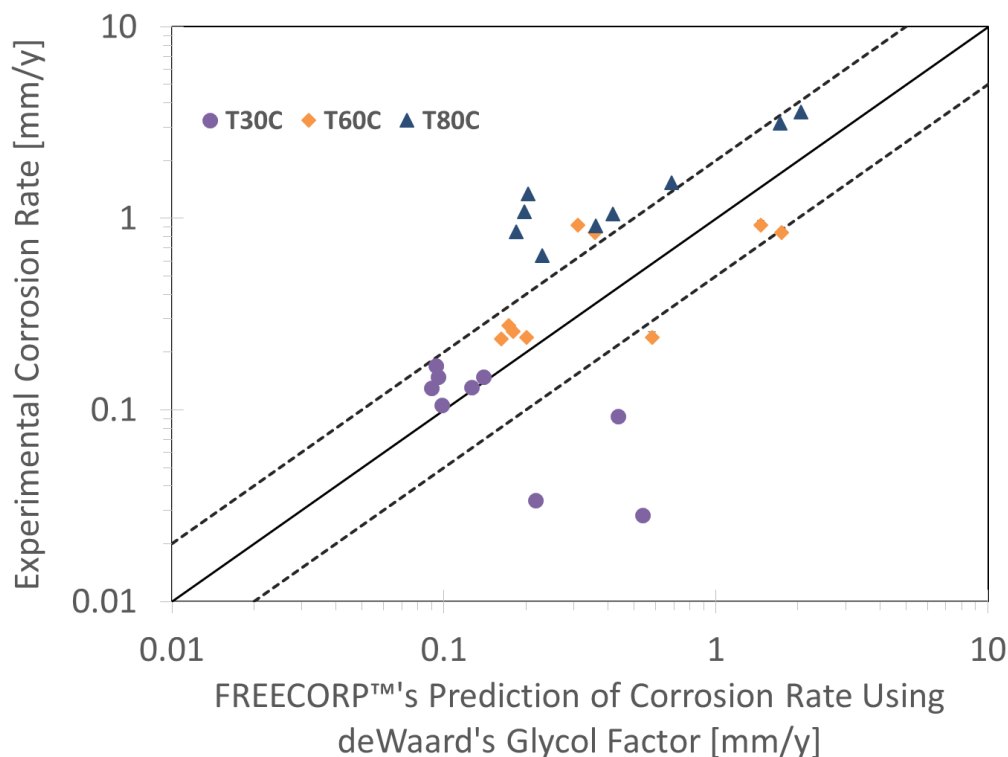


Figure 26. LPR data for 30, 60 and 80°C, at pH ~ 4.00 for a solution containing 70vol. % MEG saturated with 0.5bar CO₂, and 1wt. % NaCl.

The data points displayed for each temperature were obtained at different pH's and rotation speeds. Figure 26 also includes data obtained at 30°C, which have already been presented in Figure 23 – the under prediction of the corrosion rate noticed at pH ~ 4.00 stands out. While the experimental results and the model predictions seem to be in relatively good agreement at 60°C, the corrosion rate is clearly underestimated at 80°C. A complete database of all the data points obtained via LPR measurements for all conditions are provided in the Experimental LPR Data section in APPENDIX E EXPERIMENTAL LPR DATA. It is also encouraging to see the overall trend in under prediction of corrosion rates at high temperatures matched those results found in literature^{18,16} although different experimental setups and methodologies were applied. In these conditions (above 60°C), the

use of the deWaard glycol factor could lead to dangerous underestimation of the corrosion rate in the presence of glycol.

5.6 Summary on Experimental Findings

The results obtained by performing this systematic analysis for strong or weak acid solutions provided a better insight on the effect of glycol on corrosion rate.

From the potentiodynamic sweeps analysis, it was found that both anodic and cathodic electrochemical reactions are affected by adding MEG in solution. The effect of changes in flow, pH and temperature did not yield unexpected results in the presence of ethylene glycol and the same trend as solutions with only water were observed, albeit with much reduced rates. No changes in Tafel slopes were observed for all electrochemical reactions involved and the cathodic limiting current responded as expected to environmental conditions. Gulbrandsen et al.,¹³ proposed that the changes in physico-chemical properties of the fluid could explain the decrease in corrosion rate, as well as the possible changes in the water reduction reaction. The experimental results presented in the previous section seem to corroborate those findings, but also demonstrate that no clear effect of MEG on the water reduction water occurred. Additionally, several researchers¹³⁻¹⁷ attributed the adsorption of MEG onto the metal surface as one of the reasons for the inhibition of the anodic reaction. Furthermore, Gulbrandsen et al.,¹³ proposed an additional explanation for the inhibition of the anodic reaction. In their research, it was proposed that the activation energy for the anodic dissolution could be increased due to the presence of MEG in solution as seen in Figure 27.

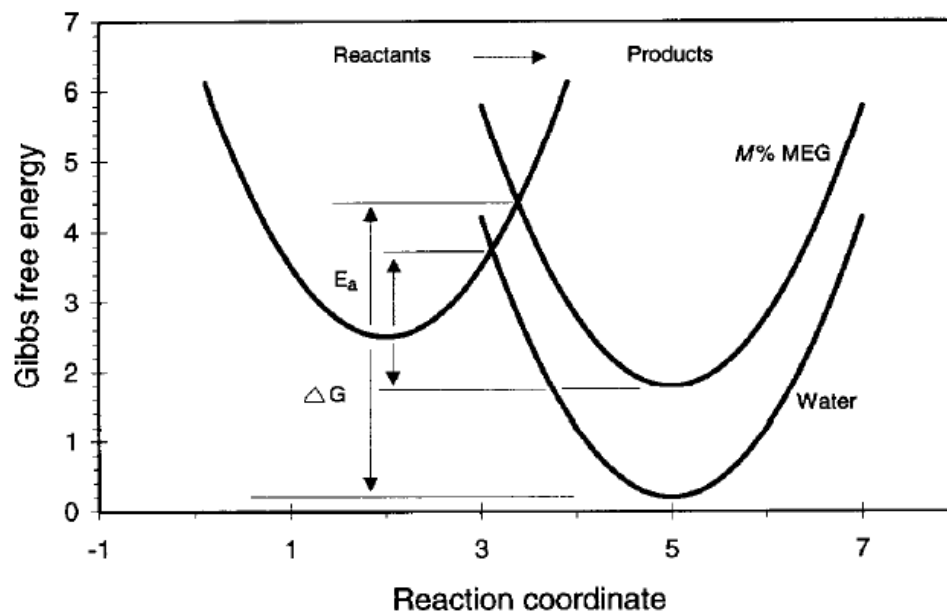


Figure 27. Activation energy schematic for iron dissolution into water and MEG-Water solutions. Reproduced with permission from NACE International, Houston, TX. All rights reserved. Gulbrandsen E and Morad J, Paper 221 presented at Corrosion/1998, San Diego California. © NACE International 1998.¹³

This proposed increase in activation energy for the iron dissolution reaction would make the release of iron ions in solution more difficult, thus affecting the rate of the anodic reaction. Results obtained in this research presented similar findings related to the clear retardation of the anodic reaction at various glycol concentrations in solution. However, the change in activation energy could not be tested or confirmed within the scope of the present study.

By corroborating existing literature findings as well as performing a new comprehensive study, a solid understanding of the effect of MEG on corrosion mechanisms is achieved. This in turn constitutes an essential step in the development of the modeling approach, which can be used to validate some of the assumptions made in this section.

The experimental LPR corrosion rates obtained in the presence of MEG can be predicted in most conditions within a factor of two using FREECORP™ in conjunction with deWaard's glycol factor. Exceptions are observed at temperature of 30°C and pH 4.00, where the corrosion rate is over-predicted, and at high temperature (above 60°C) where the corrosion is under-predicted. This last observation is more concerning as under-prediction can have serious consequences on asset integrity.

These comments mostly agree with results from previous studies, where at temperatures above 50°C, the deWaard glycol factor was not deemed to be a safe approach.

CHAPTER 6 MODELING APPROACH

This section focuses on the modeling methodology, as well as assumptions that were used to model the corrosion of mild steel in the presence of MEG. From the results found in the previous section, a number of observations could be clearly made with regards to the effect of increasing MEG content in solution:

- The Tafel slopes of the cathodic and anodic reactions are unaffected;
- At constant pH, temperature and CO₂ content, the limiting current (considering contribution from H⁺ and H₂CO₃ reductions) is clearly decreased.
- At constant pH, temperature and CO₂ content, the charge transfer rates of the cathodic reactions (H⁺, H₂O and H₂CO₃ reductions) are unaffected.
- The anodic reaction rate is clearly retarded.
- There is no effect on the water reduction in the presence of MEG.

On the cathodic side, it is hypothesized that all the changes observed can be modeled by considering the physico-chemical properties of the MEG/H₂O/CO₂ system.

For the anodic reaction, no mechanism is proposed at this stage to explain the observed reaction decrease. Although an adsorption of MEG on the steel surface or/and a change of activation energy have been proposed¹³⁻¹⁷, the present experimental results do not provide sufficient evidence to conclude. Instead, a “MEG-factor, η_{MEG} ” is used to simulate the retardation effects exhibited on the iron dissolution.

The following section presents a summary on how these changes are considered and can be divided in three main sub-sections:

1. First, the non-ideal MEG-H₂O-CO₂ is modeled and the activity of the H⁺ ion in particular (and all other species in general), is determined.
2. Next, the contribution of the H⁺ and H₂CO₃ reductions to the limiting current in glycolic solutions is calculated based on the updated electrolyte chemistry.
3. The methodology to determine the empirical MEG factor is presented.
4. Finally, the updated chemical and electrochemical models are validated using literature information and data from the present study.

These four steps cover the changes seen on the anodic and cathodic reactions due to the presence of MEG. This approach provides a clear and methodic representation of the complexity formed by CO₂ corrosion systems in non-ideal mixtures in general and in MEG containing systems in particular.

6.1 Chemistry of MEG/H₂O/CO₂ Solutions and Calculation of pH (Proton Activity)

Revisiting the literature review section, Equation (37) and Equation (38) provide an overview for the definition of the proton activity, as well as the methodology used for pH calculation in non-ideal solutions. Furthermore, highlighted in Table 1 are the equations associated in the dissolution, hydration and dissociation of carbon dioxide/carbonic species in water. Up to this point, a mathematical model can be developed to predict the concentration of protons in a system for CO₂-H₂O-NaCl. However, in order to take into account the non-ideality formed by adding MEG in solution, modifications need to be made to represent how each component concentration changes with given contents of glycol. References to these derivations link to the work presented by Lu et al.,²⁹ Kan et al.³⁰ and

Sandengen et al.,³⁴ where the solubility constant of carbon dioxide in non-ideal solutions was given earlier by Equation (39).

The thermodynamic Henry's constant used in Equation (39) can be expressed as function of concentration, partial pressure and activity coefficients:

$$K_{sol} = \frac{a_{CO_2(aq)}}{f_{CO_2(gas)}} = \frac{[CO_2(aq)] * \gamma_{CO_2(aq)}^S * \gamma_{CO_2(aq)}^M}{P_{CO_2} * \gamma_{CO_2(gas)}} \quad (45)$$

where the $\gamma_{CO_2}^{gas}$ is the CO₂ activity coefficients in the gas phase, and $\gamma_{CO_2(aq)}^S$ and $\gamma_{CO_2(aq)}^M$ are the activity coefficient contributions in the liquid phase due to the presence of salt (labeled *S*) and MEG (labelled *M*), respectively. The partial pressure for carbonic acid in this model is defined as an input. It is important to understand that the non-ideality in solution not only occurs by the presence of MEG, γ_i^M but also due to the presence of NaCl, γ_i^S . In this study, the electrolyte content in solution was fixed at 1wt. % NaCl, which resulted in minimal deviations from ideality, and therefore, it was decided to set $\gamma^S = 1$ for each component in solution.

Similarly, the dissociation of water in terms of the activity is expressed as:

$$K_{wa} = \frac{a_{H^+} * a_{OH^-}}{a_{H_2O}} = \frac{[H^+] * \gamma_{H^+}^M * [OH^-] * \gamma_{OH^-}^M}{[H_2O]} \quad (46)$$

Sandengen et al.,³⁴ demonstrated that the concentration of water can be estimated by the mole fraction of water in the system. In addition, the dissociation constant for water at various temperatures, and in the presence of different concentrations of MEG has been identified by Banerjee et al.⁵² as shown below in Table 6.

Table 6. pKa values for water-MEG as a function of temperature in Kelvin, K.

MEG Content [wt. %]	pKa	Reference
0	$29.3868 + 0.0737549*T - 7.47881*10^{-5}*T^2$	Nordsveen et al., ²¹
10	$3009.97/T + 2.77 + 0.00329*T$	Banerjee et al. ⁵²
30	$3017.70/T + 1.49 + 0.00708*T$	
50	$4172.07/T - 7.11 + 0.02271*T$	
70	$2429.05/T + 4.39 + 0.00433*T$	
90	$3560.93/T - 2.67 + 0.01711*T$	

The same procedure is then applied to express on the hydration of the aqueous carbon dioxide, and the subsequent dissociation reactions:

$$K_{hy} = \frac{a_{H_2CO_3(aq)}}{a_{H_2O} * a_{CO_2(aq)}} = \frac{[H_2CO_3] * \gamma_{H_2CO_3}^M}{[CO_2] * \gamma_{CO_2}^M * x_{H_2O}} \quad (47)$$

$$K_{ca} = \frac{a_{HCO_3^-(aq)} * a_{H^+(aq)}}{a_{H_2CO_3(aq)}} = \frac{[HCO_3^-] * \gamma_{HCO_3^-}^M * [H^+] * \gamma_{H^+}^M}{[H_2CO_3] * \gamma_{H_2CO_3}^M} \quad (48)$$

$$K_{bi} = \frac{a_{CO_3^{2-}(aq)} * a_{H^+(aq)}}{a_{HCO_3^-(aq)}} = \frac{[CO_3^{2-}] * \gamma_{CO_3^{2-}}^M * [H^+] * \gamma_{H^+}^M}{[HCO_3^-] * \gamma_{HCO_3^-}^M} \quad (49)$$

The concentrations of charged species are linked through the electron-neutrality expression.

$$[Na^+] + [H^+] = [OH^-] + [HCO_3^-] + 2 * [CO_3^{2-}] + [Cl^-] \quad (50)$$

Each concentration term in the electro-neutrality equation (besides Na^+ and Cl^-), can be expressed as function of H^+ concentration and other known parameters, such as equilibrium constants, activity coefficients and partial pressure of CO_2 . The final expression can be solved using an iterative method (Newton-Raphson) as shown by Equation (51):

$$[Na^+] - [Cl^-] + [H^+] - \frac{2 * K_{bi} * K_{ca} * K_{hy} * x_{H_2O} * [CO_2] * \gamma_{CO_2}^M}{[H^+]^2 * (\gamma_{H^+}^M)^2 * \gamma_{CO_3-2}^M} - \frac{1}{[H^+] * \gamma_{H^+}^M} \left\{ \frac{K_{ca} * K_{hy} * x_{H_2O} * [CO_2] * \gamma_{CO_2}^M}{\gamma_{HCO_3-}^M} + \frac{K_w * x_{H_2O}}{\gamma_{OH-}^M} \right\} = 0 \quad (51)$$

Ultimately, the appropriate concentration of protons in a MEG-Water-CO₂-NaCl mixture can be determined and used to calculate the pH:

$$pH = -\log([H^+] * \gamma_{H^+}^M) \quad (52)$$

The mathematical expressions of the activity coefficients are taken from two studies performed by Sandengen³⁴ and Kan³⁰ due to the similarity in the modeling approach used in both investigations.

In the present study, the gas phase can be considered ideal as the total pressure is only 1 bar and the partial pressure of MEG can be considered negligible. However, applications of this methodology to HPHT environments will definitely warrant considerations of non-ideality. The methodology for determination of fugacity is consequently presented here for consistency. The activity coefficient for carbon dioxide in the gaseous phase is determined as follows:

$$f_{CO_2(gas)} = P_{CO_2} * \gamma_{CO_2(gas)} \quad (53)$$

As described earlier, the partial pressure of carbon dioxide is an input, and therefore the fugacity, f of the gas can be determined by the van der Waals EOS as:

$$\ln\left(\frac{f_{CO_2(gas)}}{P_{CO_2}}\right) = (Z - 1) - \frac{A}{Z} - \ln(Z - B) \quad (54)$$

where Z is the compressibility factor, which can be determined as follows:

$$Z^3 - (1 + B) * Z^2 + A * Z - A * B = 0$$

$$A = \frac{aP}{(RT)^2}$$

$$B = \frac{bP}{RT} \quad (55)$$

where a and b for CO₂ are 0.3658 Pa.m⁶/mol², 4.286X10⁻⁵ m³/mol, respectively⁵⁶.

Carbon dioxide's activity coefficient in the presence of MEG in the aqueous phase and calculated on a kg of water basis is expressed as:

$$\log_{10}(\gamma_{CO_2(aq)}^M) = \left(-2.954 + \frac{691.6}{T} - (0.382 * I)/(1 + I^{0.5})\right) * x_{MEG} - \frac{151.9}{T} * x_{MEG}^2 - 0.67 * x_{MEG}^4 \quad (56)$$

where x_{MEG} is the mole fraction of MEG in solution, T, is the temperature in Kelvin, and I is the ionic strength in molality.

Similarly, the activity coefficients for the remaining species in solution (HCO₃⁻, CO₃⁻², and OH⁻), this time evaluated of a kg of solvent basis, are expressed as follows:

$$\ln(\gamma_{i(aq)}^M) = (r_1 + t_1 * [T - 298] * x_{MEG} + (r_2 + t_2 * [T - 298] * x_{MEG}^2) + (r_3 + t_3 * [T - 298] * x_{MEG}^3)) * x_{MEG} - \frac{151.9}{T} * x_{MEG}^2 - 0.67 * x_{MEG}^4 \quad (57)$$

where the coefficients r_i and t_i are defined in Table 7.

Table 7. Coefficients used for the calculation of MEG dependence on activity coefficients for components. Discussion of the results are presented by Sandengen et al.³⁴

Species	r ₁	r ₂	r ₃	t ₁	t ₂	t ₃	T [°C]
HCO ₃ ⁻	3.4648	-1.7839	-1.3926	2.0977E-2	6.7566E-3	-1.9826E-2	25-90
CO ₃ ⁻²	11.240	-9.7739	4.0510	0	0	0	25-80
OH ⁻	-6.6801	11.953	-8.2732	0	0	0	25-50

Finally, the dependence of MEG on the hydronium ion, H^+ , again listed on a kg of solvent basis, is listed as follows:

$$\ln(\gamma_{H^+}^M(aq)) = 1.4457 * x_{MEG} - 3.9428 * x_{MEG}^2 + 5.6753 * x_{MEG}^3 + \frac{A * I^{0.5}}{1 + B * I^{0.5}}$$

$$A = -1.17 * W_{MEG} - 0.82 * W_{MEG}^2$$

$$B = 9.92 * W_{MEG} - 3.65 * W_{MEG}^2 \quad (58)$$

where x_{MEG} and I are the mole fraction of MEG in solution, and the solution's ionic strength in molality respectively, and W_{MEG} is the mass fraction of MEG in the mixture. Unlike for HCO_3^- , CO_3^{2-} , OH^- (Table 7), the expression of the activity coefficient of H^+ in the presence of MEG depends not only on glycol concentration and temperature but also on the ionic strength of the solution.

By combining these expressions, an example of calculated pH in MEG/H₂O system for a given temperature, ionic strength in solution, partial pressure of carbon dioxide is shown in Table 8.

Table 8. Calculations of the pH for a solution saturated with 0.5bar CO₂, at 30°C and 1wt. % NaCl.

MEG Content in Solution		pH_calculated	pH_measured without correction	pH_measured with correction
Vol. %	Wt. %			
0	0	4.00	4.00 ± 0.03	4.00 ± 0.03
40	42	4.18	4.01 ± 0.06	4.20 ± 0.06
55	57	4.27	4.05 ± 0.05	4.19 ± 0.05
70	71.5	4.37	4.06 ± 0.04	4.32 ± 0.04
85	85.4	4.41	4.04 ± 0.06	4.52 ± 0.06

As expected, the addition of MEG in solution causes an increase in pH according to the model, as well as the experimental results. However, when the pH is measured during the experiment, it can be seen that there are no visible increases in the measured value obtained by the pH meter. This is because the pH meter readings need to be corrected in the presence of MEG. By combining the data from Table 2 (delta pH_MEG values) and Table 8, a better correlation is obtained between what the model predicts, and what is measured experimentally (pH with correction v.s. pH without correction). Determining the speciation of the non-ideal MEG/H₂O/CO₂ is an essential and necessary step for the calculation of the electrochemical reaction rates and, when appropriate, the associated limiting currents.

6.2 Calculation of the H⁺ and HCO₃⁻ Limiting Current in the Presence of MEG

As presented earlier, for an ideal system the limiting currents for the protons and bicarbonate reduction reactions can be estimated by Equation (59) and Equation (60), respectively. These equations are repeated here for clarity purposes.

$$i_{lim}^d(H^+) = k_m * F * [H^+]_b \quad (59)$$

$$i_{lim}(H_2CO_3) = F * [CO_2]_b * f * \sqrt{(D_{H_2CO_3} * k_{f,Hyd} * K_{Hyd})} \quad (60)$$

Both reactions are modeled individually and then combined to represent the overall limiting current of the net cathodic reaction in the system as shown below:

$$\frac{1}{i_{total}(H^+)} = \frac{1}{i_{charge\ transfer}(H^+)} + \frac{1}{i_{limiting\ current}^d(H^+)} \quad (61)$$

and

$$\frac{1}{i_{total}(H_2CO_3)} = \frac{1}{i_{charge\ transfer}(H_2CO_3)} + \frac{1}{i_{limiting\ current}(H_2CO_3)} \quad (62)$$

where the net cathodic current is the sum of all cathodic reactions, including those contributions coming from the water reduction.

This section focuses on the determination of the limiting current and on the effects of fluid properties. Fluid properties are also significantly affected by the presence of MEG. When appropriate, species activities are also considered instead of concentrations. Expressions of the mass transfer coefficients in glycolic solutions are developed so that an appropriate representation of the limiting current can be obtained. As explained earlier, correlations exist to express the mass transfer coefficient in a specific system. For a rotating cylinder electrode, the mass transfer coefficient is obtained through the Sherwood correlation as follows:

$$k_m = \frac{D_{AB}}{d_{cyl}} * 0.0791 * Re^{0.7} * Sc^{0.356} \quad (63)$$

The Reynolds number is a function of the density, dynamic viscosity and fluid velocity. The Schmidt number relates the dynamic viscosity and the diffusion coefficient of ions in solution. The expressions selected for the determination of these parameters for MEG/water solutions are listed in Table 16 in APPENDIX B COEFFICIENTS USED FOR MODELING THE ELECTROCHEMICAL REACTIONS.

The diffusion coefficients of H^+ or H_2CO_3 in water can be estimated as demonstrated by Nordsveen²⁹, using the Nernst-Einstein equation, which is reduced to the following format:

$$D_i = D_{ref} * \frac{T}{T_{ref}} * \frac{\mu_{ref}}{\mu} \quad (64)$$

where the dynamic viscosity can be estimated by the equations listed in Table 16. One key aspect of this calculation lies in the use of a reference diffusion coefficient for a given

component in solution. The authors in that investigation listed the reference diffusion coefficient for many compounds in water, including those referenced herein:

Table 9. Table of reference diffusion coefficients of species in water used in the model.²⁹

Species	Diffusion Coefficient (m ² /s)
CO ₂	1.96*10 ⁻⁹
H ₂ CO ₃	2.00*10 ⁻⁹
H ⁺	9.31*10 ⁻⁹

This value is important because it highlights the mobility of a particular ion or molecule in solution, which is naturally affected by the presence of MEG. Won et al.³⁹ and Hayduk et al.,³⁸ obtained values for the diffusivity of carbon dioxide in water-ethylene glycol solutions at 25°C. However, no data regarding the diffusivity of carbonic acid in glycolic solutions was found. Nevertheless, as can be seen from

Table 9, the diffusivity of carbon dioxide and carbonic acid in pure water are similar: 1.96 and 2.00*10⁻⁹ m²/s, respectively. Consequently, it was assumed that both molecules would diffuse in a similar manner in glycolic solutions. A fitting equation was developed with the literature results obtained for carbon dioxide diffusivity in MEG-Water solutions and was then applied directly to carbonic acid to extrapolate its diffusivity in the same systems.

Similarly, the diffusion coefficient for H⁺ in MEG-Water solutions was also problematic to obtain. However, investigations by Garner et al.⁴⁰, Byers, et al.,⁴¹ and Ternstrom et al.,⁴² presented data regarding the diffusion coefficients of water in MEG-water systems at various temperatures, one of which was 25°C. These results were used to represent the diffusivity of an H⁺ ion in a MEG-Water solution. These assumptions proved

to be valid as increasing glycol content in solution lead to a lower diffusivity (and hence lower ion mobility). This trend was related to a postulate presented by Gulbrandsen's research,¹³ where an increase in glycol content would result in restricted ion mobility for CO₂ and H⁺ as shown by Figure 28 and Figure 29.

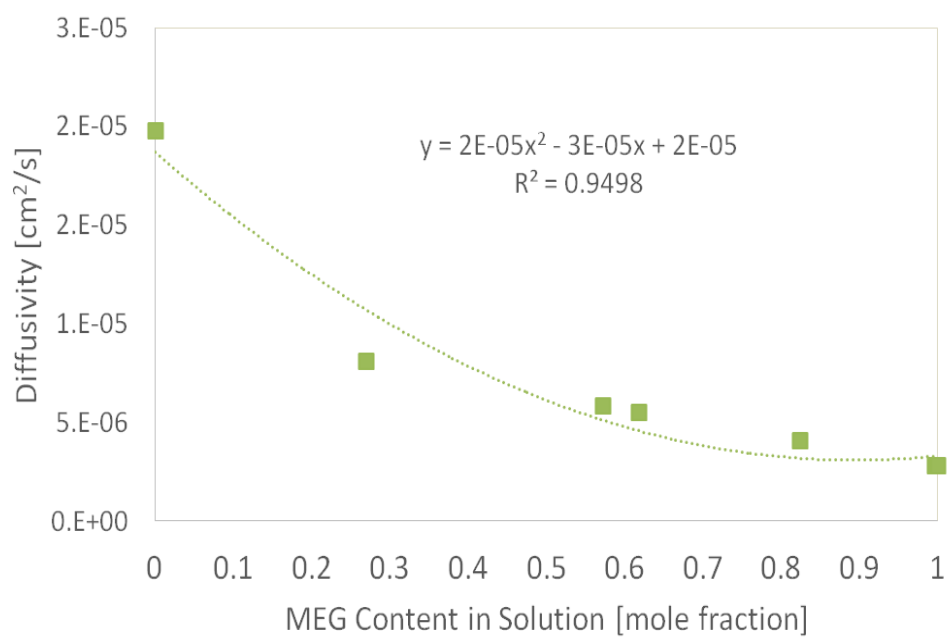


Figure 28. Reference diffusivity for CO₂ in MEG-Water solutions at 25°C.

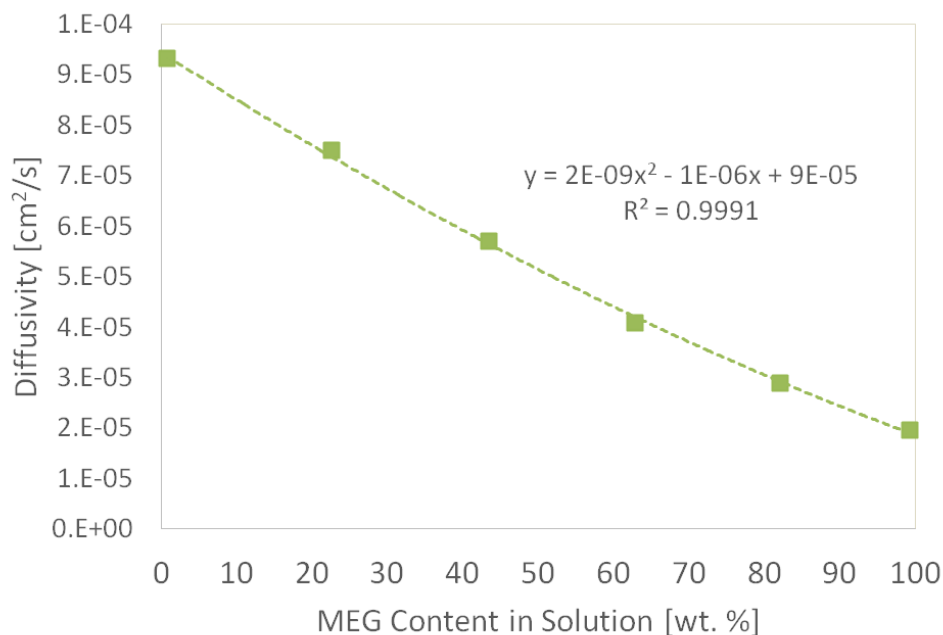


Figure 29. Reference diffusivity for H^+ in MEG-Water solutions at 25°C.

It can be seen that by increasing glycol content, a lower reference diffusivity is obtained for each compound in solution.

Next, the density of the mixture was calculated as follows:

$$\rho_{mixture} = \frac{mass_{total}}{\left(\frac{mass_{H_2O}}{\rho_{H_2O}} + \frac{mass_{MEG}}{\rho_{MEG}}\right)} \quad (65)$$

where the temperature-dependent density of each component can be found in Table 16 in

APPENDIX D LIQUID DENSITY AND VISCOSITY INFORMATION FOR WATER AND MONOETHYLENEGLYCOL.

For the viscosity of the mixture, the following procedure was used according to the methodology provided in Maples' Petroleum Refinery Book⁵³. This approach used the Refutas method, which accounts for mass-based ratio of the viscosity. However, an update was done by Chevron to account for volumetric-base calculations, which is a similar

approach used in this study.⁵³ For this method, a viscosity blending index (VBI) is determined for MEG and water. This VBI number depends on the viscosity in centistokes, C_s for each fluid in solution.

$$VBI = \frac{\ln(C_s)}{\ln(1000 * C_s)} \quad (66)$$

Then, the viscosity of the mixture is then calculated as:

$$VBI_{MIXTURE} = \sum_{i=0}^N v_i * VBI_i \quad (67)$$

where the volume fraction of each component, v_i is multiplied to its respective VBI to obtain the $VBI_{MIXTURE}$; this value in turn is used to determine the viscosity of the mixture as:

$$C_{S_{MIXTURE}} = EXP\left(\frac{VBI_{MIXTURE} * \ln(1000)}{(1 - VBI_{MIXTURE})}\right) \quad (68)$$

This is a very important parameter to determine as it is directly related the Reynolds and Schmidt numbers.

Lastly, it is important to define clearly how the fluid velocity is determined in the modeling approach since it is used for the calculation of the Reynolds number. When comparing modeling and experimental results obtained in RCE, the working electrode rotational velocity, in RPM, has to be converted to m/s. However, since the primary application of this work is geared towards the oil and gas industry, it is often useful to determine the pipeline velocity that is equivalent to this rotational velocity obtained in the experimental setup. This is typically done by equating either the mass transfer coefficient or the shear stress in RCE and pipe. Considering the scope of this study, it is more meaningful to determine fluid velocities based on equivalent mass transfer coefficients.

Silverman developed a correlation defining the relationship between the RPM velocity and pipeline velocity for this purpose.⁵⁴

$$U_{pipe} = \left(\frac{U_{cyl}}{0.1185 * \left(\frac{\rho}{\mu}\right)^{\frac{1}{4}} * \left(\frac{d_{cyl}^{\frac{3}{5}}}{d_p^{\frac{28}{5}}}\right) * Sc^{-0.0857}} \right)^{\frac{4}{5}} \quad (69)$$

It can be seen that the Schmidt number, as well as the density and viscosity of the liquid mixture are involved in this calculation as shown by Equation (69). By adding MEG in solution, these parameters have to be adjusted accordingly to show the behavior in flow in the non-ideal mixture.

In summary, the following adjustments were implemented to represent accurately the properties of the MEG/H₂O/CO₂ system and to model both chemical and electrochemical reactions:

- Determination of all activity coefficients of all involved species.
- Update of fluid density and viscosity.
- Determination of diffusion coefficients of H⁺ and H₂CO₃ in glycolic solution.
- Update in calculation methodology for the limiting current for cathodic and anodic reactions.

6.3 Modeling the Anodic Reaction in the Presence of MEG

Up to this point, the modeling approach focused on the effect of MEG on the cathodic reactions. Experimental results also show a clear retardation of the anodic

reactions in glycolic solutions. This section focuses on the method used to simulate the effect of MEG on the anodic reaction. It is important to note that a mechanistic approach was utilized for the total cathodic currents, mostly by recalculating the mixture properties and considering a non-ideal liquid phase. No further change in reaction rate parameters seemed to be required. For the anodic reaction, on the other hand, the clear decrease in reaction rate cannot be explained by changes in fluid properties alone. Although the experimental results obtained in this study constitute a very useful and comprehensive database, they cannot be used directly to decipher the mechanism involved on the anodic side. Assuming that adsorption of MEG on the metal surface does occur, a fitting exercise, based on the results seen in the experimental results chapter, was executed without additional attempt to investigate the nature of the bonding at the steel/electrolyte interface.

Before explaining the procedure applied to represent the MEG effects on the anodic reaction, it is important to describe the complexity of the representation of iron dissolution in the presence of CO₂ in water. First, Nescic et al.,⁵⁵ described that there exist various dominating mechanisms in the dissolution of iron into solution. Furthermore, the anodic Tafel slope – which was continually assumed to be a constant value prior to that work – was demonstrated to change depending on the pH of the solution. It was also determined in that investigation that a solution with pH in-between 4.00 and 5.00 would exhibit behaviors that would signal a different reaction order. Even though the purpose of the present study is not to further investigate the mechanisms involved with the dissolution of iron, the results presented by Nescic's research showed that even for water-based systems – and for a given pH – the dissolution of iron is a complex topic to understand and to model.

Moreover, the validity of some of these assumptions have not been verified extensively. Due to the uncertainty of the new finding presented at the time, it was proposed to model the anodic reaction in a simpler way, mimicking the approach selected in FREECORP™. Since one of the objectives of this work is to upgrade FREECORP™, it does make sense to use the same basic framework, which is presented below.

Table 10. Comparison between literature and FREECORP™'s values for anodic Tafel slope for iron dissolution.

	Anodic Tafel Slope, b_{anodic} [mV/decade], Literature ²¹	Anodic Tafel Slope, b_{anodic} [mV/decade], FREECORP™
$Fe \rightarrow Fe^{+2} + 2e^{-}$	0.03 for pH <4	0.04 over entire pH range
	0.08 for 4 < pH < 5	
	0.12 for pH > 5	

Similarly, the method to estimate the exchange current density of the anodic dissolution was proposed by Nordsveen et al.²¹, as it was demonstrated in literature review section, (as well as Table 13 in APPENDIX B COEFFICIENTS USED FOR MODELING THE ELECTROCHEMICAL REACTIONS) to be a function of various parameters as shown by Equation (71):

$$i_o = i_{o_ref} * \left(\frac{c_{H+}}{c_{H+_ref}} \right)^{a1} * \left(\frac{c_{CO2}}{c_{CO2_ref}} \right)^{a2} * \left(\frac{c_{H2CO3}}{c_{H2CO3_ref}} \right)^{a3} * e^{\frac{-\Delta H^*}{R} * \left(\frac{1}{T} - \frac{1}{T_{ref}} \right)} \quad (70)$$

It is important to highlight that some uncertainties exist about the validity of these coefficients over different ranges of pH and CO₂ partial pressure. In an effort to remain consistent with the approach adopted in FREECORP™, the following values were applied to the concentration dependent coefficients (a1, a2, a3) for the anodic exchange current density as shown by Table 11.

Table 11. Values for the anodic exchange current density coefficients used in this research.

	i_{oref} [A/m ²]	a_1	$C_{H^+_{ref}}$ [Molar]	a_2	$C_{CO_2}_{ref}$ [Molar]	a_3	$C_{H_2CO_3}_{ref}$ [Molar]	ΔH [kJ/mol]	T_{ref} [°C]	E_{rev} [V vs. SHE]	b_{anodic} [mV/decade]
$Fe \rightarrow Fe^{+2} + 2e^-$	1	0	10^{-4}	1 for $p_{CO_2} < 1 \text{ bar}$	0.0366	0	0	37.5	25	-0.488	$2.303 * R * T / (1.5 * F)$

These assumptions served as the basis for the modeling of the anodic reaction in the presence of MEG, and helped simplify Equation (25). In addition, the MEG factor, η_{MEG} , is added to the expression of the exchange current density as follows:

$$i_o = i_{o_MEG} * \left(\frac{a_{CO_2}}{a_{CO_2ref}} \right)^1 * e^{\frac{-\Delta H}{R} * \left(\frac{1}{T} - \frac{1}{T_{ref}} \right)} \quad (71)$$

where,

$$i_{o_MEG} = i_{o_ref} * \eta_{MEG}$$

As shown in the simplified expression obtained in Equation (71), the anodic exchange current density used in this model does not depend on pH, nor on the carbonic acid concentration. The only dependence is the activity of carbon dioxide.

In order to determine this MEG factor, a fitting exercise is applied based the experimental corrosion potential, E_{corr} . For each experimental condition, the predicted corrosion potential is matched to the experimental one by changing the value of the MEG factor. The values for η_{MEG} obtained through the fitting exercise are then plotted against the MEG content in order to investigate if a trend can be extrapolated. The results from this approach considering all experimental data obtained at 30°C are presented in Figure 30.

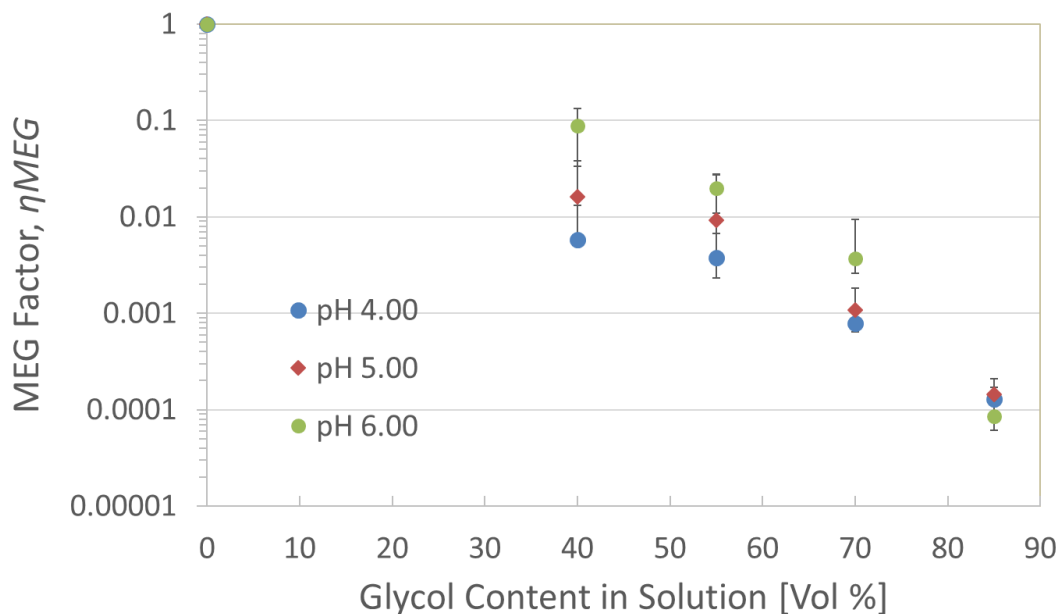


Figure 30. MEG Factor, η_{MEG} calculated from experimental E_{corr} values at various pH ranges for solutions at 30°C saturated with 0.5bar CO₂ and 1wt. % NaCl.

It is important to note that this MEG factor is not the same as the one proposed by deWaard¹⁸. η_{MEG} is determined based on the assumptions made for the determination of the Tafel slope, and the exchange current density of the iron dissolution. Any change in these assumptions will generate a different value of the MEG factor.

It can be determined from these results that with increasing concentrations of glycol in solution, there is a resulting decrease in the MEG factor. Furthermore, it was found that pH had minimal effects on the value of the MEG factor. On the other hand, changes in temperature for a fixed glycol concentration altered considerably the MEG factor value, as shown in Figure 31.

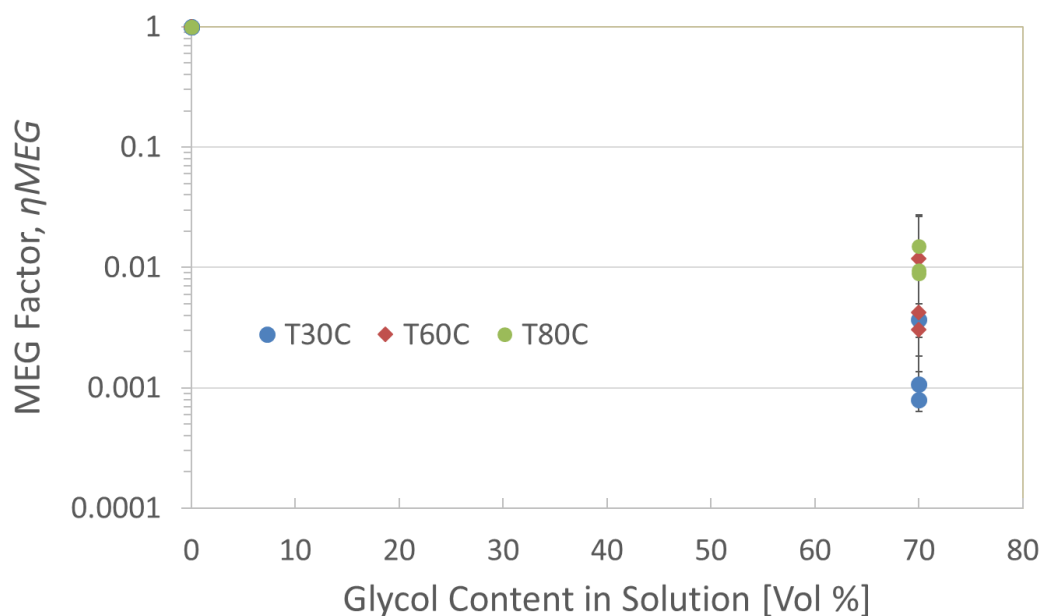


Figure 31. Changes in MEG factor with alterations in temperatures for a solution saturated with 1wt. % NaCl, 0.5bar CO₂ and 70vol. % MEG in solution.

The reasons behind this strong dependence on temperature are unclear but could be due to the assumptions made for the determination of the Tafel slope and the exchange current density in the anodic reaction.

6.4 MEG-H₂O-CO₂-NaCl Electrochemical Model Performance

A parametric analysis of the model's behavior is presented in this section. The goal here is to verify that the model predictions are sensible and agree with the experimental trends. The predictions are shown through several plots of net anodic and cathodic sweeps representing the effect of the parameters tested on the corrosion mechanism.

Figure 32 shows how the model responds to changes in temperature in the presence of 70vol. % MEG.

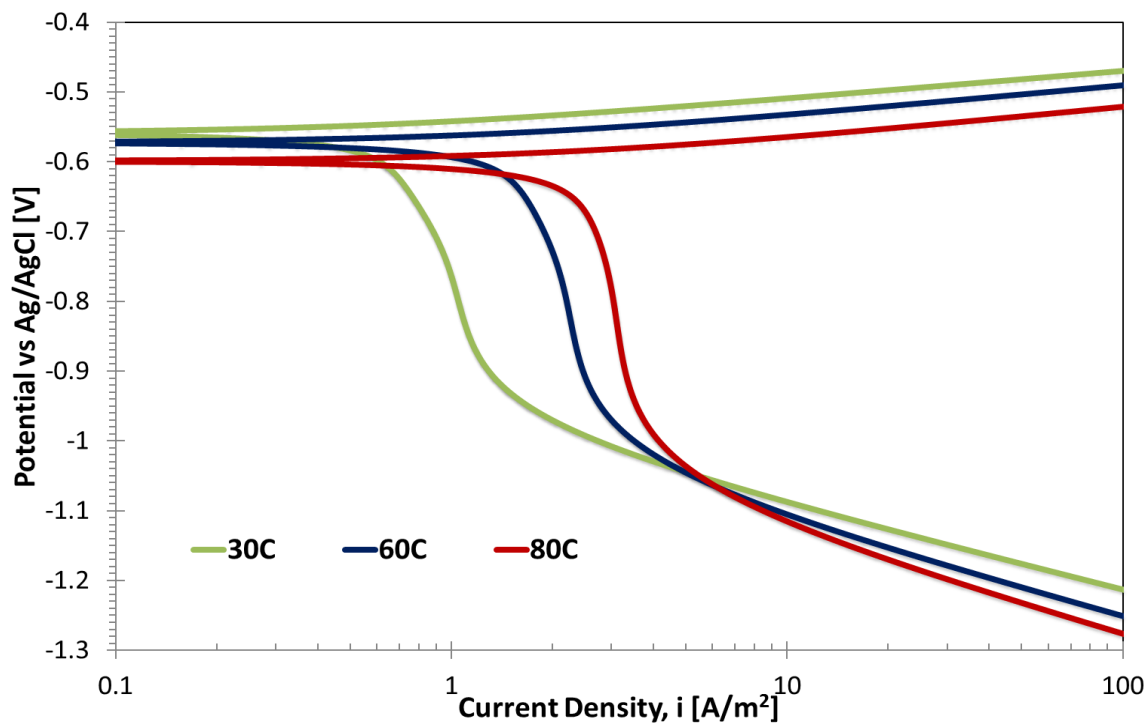


Figure 32. Model predictions - Potentiodynamic sweeps for a solution saturated with 0.5bar CO₂, 1wt. % NaCl and with a MEG content of 70vol. % MEG at 30°C, 60°C and 80°C and pH 4.00.

As shown in the plot above, the effect of temperature is seen mostly through the limiting current of the H⁺ reduction and on the Tafel slope of the water reduction. These changes are expected and a similar behavior would be obtained in the absence of MEG. Lastly, there is a visible change in corrosion potential, but as it was previously explained, these changes came from the strong dependence in temperature of η_{MEG} .

The model dependency on pH is shown in Figure 33.

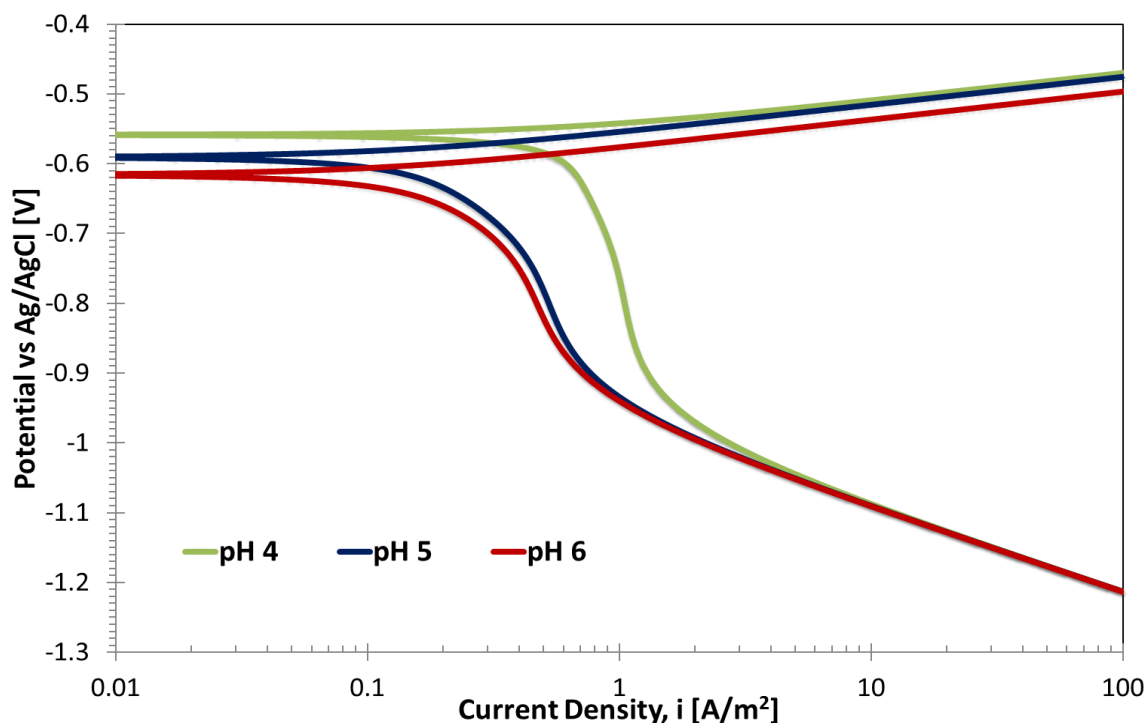


Figure 33. Model predictions - Potentiodynamic sweeps for a solution at 30°C saturated with 0.5bar CO₂, 1wt. % NaCl and with a MEG content of 70vol. % MEG and pH 4.00, 5.00 and 6.00.

Changes in pH have little effect on the anodic reaction and the water reduction, as expected. Changes are seen in the limiting current, which is logically decreased as the pH is increased. There is much more difference in the limiting current between pH 4 and 5 than between pH 5 and 6 - this is due to the fact that at high pH the net cathodic current is dominated by the H₂CO₃ reduction rather than the H⁺ reduction. Additionally, there are no changes in the reduction of water in the system, and all curves converge at the same point. These behaviors are also expected in a solution without MEG present.

The effect of flow in the presence of MEG-Water solutions is shown in Figure 34.

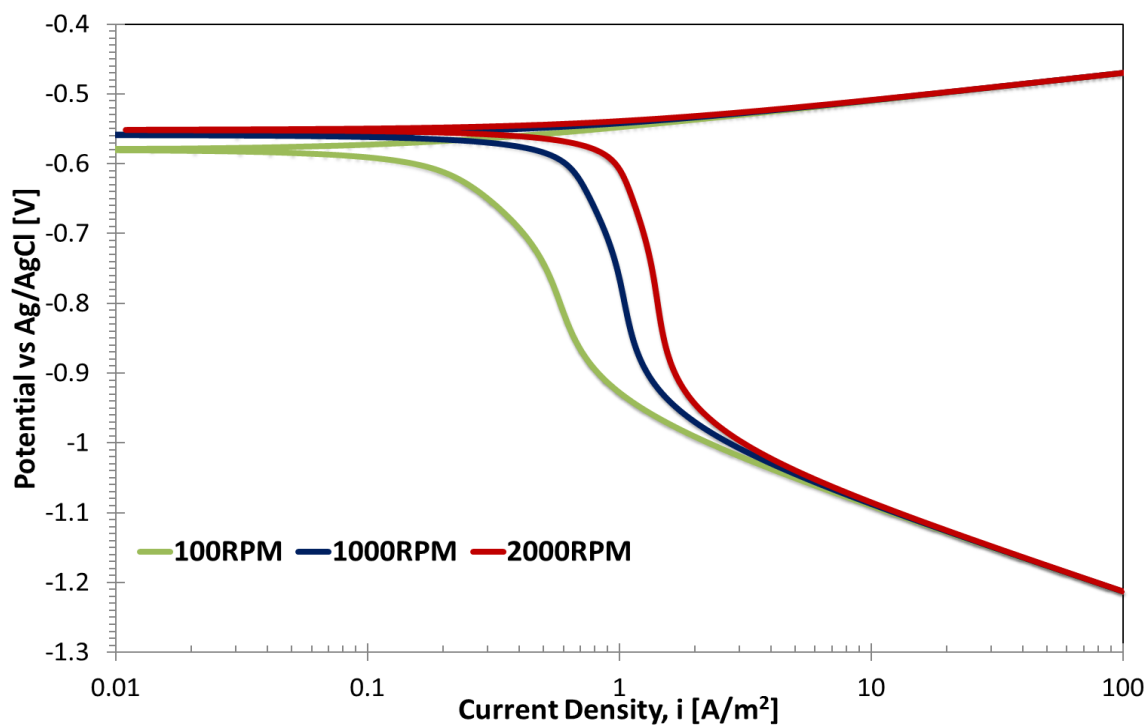


Figure 34. Model predictions - Potentiodynamic sweeps for a solution at 30°C and pH 4.00 saturated with 0.5bar CO₂, 1wt. % NaCl and a MEG content of 70vol. % MEG for RCE rotation of 100, 1000 and 2000RPM.

Figure 34 shows that the effect of flow is only visible on the limiting current of the cathodic reaction, dominated by the H⁺ reduction at pH 4.00. These results again fall in line with expected results.

Lastly, the effect of increasing glycol content on the model predictions, for a set of fixed operating parameters, is shown in Figure 35.

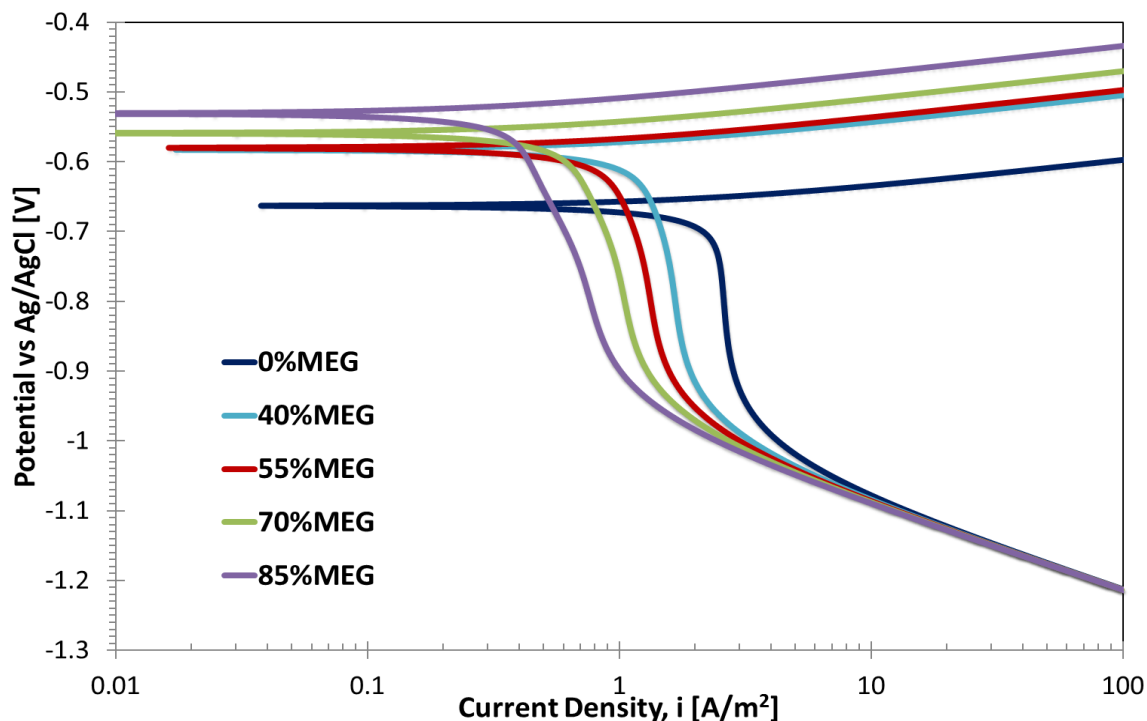


Figure 35. Model predictions - Potentiodynamic sweeps for an RCE velocity of 1000RPM for a solution at 30°C and pH 4.00 saturated with 0.5bar CO₂, 1wt. % NaCl and with a MEG content of 0, 40, 55, 70 and 85vol. % MEG.

As it is shown in Figure 35, the model predicts that increasing MEG content does not have any effect on the water reduction, nor the Tafel slopes of electrochemical reactions. In addition, increases in glycol concentration causes a decrease in the cathodic limiting current and a retardation of the anodic reaction, which is visible by the increases in corrosion potential.

All the results presented in this parametric study naturally agree with the trends observed with the experimental results. Validation of the numerical values of current and potential is the next step in the model development and is presented in the next section.

6.5 MEG Model Validation

This section presents a validation of the modeling approach using experimental data obtained through the literature and the present study. It is divided into two parts: validation of the modeling of MEG/H₂O/CO₂ chemistry and validation of the electrochemical model. Only a summary of the validation effort is shown here while more comparisons are shown in APPENDIX F VALIDATION OF CHEMISTRY MODEL USING LITERATURE DATA and APPENDIX G MODEL VALIDATION – EFFECT OF FLOW.

6.5.1 Validation of the Chemistry Model

The accurate determination of the pH of MEG-Water-CO₂-NaCl solutions is probably one of the most important parts of the chemical model. An effort to validate the modeling approach is already shown in Table 8 for the experimental values of MEG concentrations tested in this work. The validation of the model over a wider range of MEG content in solution can be shown in Figure 36.

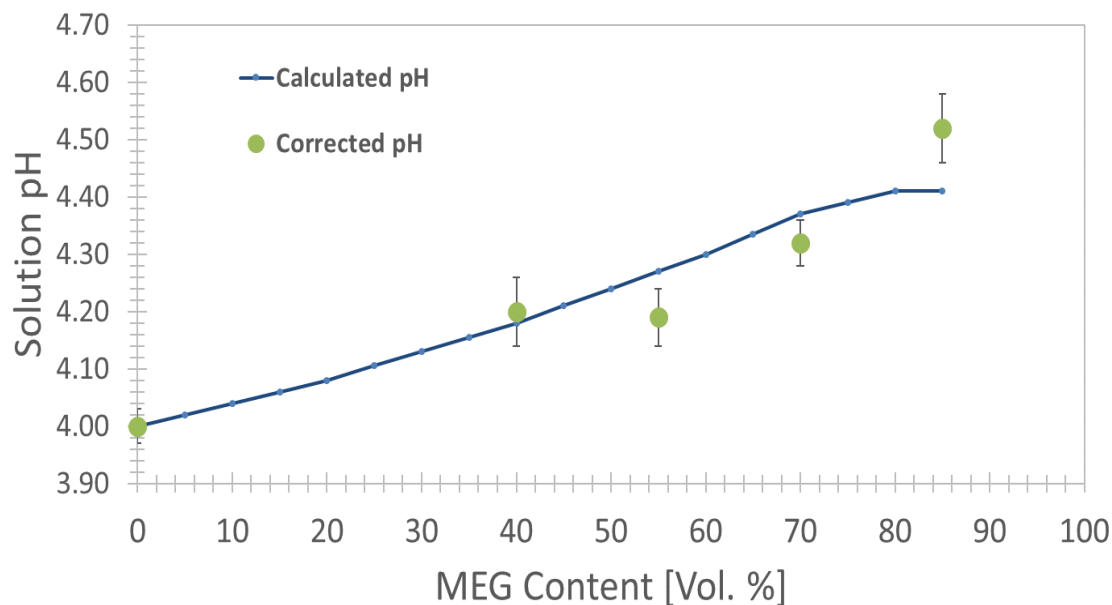


Figure 36. MEG model prediction of solution pH for a system saturated with 0.5bar CO₂, 1wt. % NaCl and at 30°C.

As expected, the addition of MEG in solution results in a decrease in solution acidity, which is well captured by the model.

An additional and very important property that can be validated with this model is the solubility of carbon dioxide in glycolic solutions. It was demonstrated in the literature review section that the solubility of CO₂ in MEG-Water solutions decreases up to 70wt. % MEG and then increases.^{13,29-35, 44-46} Figure 37 presents a prediction of the solubility of carbon dioxide in glycolic solutions at 30°C and with 0.5bar CO₂.

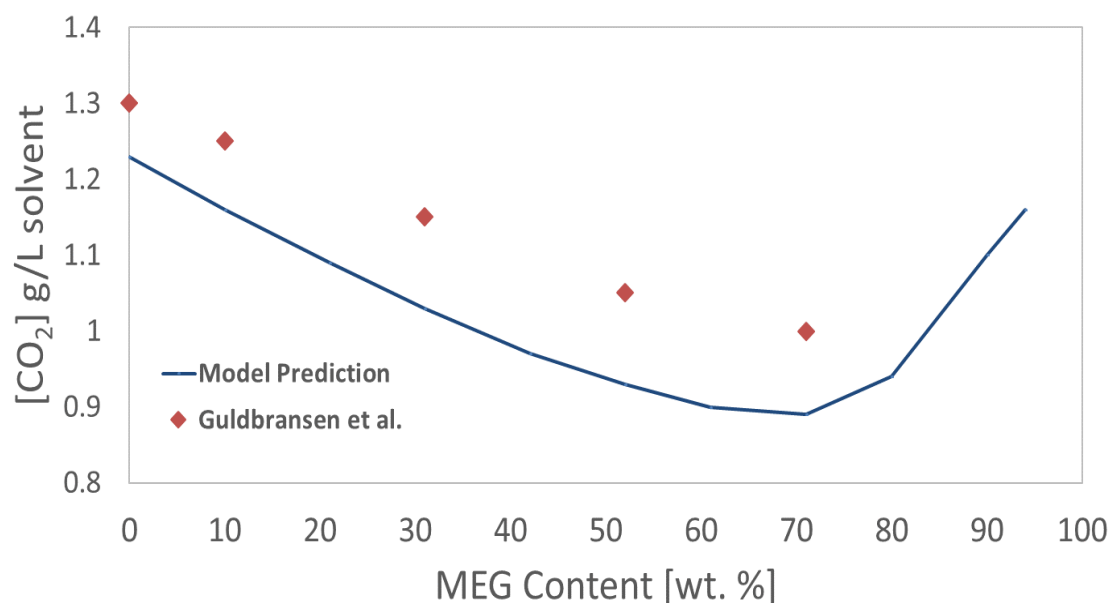


Figure 37. Comparison between model prediction (blue solid line) and Gulbrandsen's results (red dots) for of carbon dioxide's solubility as a function of glycol content for a solution at 30°C, 1bar CO₂ and 1wt. % NaCl.

From the results above, the trend predicted by the model is very similar compared to what was obtained by Gulbrandsen et al.¹³ where the solubility of CO₂ decreased up to about 70wt. %, and then increased. Further validation of the model using literature data is presented in APPENDIX F VALIDATION OF CHEMISTRY MODEL USING LITERATURE DATA.

6.5.2 Validation of the Electrochemical Model

This section presents an extensive effort to compare model predictions with experimental data, and to highlight areas of good agreement as well as discrepancies. In each of the following figures, experimental potentiodynamic curves (dotted lines) are plotted together with predicted total anodic and cathodic current vs. potential curves (continuous lines). In addition, the individual curves representing the H⁺, H₂CO₃ and H₂O

reduction reactions are also predicted and plotted to highlight their contribution to the overall mechanism.

6.5.2.1 Effect of MEG

Before demonstrating the performance of the model in glycolic solutions, it is important to validate the model in pure water systems. Figure 38 shows that for a solution without MEG and at a pH of 4.00, the model predictions fit the experimental results relatively well.

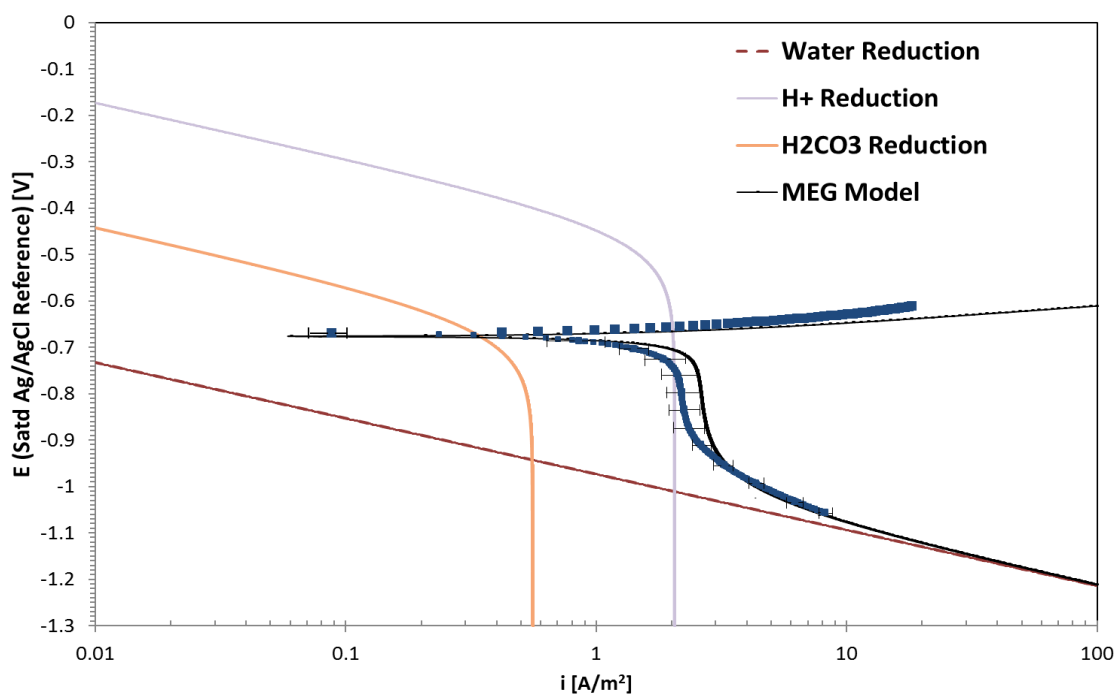


Figure 38. Comparison between model predictions (black continuous line) and experimental results (blue dotted line) for a solution saturated with 0.5bar CO₂, 1wt. % NaCl, 0% MEG at pH 4.00, 30°C and for a $V_{RCE} = 1000\text{RPM}$.

The predictions of the open circuit potential and the iron dissolution and water reduction lines are quite satisfactory. A discrepancy is observed on the prediction of the

total limiting current but only represents 18% over-prediction (2.6 A/m^2 for the model and 2.2 A/m^2 for the experimental data). More comparisons are available in upcoming sections that show in general, a satisfactory agreement with experimental data. Even though there are small differences, these results in pure water are very encouraging and provide the necessary confidence to extend the model application for simulation in non-ideal MEG/H₂O mixtures.

Figure 39 shows the comparison between experimental results and model predictions for 40vol. % MEG in solution.

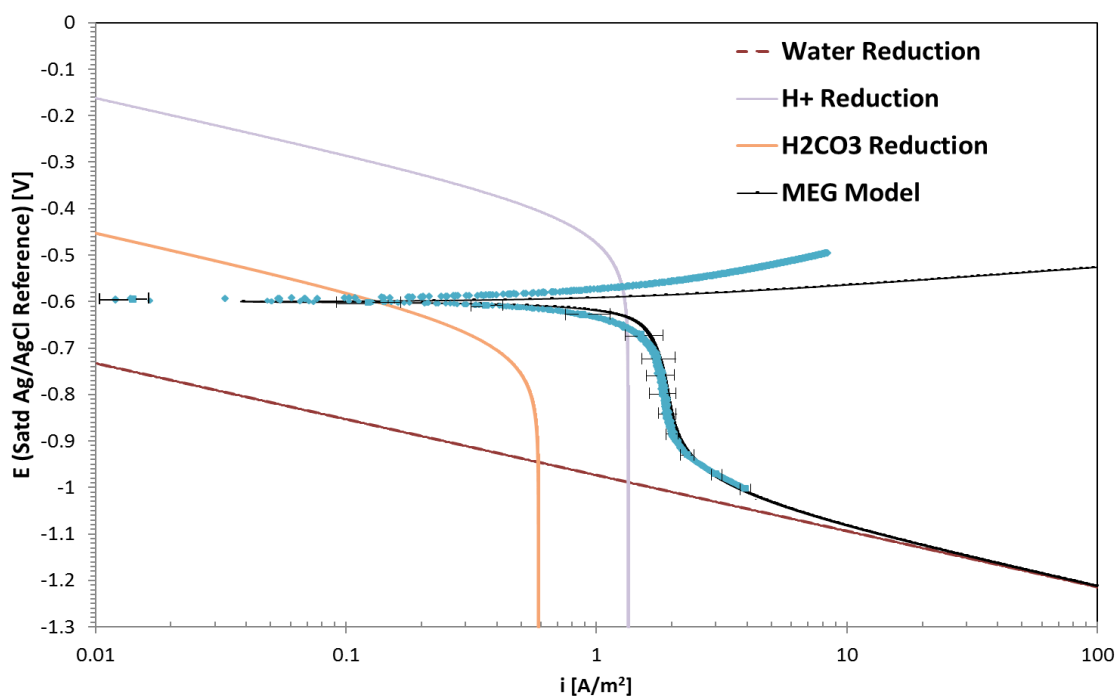


Figure 39. Comparison between model predictions (black continuous line) and experimental results (blue dotted line) for a solution saturated with 0.5bar CO₂, 1wt. % NaCl, 40vol. % MEG at pH 3.91, 30°C and for a $V_{RCE} = 1000\text{RPM}$.

It can be seen from Figure 39 that, for a glycol content of 40vol. %, the model provides an excellent representation of the measured CO₂ corrosion behavior. The predicted and experimental OCP, and the anodic line match well; this is fully expected since the modeling data is fitted to the experimental results for these two parameters. This point will be valid in this entire section, as the fitting exercise was applied for all conditions tested. The predicted total cathodic polarization curves, including the limiting current, are also in excellent agreement with the measured data. No fitting exercise was performed for the cathodic reactions and the results are only the consequence of updates implemented in the physicochemical properties of the solution. The modeling results also indicate that the reduction of H⁺ is the main cathodic reaction influencing the corrosion rate at pH of 3.91 and that the system is under mixed charge transfer / mass transfer control.

As for 40vol. % MEG, Figure 40 shows very good agreement between prediction and experimental results with 55vol. % MEG in solution.

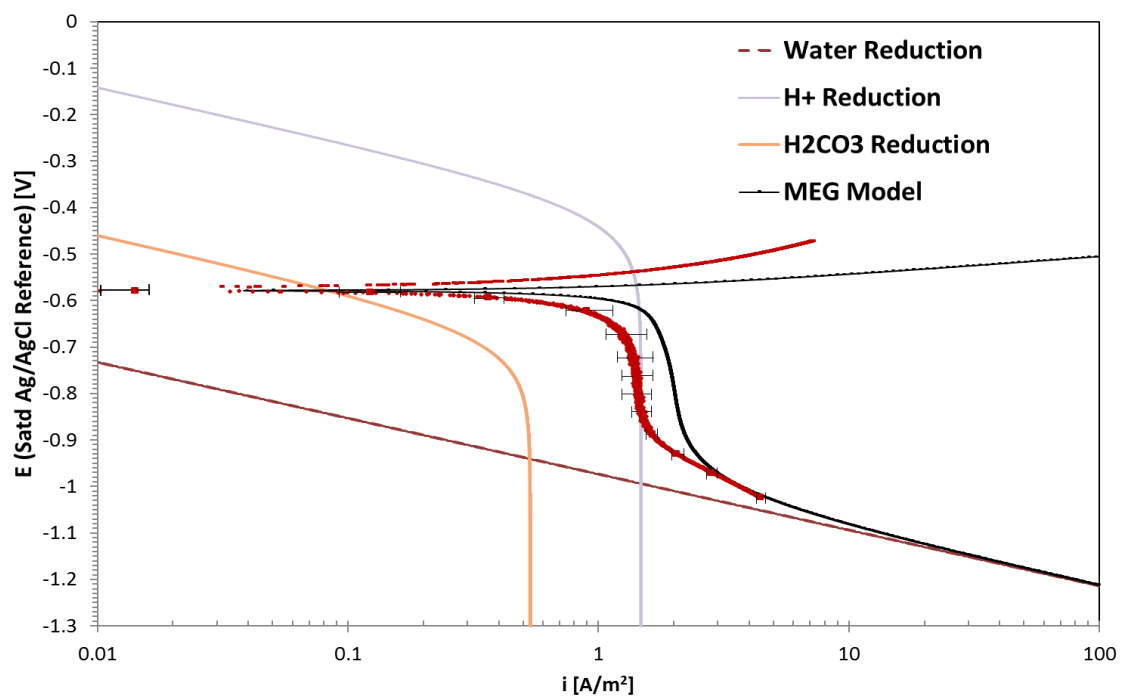


Figure 40. Comparison between model predictions (black continuous line) and experimental results (red dotted line) for a solution saturated with 0.5bar CO₂, 1wt. % NaCl, 55vol. % MEG at pH 3.77, 30°C and for a $V_{RCE} = 1000\text{RPM}$.

Figure 41 presents the results obtained with 70vol. % MEG in solution.

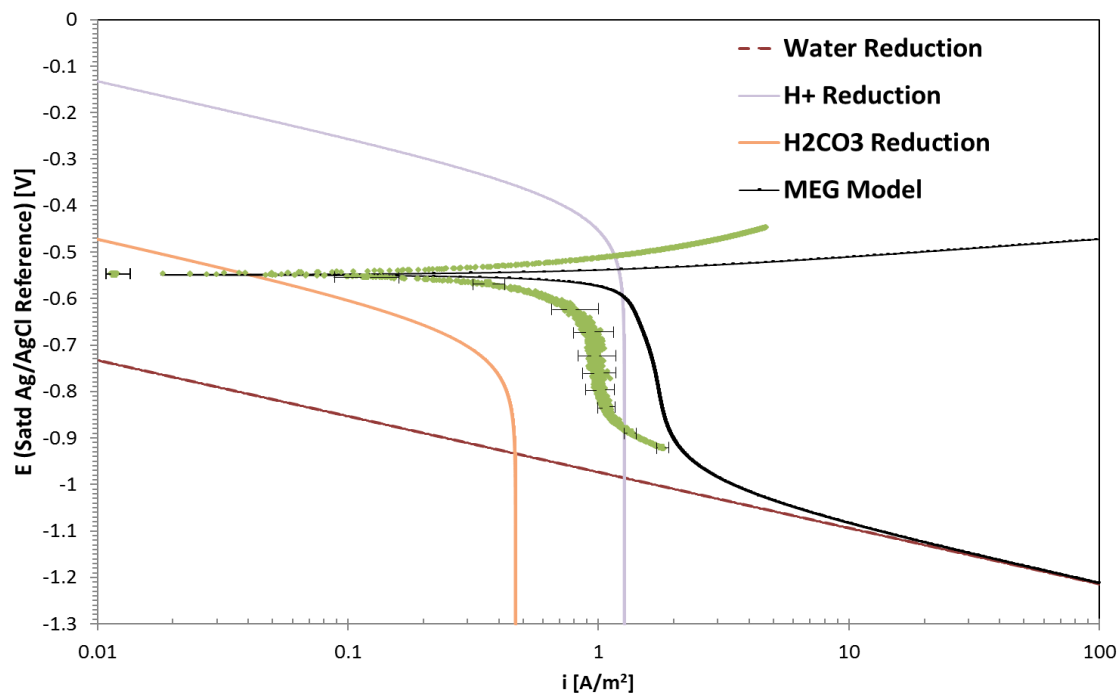


Figure 41. Comparison between model predictions (black continuous line) and experimental results (green dotted line) for a solution saturated with 0.5bar CO_2 , 1wt. % NaCl, 70vol. % MEG at pH 3.66, 30°C and for a $V_{\text{RCE}} = 1000\text{RPM}$.

For the prediction for a solution containing 70vol. % MEG in solution the discrepancies in results start to appear. Although there is a relatively good agreement between the model and experimental results, the main source of discrepancy lies in the limiting current; this however can be related to the logarithmic nature of the diagram. When analyzing the values obtained between the experimental results, and the predicted values in net limiting current, the discrepancy is about $+0.9 \text{ A/m}^2$. Additionally, it can be noted that the main contributor to the net proton reduction reaction is the proton reduction.

Figure 42 shows the results obtained with 85vol. % MEG in solution.

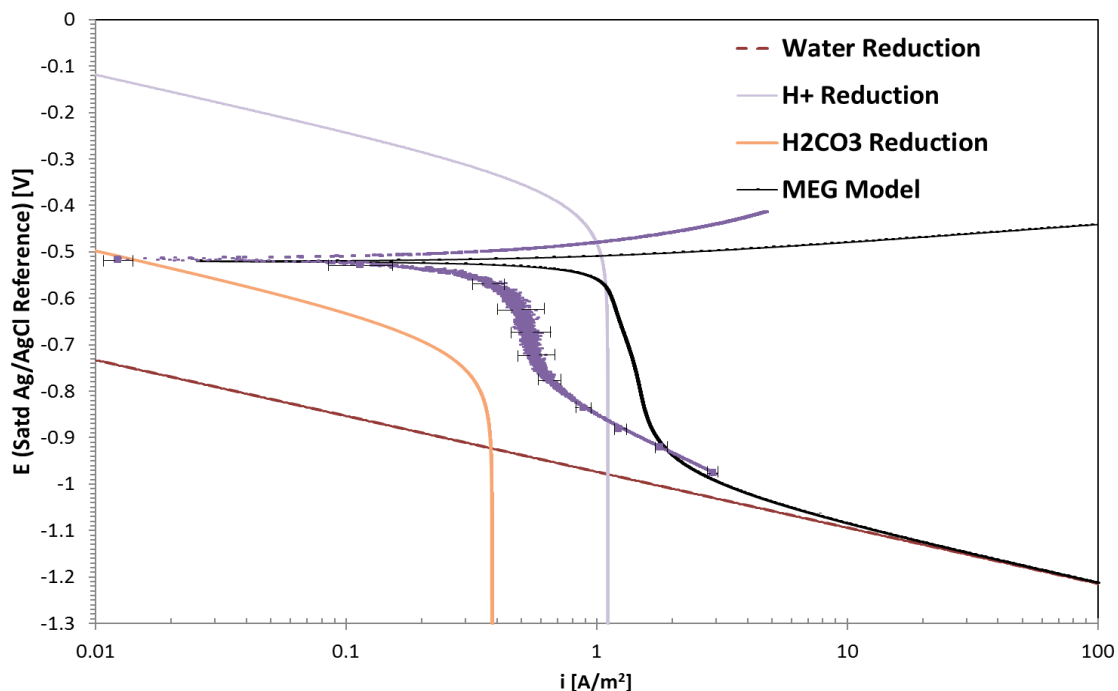


Figure 42. Comparison between model predictions (black continuous line) and experimental results (purple dotted line) for a solution saturated with 0.5bar CO₂, 1wt. % NaCl, 85vol. % MEG at pH 3.54, 30°C and for a $V_{RCE} = 1000\text{RPM}$.

For this higher MEG concentration, the comparison between prediction and experimental results show a greater degree of variation. Again, these changes occur mainly in the total limiting current which is again dominated by the reduction of H⁺. The discrepancies in these predictions may come from the assumptions made for the values of reference diffusion coefficients in MEG-Water solutions. In addition, it is important to note that the predicted limiting current is very sensitive to pH, and that the experimental methodology to adjust the pH during the test also holds some level of uncertainty. Experimental errors in the pH measurements could help explain the discrepancy obtained in limiting current.

6.5.2.2 Effect of Flow

Another aspect that was investigated in this study was the effect of various flowing conditions on electrochemical reactions in the presence of glycol. It was shown in the results section that the effect of flow, and hence mass transfer, behaved similarly in pure water solutions and in glycolic solutions.

Figure 43 clearly shows that this behavior is captured by the model since there is a relatively good correlation between the model predictions and experimental results.

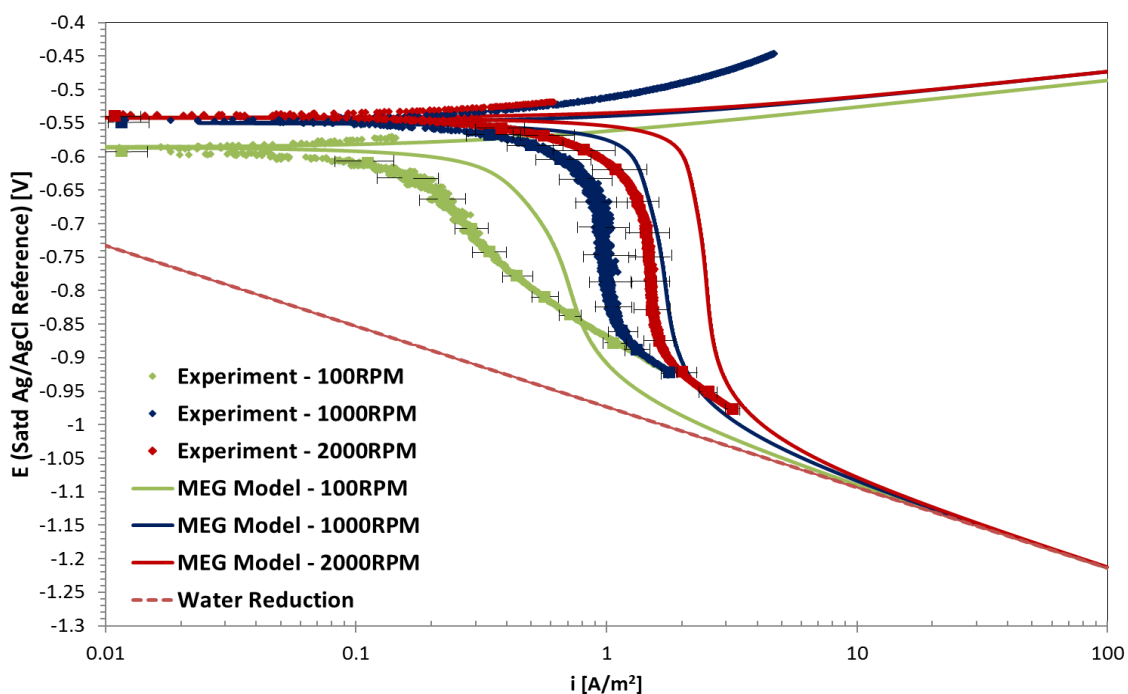


Figure 43. Comparisons between model predictions (solid continuous lines) and experimental results (dotted lines) for a solution at 30°C and pH 3.66 saturated with 0.5bar CO₂, 70vol. % MEG and 1wt. % NaCl.

By testing the effect of flow in glycolic solutions, the methodology presented in the previous section regarding the use of Silverman's mass transfer correlation for RCE

configurations⁵⁴ was validated. From the results presented in Figure 43, it can be seen from that there is an overprediction of about 1 A/m² mainly in the value of the limiting current for each RCE rotation. While there is a small discrepancy in the correlation between the model and the experimental results, it can be appreciated that the effect of flow on CO₂ corrosion mechanisms in the presence of MEG can be well simulated by using the model. Additional results regarding the effect of flow for various conditions can be found in APPENDIX G MODEL VALIDATION – EFFECT OF FLOW.

6.5.2.3 Effect of Temperature

Temperature was also tested for a fixed content of ethylene glycol in solution, and similar to the previous section, the results shown in Figure 44 illustrate the performance of the model in predicting temperature changes in the presence of MEG.

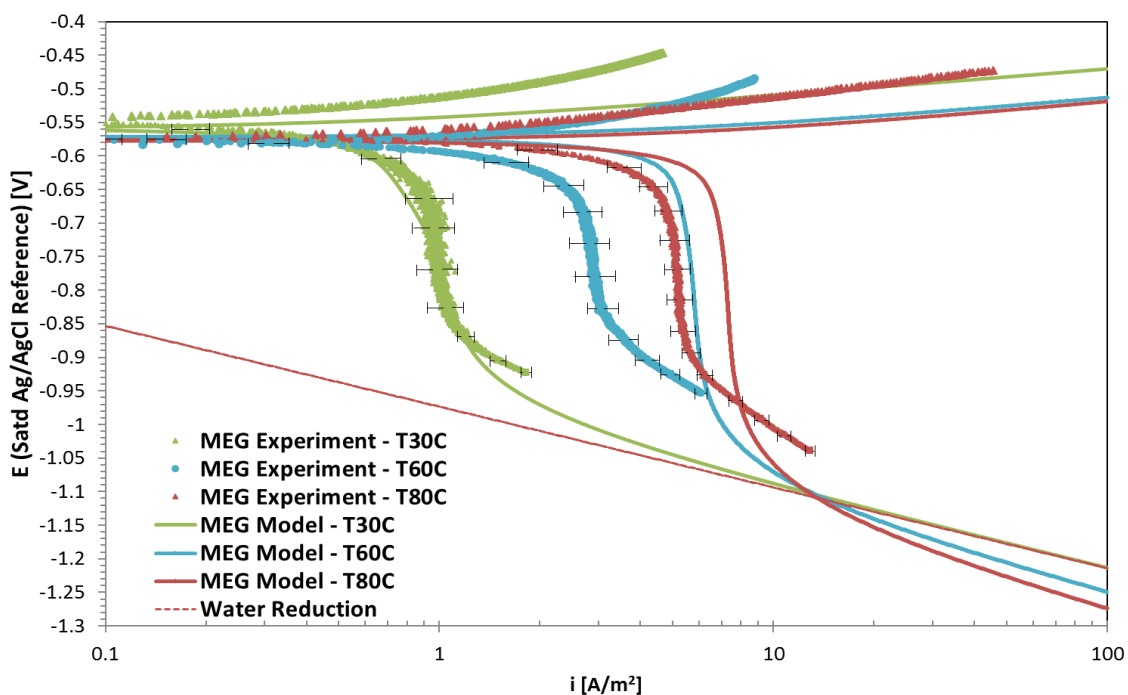


Figure 44. Comparisons between the model predictions (solid continuous lines) and experimental results (dotted lines) for solutions saturated with 0.5bar CO₂, 70vol. % MEG, 1wt. % NaCl, 1000RPM and pH 3.66 (30°C), 3.44 (60°C) and 3.52 (80°C).

As can be noted from the results illustrated in Figure 44, there is a good agreement between the model predictions and the experimental results at 30°C. However, as the temperature is increased to 60°C, there is a level of discrepancy mainly with the differences in values for the limiting current for the experimental results and the model predictions. For this condition, there is an overprediction by the model, which causes a difference in limiting current values of about 4 A/m². However, this discrepancy decreases as the temperature reaches 80°C, where this overprediction is only about a 1.5 A/m². Lastly, there is a noticeable change in the Tafel slopes for the water reduction part of the cathodic curve predicted by the model for each temperature. This is expected as the Tafel slopes depend

on temperature as it was shown in Table 13 in APPENDIX B COEFFICIENTS USED FOR MODELING THE ELECTROCHEMICAL REACTIONS.

6.5.2.4 Effect of pH

This section presents the comparison between predicted and experimental results over a pH range from 4.00 to 6.00. First, the comparison is made at pH 6.00 and in pure water Figure 45.

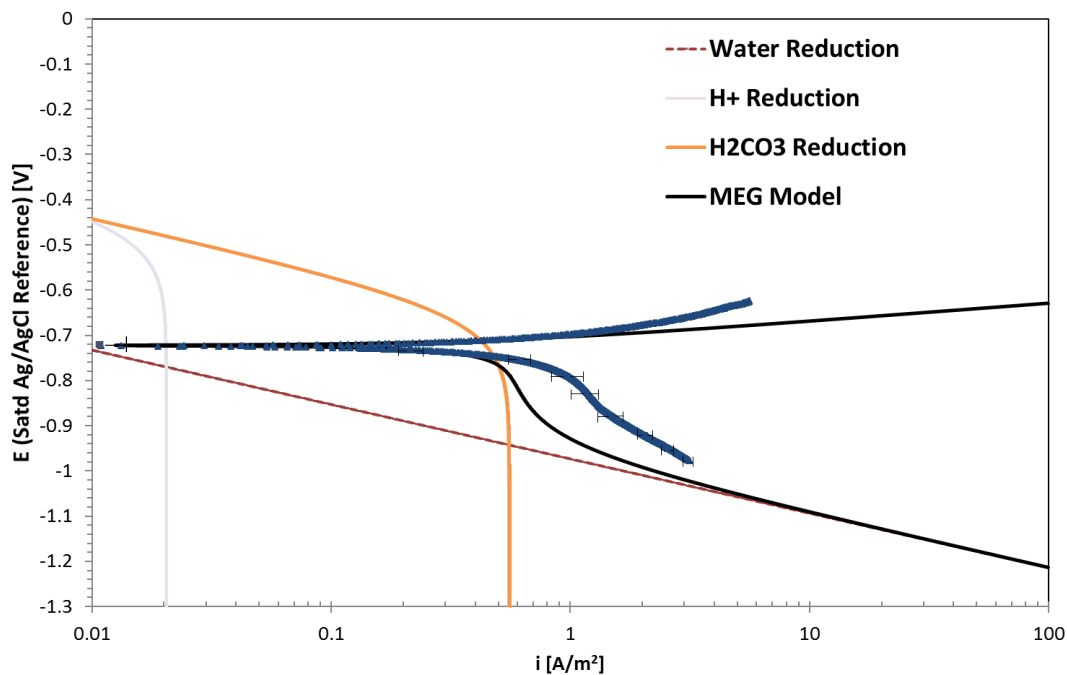


Figure 45. Comparison between model predictions (black continuous line) and experimental results (blue dotted line) for a solution saturated with 0.5bar CO₂, 1wt. % NaCl, 0vol. % MEG at pH 6.00, 30°C and for a $V_{RCE} = 1000\text{RPM}$.

At a pH of 6.00, the concentration of proton is low enough so that the total cathodic current is dominated by the carbonic acid reduction reaction. This can be clearly seen in the Evans diagram where the H₂CO₃ reduction is the main contributor to the overall

reduction reaction. For this condition, the predicted cathodic limiting current does not agree very well with the experimental results. The reason for this discrepancy is unclear as there were no real indications for any uncertainties during the execution of this experimental trial.

Figure 46 shows the results for a solution at pH 5.91 with 40vol. % MEG in solution.

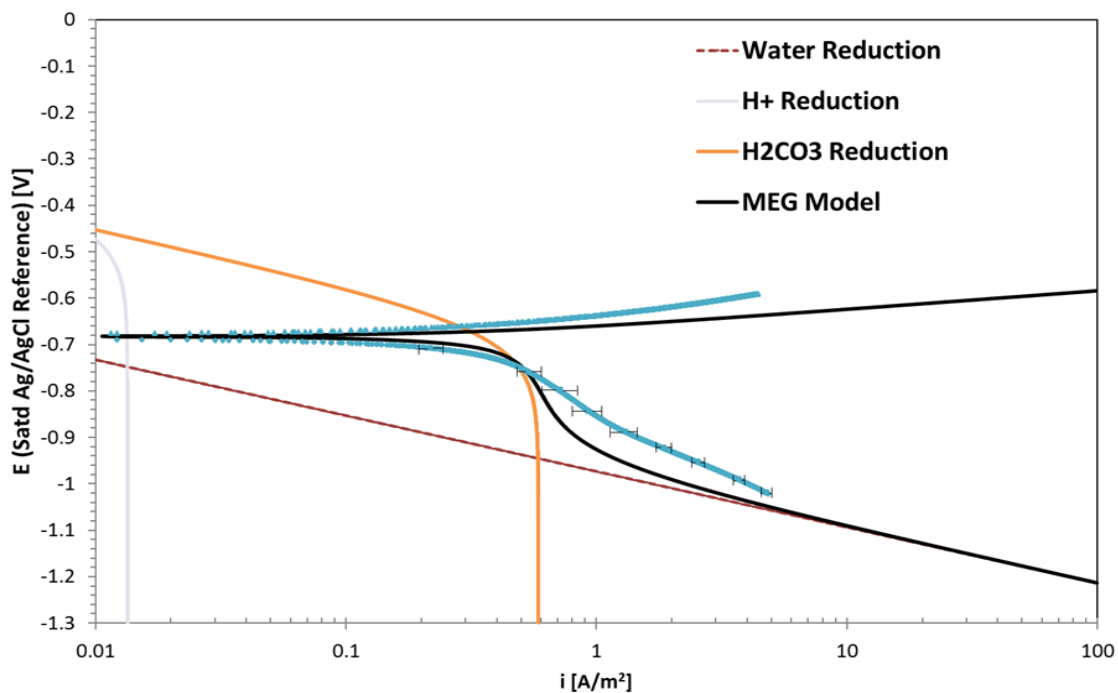


Figure 46. Comparison between model predictions (black continuous line) and experimental results (blue dotted line) for a solution saturated with 0.5bar CO₂, 1wt. % NaCl, 40vol. % MEG at pH 5.91, 30°C and $V_{RCE} = 1000\text{RPM}$.

It can be seen from Figure 46 that there is a great correlation between the experimental results and the predictions provided by the model, again mainly in the values of the limiting current.

For a solution with 55vol. % MEG in solution, similar relationships are obtained as shown by Figure 47.

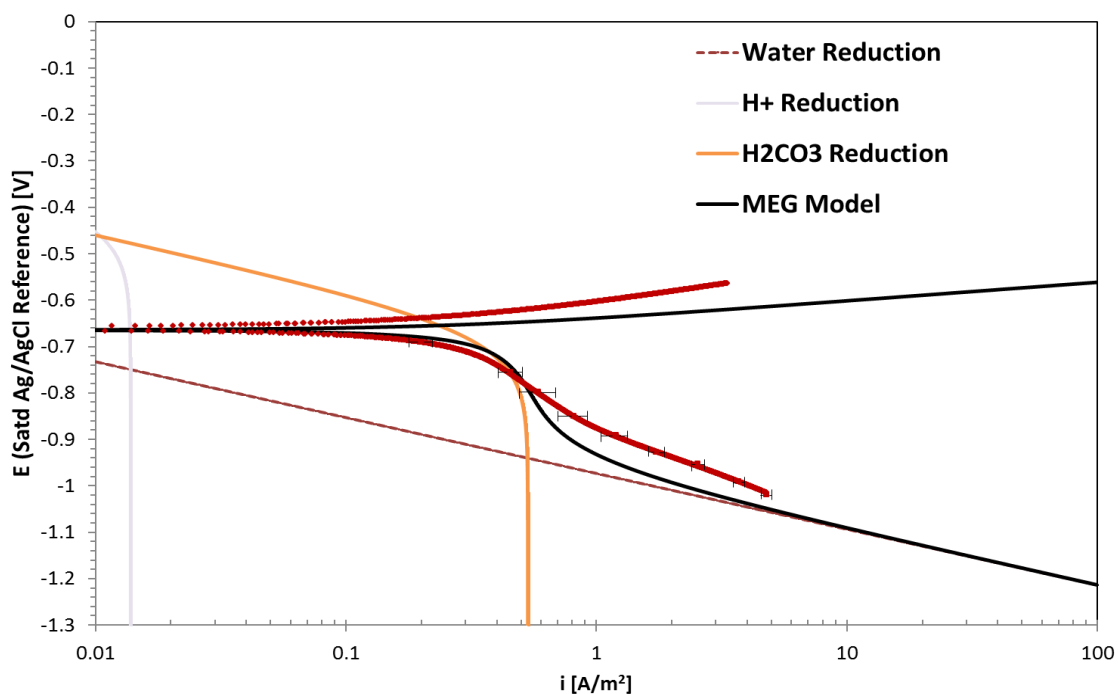


Figure 47. Comparison between model predictions (black continuous line) and experimental results (red dotted line) for a solution saturated with 0.5bar CO₂, 1wt. % NaCl, 55vol. % MEG at pH 5.77, 30°C and $V_{RCE} = 1000\text{RPM}$.

As can be seen from the results above, the correlation between model and experiments is still satisfactory. The match in corrosion potential is due to the fitting exercise, however, the match obtained in limiting current values demonstrates that the model can successfully predict the effect of ethylene glycol in solution at higher alkalinities.

The results for a solution with 70vol. % MEG and pH 5.66 are shown in Figure 48.

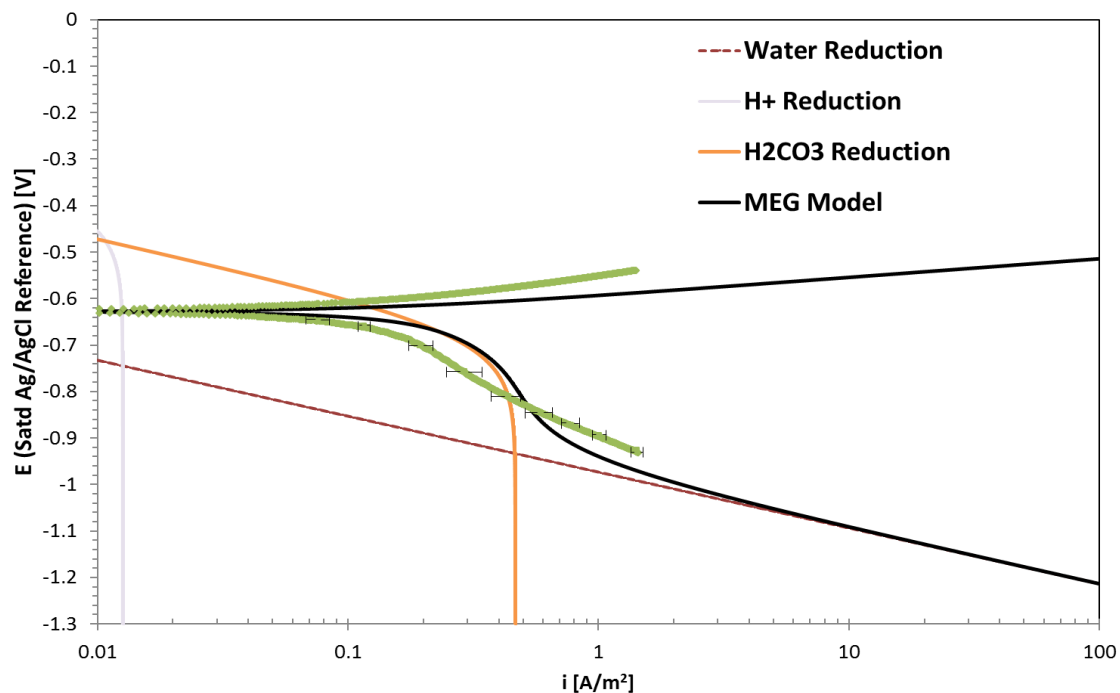


Figure 48. Comparison between model predictions (black continuous line) and experimental results (green dotted line) for a solution saturated with 0.5bar CO₂, 1wt. % NaCl, 70vol. % MEG at pH 5.66, 30°C and for a $V_{RCE} = 1000\text{RPM}$.

As can be seen by Figure 48, the predicted results at high pH and higher MEG content are quite satisfactory. On the total cathodic side, the predictions show a really good agreement with the experimental results. As expected, the corrosion rate is controlled by the reduction of carbonic acid.

Laslty, the results for a solution with 85vol. % and pH 5.54 are shown in Figure 49. Once again, the agreement is satisfactory.

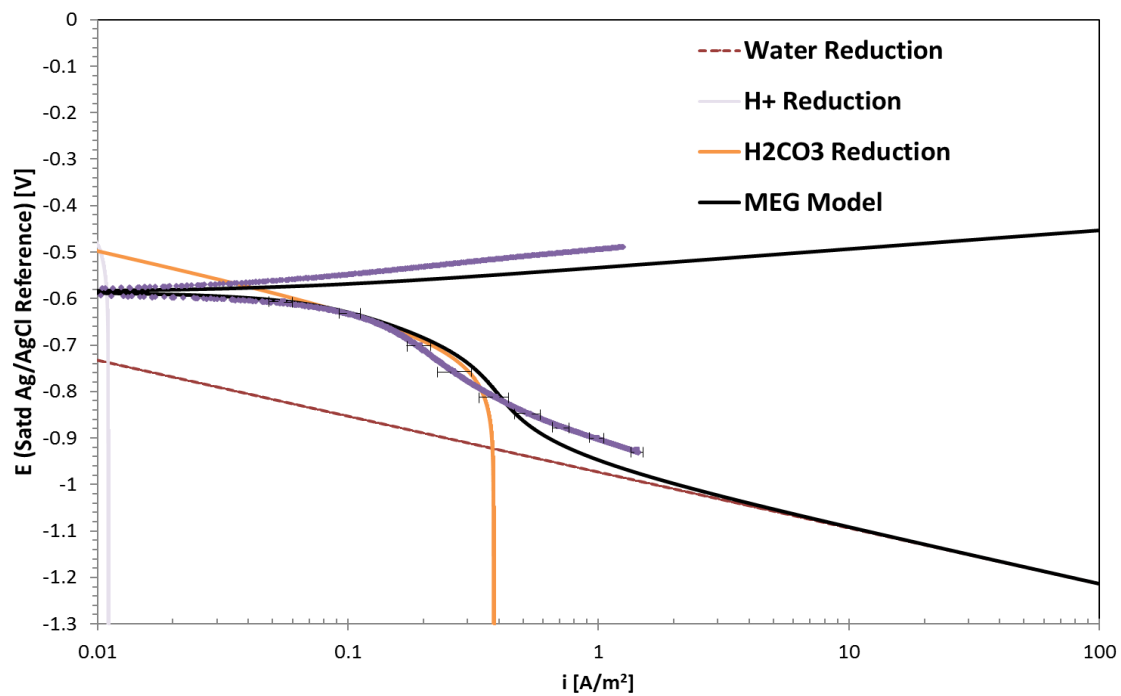


Figure 49. Comparison between model predictions (black continuous line) and experimental results (purple dotted line) for a solution saturated with 0.5bar CO₂, 1wt. % NaCl, 85vol. % MEG at pH 5.54, 30°C and $V_{RCE} = 1000$ RPM.

The results between the comparison between experimental trials and predictions obtained at pH 5.00 are shown in Figure 50.

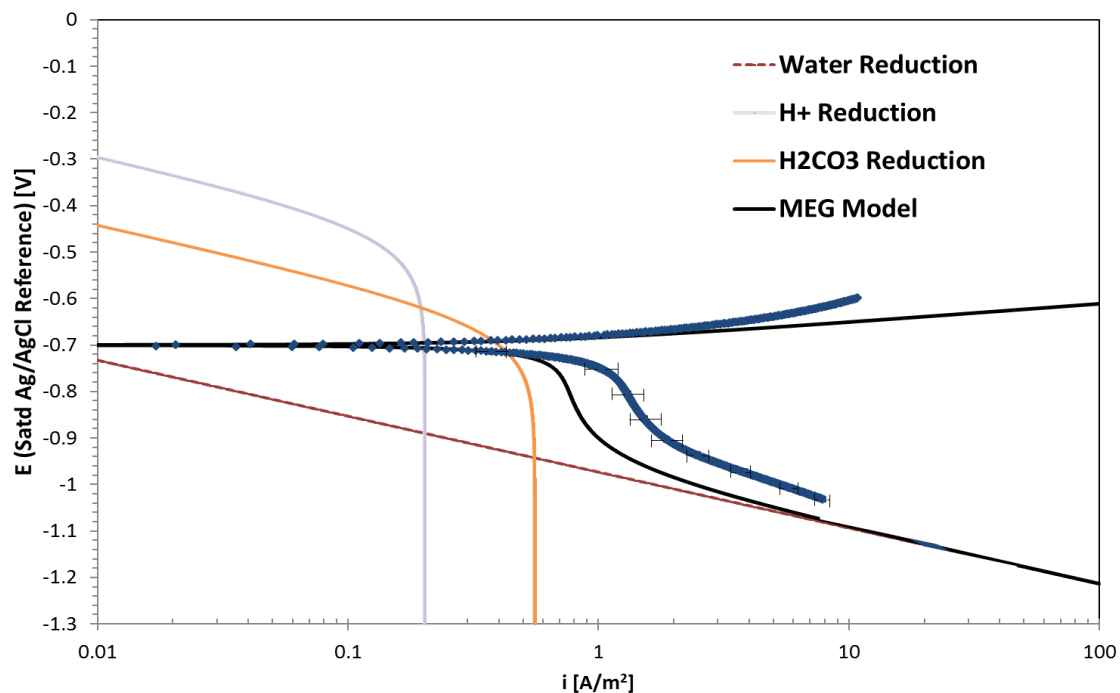


Figure 50. Comparison between model predictions (black continuous line) and experimental results (blue dotted line) for a solution saturated with 0.5bar CO₂, 1wt. % NaCl, 0% MEG at pH 5.00, 30°C and for a $V_{RCE} = 1000\text{RPM}$.

As the alkalinity in solution is decreased, the contribution of the H⁺ reduction to the overall corrosion process is greater with the reduction of carbonic acid still being the more dominant mechanism as demonstrated by Figure 50. Better overall agreement between predictions and experimental results are obtained at this lower pH. The total limiting current for the model is 0.8 A/m², whereas the experimental value is about 1.05 A/m².

Figure 51 shows the results for the same system with a 40vol. % MEG at a pH of 4.91.

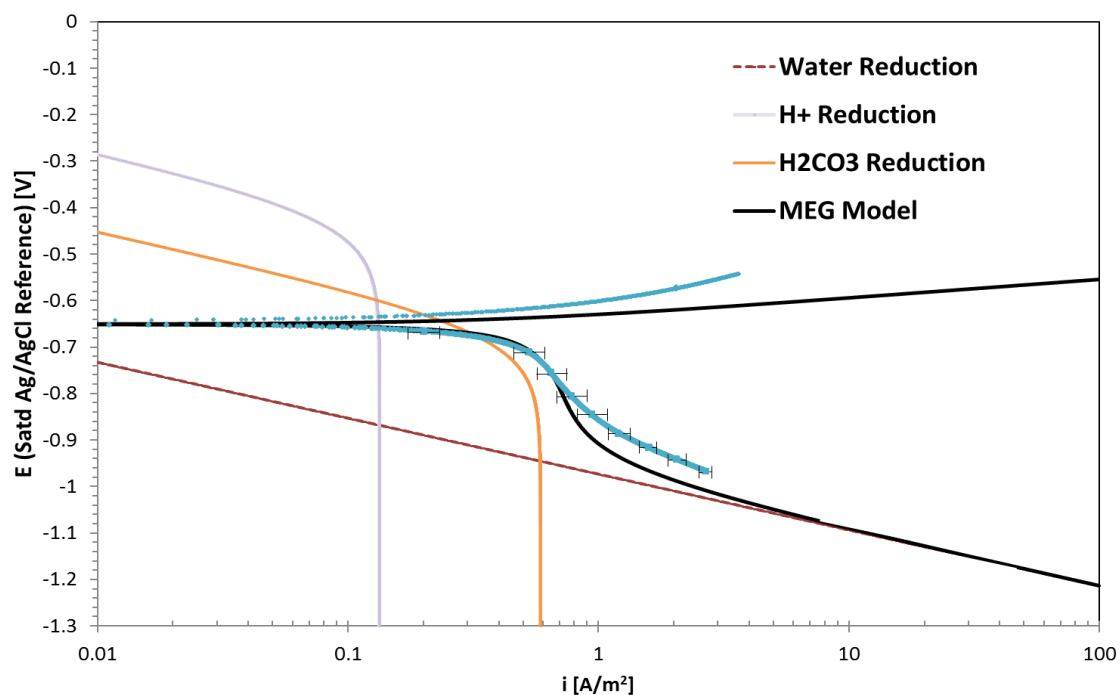


Figure 51. Comparison between model predictions (black continuous line) and experimental results (blue dotted line) for a solution saturated with 0.5bar CO₂, 1wt. % NaCl, 40vol. % MEG at pH 4.91, 30°C and $V_{RCE} = 1000\text{RPM}$.

As it was seen for solutions with pH around 6.00, the same behavior is obtained when a solution contains 40vol. % at pH 5.00. The predicted and experimental limiting current results show remarkable agreement. Lastly, as the alkalinity was lowered by an order of magnitude, it is also clear to note that the influence of H⁺ reduction in the system increased, even though the main dominating mechanism is the reduction of carbonic acid.

For a solution containing 55vol. % MEG in solution and pH 5.77, the results are shown in Figure 52. There is an excellent agreement between the predictions and the experimental results.

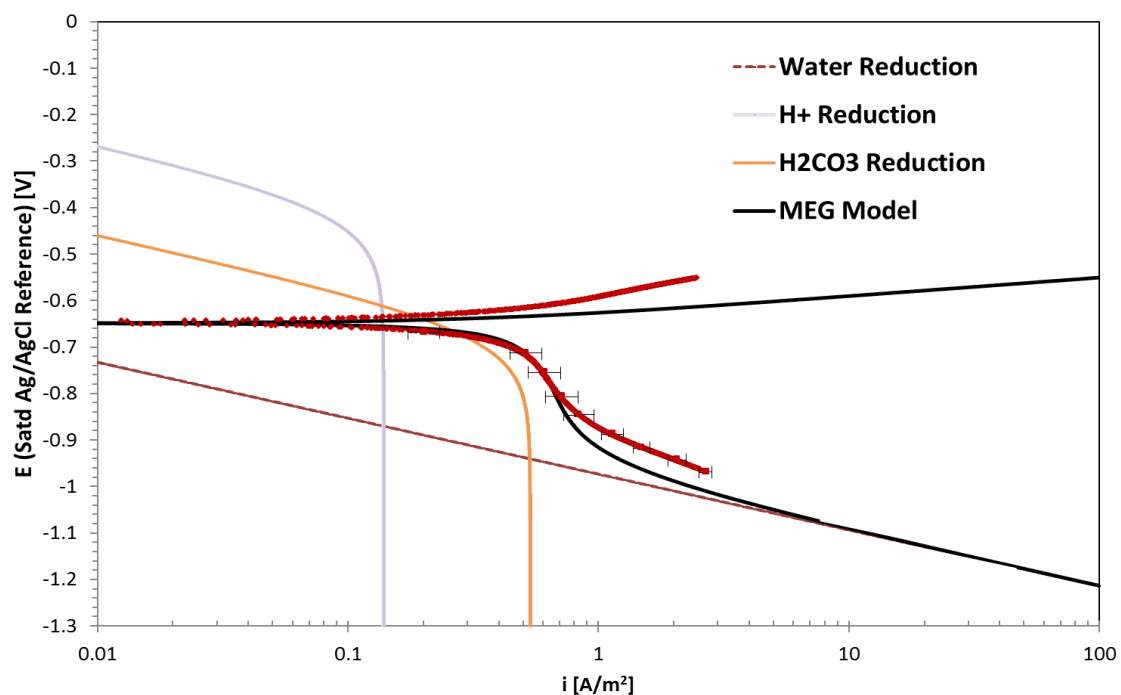


Figure 52. Comparison between model predictions (black continuous line) and experimental results (red dotted line) for a solution saturated with 0.5bar CO₂, 1wt. % NaCl, 55vol. % MEG at pH 4.77, 30°C and $V_{RCE} = 1000\text{RPM}$.

Figure 53 shows the results for the same system with a 70vol. % MEG at a pH of 4.66. A relatively good agreement is also obtained.

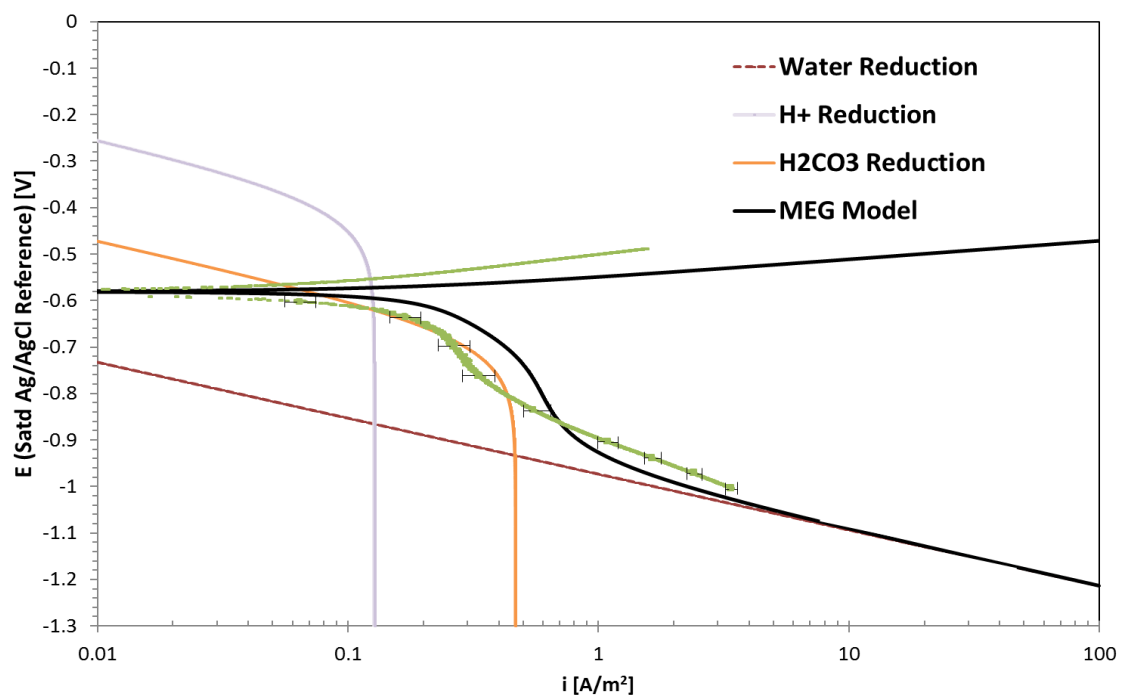


Figure 53. Comparison between model predictions (black continuous line) and experimental results (green dotted line) for a solution saturated with 0.5bar CO₂, 1wt. % NaCl, 70vol. % MEG at pH 4.66, 30°C and for a $V_{RCE} = 1000\text{RPM}$.

For a solution with 85vol. % MEG in solution at pH 4.54, the results are given by

Figure 54.

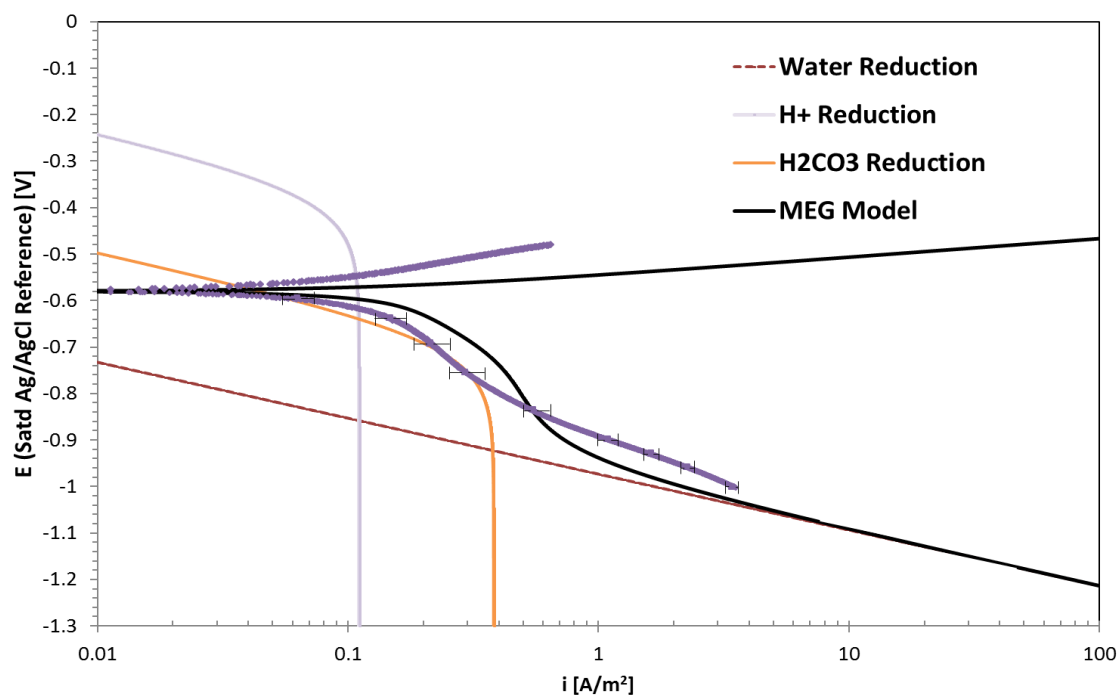


Figure 54. Comparison between model predictions (black continuous line) and experimental results (purple dotted line) for a solution saturated with 0.5bar CO₂, 1wt. % NaCl, 85vol. % MEG at pH 4.54, 30°C and $V_{RCE} = 1000\text{RPM}$.

From the results presented in Figure 54, a similar correlation is obtained compared with a solution with 70vol. % MEG. A small discrepancy is only visible in the values for the limiting current obtained. This value however, is only about 1 A/m², and the dominating mechanism for these conditions is still the reduction of carbonic acid.

The results obtained at pH of 5 and 6 in the presence of MEG show in general an excellent agreement between the predictions provided by the model and the experimental results, mainly in the value of the limiting current. For the anodic portion of the polarization curve, there was an obvious fit in corrosion potentials, but this was expected as the fitting exercise was adopted.

Overall, each parameter tested (pH, Temperature, MEG Content, Flow) resulted in good agreement when compared with experimental results.

6.6 Electrochemical Model Limitations

Thus far, the results presented have shown that the model behaves well in predicting the overall trends in electrochemical reactions, when considering the effect of testing parameters such as pH, temperature, flow and MEG content. However, there are known limitations in the model validity that need to be highlighted in order to prevent incorrect predictions:

- Lack of validation in the model predictions at high temperatures ($>60^{\circ}\text{C}$).
- No validation for CO_2 concentrations higher than 1bar.
- No validation outside of the pH range of 3.00 to 6.00.
- No validation of the model to predict chemistry or electrochemistry behaviors/trends at high NaCl content ($>1\text{ wt. } \%$) in glycolic solutions.

6.7 Discussion on Modeling Approach

Investigating the physico-chemical properties of the fluid to represent the effect of MEG proved to be a valid approach. These changes in fluid chemistry seen with increasing concentrations of glycol (Table 8) could explain most of the obtained results. The necessity to consider activity coefficients in this non-ideal solution was also highlighted. When validating the model with experimental results, there seemed to be a good agreement at various levels of alkalinity. Depending on the pH (mainly at low pH) and the glycol content, minor discrepancies were still identified, especially in the predicted and experimental values of the limiting current. Moreover, the results demonstrating the effect

of flow also matched those predictions relatively well, particularly at low MEG content. However, higher glycol content led to instances where the model over-predicted the effect of flow. This overprediction occurred particularly in the value of the limiting current.

Changes in temperature seemed to cause the largest discrepancies when validating the experimental with the model predictions. At low temperatures (30°C), the accuracy of predicted limiting current was good. However, as the temperature was increased, the model overpredicted the behavior of the cathodic reactions by providing a greater value in limiting current. More experimental work is definitely needed at and above 60°C as current model predictions could be misleading.

The discrepancies that were found throughout the model may have arisen from the methodology selected to describe the physico-chemical properties of the non-ideal solution. As an example, the best fit approach used to obtain the value of the reference diffusivity for H^+/CO_2 in glycolic solutions may have caused prediction errors, especially as they related to the determination of limiting current.

While the cathodic aspect of the model was built following a mechanistic approach, the method used to describe the anodic retardation due to the presence of glycol was clearly empirical since no fully physical explanation could be developed. The fitting exercise, which led to the MEG factor was also based on certain assumptions related to the dependency of anodic kinetic parameters on the activities of components in solution. While extracting the value for the corrosion potentials for each experimental trial, it was assumed that the average corrosion potential obtained at each RCE velocity was the same. This led to the assumption that MEG factor was not flow dependent, and that changes in corrosion

potential, E_{corr} obtained with the model were due to other controlling mechanisms. This said, all corrosion potentials seemed to agree very well when this approach was implemented during the validation portion.

With regards to the anodic reaction, the model captured the behavior of the iron dissolution very well. At higher pH, there seemed to be a slight deviation in the experimental Tafel slope, however, this trend was not reflected in the model, which assumed a constant value. However, it was demonstrated in the literature section that for solutions where water is the main electrolyte, there are still uncertainties with regards to dependence of pH on Tafel slopes.

Lastly, revisiting the proposed hypotheses for this research, the following conclusions can be made:

1. It was intended to demonstrate that the addition of MEG to a CO₂-H₂O system does not change the commonly accepted corrosion behaviors of mild steel with respect to temperature, pH and flow changes. It has been shown that these trends and corrosion behaviors followed the same mechanisms when MEG was present in solution.
2. Additionally, since it was known that MEG was not an electroactive specie, it was noted throughout the results section that there were no changes in Tafel slopes of the anodic or cathodic reactions. The changes in the net cathodic reaction were well simulated by considering physico-chemical characteristics of the MEG-Water solution such as proton activity, viscosity, density, CO₂ solubility. On the other hand, the retardation of the anodic reaction could not be explained by the fluid

properties. An adsorption of MEG on the metal surface and/or a decrease in the iron dissolution activation energy, leading to a decrease in the anodic exchange current density is postulated. However, this study only presents an empirical representation of this behavior with the implementation of a MEG factor that illustrated the retardation effect observed in the experimental results.

CHAPTER 7 CONCLUSIONS

This research work presents a comprehensive and systematic experimental study of the effect of MEG on CO₂ corrosion mechanisms of carbon steel. Using this new set of experimental data, a renewed understanding of the underlying mechanisms in the presence of MEG for sweet corrosion could be developed. The chemistry of MEG/H₂O/CO₂ systems was modeled, leading to a good understanding of solution speciation (including solution pH) considering various concentrations of glycol. From an electrochemical perspective, a mechanistic attempt to model the corrosion of carbon steel in glycolic solutions was presented, describing procedures, methodologies as well as assumptions. A comprehensive validation effort was also implemented comparing model predictions and experimental results, highlighting the effect of MEG content, pH, temperature and flow.

The main takeaways from this research are as follows:

- The presence of MEG has minimal to no effect on the anodic and cathodic Tafel slopes for the electrochemical reactions in sweet corrosion mechanisms.
- From a cathodic stand point, as MEG is increased in solution, a decrease in value of the limiting current is obtained.
- From an anodic perspective, as more glycol is added into solution a retardation of the anodic reaction rate is seen.
- The presence of MEG in solution has no effect on the Tafel slope or the exchange current density of the water reduction.
- The effect of flow in glycolic solutions follows a similar trend as in those MEG-free solutions.

CHAPTER 8 FUTURE WORK

The goal of this study was to investigate the role MEG plays in sweet corrosion mechanisms. Although the study covered a wide range of experimental conditions, there are still areas that are not fully understood. The chemistry of MEG/Water/CO₂/NaCl solutions is a key aspect that can use further investigation. Whether it is the procedure to adjust the pH of the solution in a three-electrode set-up, or simply considering the effect of NaCl, the accurate representation of the proton activity is a key aspect for this research. Direct measurements of species concentrations would fortify its validity and allow for more accurate estimates. Additionally, further investigation of sweet corrosion in glycolic solutions at temperatures above 60°C, would expand on the work presented in this research, and hopefully close the gap on uncertainties witnessed for these conditions. Although satisfactory trends were obtained for most of the parameters tested, considering that during deep-water exploration chemicals such as corrosion, wax and scaling inhibitors are injected (in conjunction with hydrate inhibitors - MEG) to prevent flow related challenges, the following investigations could lead to greater knowledge on the effect of MEG in corrosion mechanism in a more realistic environment:

- The effect of MEG at high temperature, high pressure (HTHP) environments,
- The effect of MEG on H₂S (Sour) corrosion mechanisms,
- The effect of MEG on combined CO₂/H₂S environments,
- The effect of high NaCl content in a CO₂ and/or H₂S in glycolic solutions,
- The role of MEG in CO₂ corrosion mechanisms in the presence of corrosion inhibitors,

- The effect of MEG in a HAc-CO₂ saturated environment, as well as HAc-H₂S systems,
- Scale formation in the presence of MEG.

The completion of this investigation can be considered as the gateway for the modeling of corrosion in the presence of MEG and other corroding agents such as H₂S and HAc, in order to further develop FREECORP™'s current prediction capabilities.

REFERENCES

1. Koch, G.H: Federal Study (2002). Retrieved February 16, 2015, from <https://www.nace.org/uploadedFiles/Publications/ccsupp.pdf>
2. G2MTLabs. (2014). Retrieved February 15, 2016, from <http://www.g2mtlabs.com/2011/06/nace-cost-of-corrosion-study-update/>
3. Simmons, M. R. (2008). Corrosion in the Oil and Gas Industry. Retrieved from [https://www.nace.org/Corrosion-Central/Industries/Oil---Gas-Production/Offshore Technology Conference \(OTC\) Presentation](https://www.nace.org/Corrosion-Central/Industries/Oil---Gas-Production/Offshore%20Technology%20Conference%20(OTC)%20Presentation).
4. Dugstad, A., Lunde, L., & Nesic, S. (1994). Control of Internal Corrosion in Multiphase Oil and Gas Pipelines. *Prevention of Pipeline Corrosion/94*, Gulf Publishing Co.
5. Kvarekvål, J., & Pedersen, A. (2013). An Electrochemical Study of Corrosion Inhibition of Carbon Steel in Sour Glycol Solutions. *CORROSION/2013*. Paper No. 2447.
6. Dugstad, A., & Dronen, P. E. (1999). Efficient Corrosion Control of Gas Condensate Pipelines by pH-stabilization. *CORROSION/99*. Paper No. 20.
7. Olsen, S., Lunde, O., & Dugstad, A. (1999). pH-stabilization in the Troll Gas-Condensate Pipelines. *CORROSION/99*. Paper No. 19.
8. vanBodegom, L., & vanGelder, K. (1990). Effect of Glycol and Methanol on CO₂ Corrosion of Carbon Steel. *CORROSION/87*. Paper No. 55.
9. Crolet, J., & Samaran, J. (1993). The Use of the Anti-Hydrate Treatment for the Prevention of CO₂ Corrosion in Long Crude Gas Pipelines. *CORROSION/93*. Paper No. 102.

10. Gonzalez, J. J., Alfonso, M. E., & Pellegrino, G. (2000). Corrosion of Carbon Steels in Monoethylene Glycol. *CORROSION/2000*. Paper No. 498.
11. Kvarekval, J., & Dugstad, A. (2005). Pitting Corrosion in CO₂/H₂S Containing Glycol Solutions Under Flowing Conditions. *CORROSION/2005*. Paper No. 5631.
12. Ivonye, I., Wang, C., Hu, X., & Neville, A. (2013). Corrosion Study of Carbon Steel in the Presence of Monoethylene Glycol (MEG) and Corrosion Inhibitors in Acid. *CORROSION/2013*. Paper No. 2349.
13. Gulbrandsen, E., & Morad, J. H. (1998). Why Does Glycol Inhibit CO₂ Corrosion?. *CORROSION/98*. Paper No. 221.
14. Pojtanabuntoeng, T., Salasi, M., & Gubner, R. (2014). The Influence of Mono Ethylene Glycol (MEG) on CO₂ Corrosion of Carbon Steel at Elevated Temperatures (80 to 120°C). *CORROSION/2014*. Paper No. 4176.
15. Ehsani, H. (2013). Influence of Monoethylene Glycol (MEG) on the corrosion inhibition of wet-gas flow lines (*Doctoral dissertation, Curtin University*).
16. Javidi, M., & Khodaparast, M. (2015). Inhibitive Performance of Monoethylene Glycol on CO₂ Corrosion of API 5L X52 Steel. *Journal of Materials Engineering and Performance*, 24(4), 1417-1425.
17. Ekawati, D., Berntsen, T., Seiersten, M., & Hemmingsen, T. (2017). Effect of Temperature, Bicarbonate, and MEG Concentrations on CO₂ Corrosion of Carbon Steels. *Corrosion Journal*, 73(9), 1-11.

18. De Waard, C., Lotz, U., & Milliams, D. E. (1991). Predictive Model for CO₂ Corrosion Engineering in Wet Natural Gas Pipelines. *Corrosion Journal*, 47(12), 976-985.
19. Gunaltun, Y. M., & Larrey, D. (2000). Water-Condensation Rate Critical in Predicting, Preventing TLC in Wet-Gas Lines. *Oil & Gas Journal*, 98(28), 58-58.
20. Nestic, S., Postlethwaite, J., & Olsen, S. (1996). An Electrochemical Model for Prediction of Corrosion of Mild Steel in Aqueous Carbon Dioxide Solutions. *Corrosion Journal*, 52(4), 280-294.
21. Nordsveen, M., Nešić, S., Nyborg, R., & Stangeland, A. (2003). A Mechanistic Model for Carbon Dioxide Corrosion of Mild Steel in the Presence of Protective Iron Carbonate Films-Part 1: Theory and Verification. *Corrosion Journal*, 59(5), 443-456.
22. FREECORP Document. (N.d.) Detailed Description of Modeling Approach Corrosion Processes. Athens, Ohio. Pg. 24. Unpublished.
23. Sandler, S. I. (2006). *Chemical, Biochemical, and Engineering Thermodynamics* (4th Edition). Hoboken, NJ: John Wiley. Pg. 250-251.
24. Jones, D (1996). The Technology and Evaluation of Corrosion; In *Principles and Prevention of Corrosion* (2nd Edition), Upper Saddle River, NJ. Prentice-Hall, Pg. 3-4.
25. Bird, B; Stewart, W; Lightfoot, E (2006); *Transport Phenomena*, Revised (2nd Edition). John Wiley & Sons, Inc; New York. Pg. 678-679.
26. Bates, R. G., Paabo, M., & Robinson, R. (1963). Interpretation of pH Measurements in Alcohol—Water Solvents. *The Journal of Physical Chemistry*, 67(9), 1833-1838.
27. Pitzer, K. S. (1976). *Thermodynamics* (3rd Edition). McGraw-Hill. Pg. 182-224

28. Nešić, S., Li, H., Huang, J., & Sormaz, D. (2009). An Open Source Mechanistic Model for CO₂/H₂S Corrosion of Carbon Steel. *CORROSION/09*. Paper No. 09572.
29. Lu, H., Kan, A. T., & Tomson, M. B. (2010). Effects of Monoethylene Glycol on Carbonate Equilibrium and Calcite Solubility in Gas/Monoethylene-Glycol/NaCl/Water Mixed Systems. *SPE Journal*, 15(03), 714-725.
30. Kan, A. T., Lu, H., & Tomson, M. B. (2010). Effects of Monoethylene Glycol on Carbon Dioxide Partitioning in Gas/Monoethylene Glycol/Water/Salt Mixed Systems. *Industrial & Engineering Chemistry Research*, 49(12), 5884-5890.
31. Kan, A. T., Fu, G., & Tomson, M. B. (2002). Effect of Methanol on Carbonate Equilibrium and Calcite Solubility in a Gas/Methanol/Water/Salt Mixed System. *Langmuir*, 18(25), 9713-9725.
32. Kan, A. T., Fu, G., & Tomson, M. B. (2003). Effect of Methanol and Ethylene Glycol on Sulfates and Halite Scale Formation. *Industrial & Engineering Chemistry Research*, 42(11), 2399-2408.
33. Seiersten, M., Dugstad, A., & Gulbrandsen, E. (2003). Conditions for Scaling in Pipelines-pH in Glycol Solutions. *SPE International/2003*. Paper No. 80393.
34. Sandengen, K. (2006). Prediction of Mineral Scale Formation in Wet Gas Condensate Pipelines and in MEG (Mono Ethylene Glycol) Regeneration Plants. (*Doctoral dissertation, Norwegian University of Science & Technology*).
35. Fosbøl, P. L., Thomsen, K., & Stenby, E. H. (2009). Solubility Measurements in the Mixed Solvent Electrolyte System Na₂CO₃- NaHCO₃- Monoethylene Glycol-Water. *Industrial & Engineering Chemistry Research*, 48(4), 2218-2228.

36. Abe, T. (1986). A Modification of the Born Equation. *The Journal of Physical Chemistry*, 90(5), 713-715.
37. He, S., & Morse, J. W. (1993). The Carbonic Acid System and Calcite Solubility in Aqueous Na-K-Ca-Mg-Cl-SO₄ Solutions from 0 to 90°C. *Geochimica et Cosmochimica Acta*, 57(15), 3533-3554.
38. Hayduk, W., & Malik, V. K. (1971). Density, Viscosity, and Carbon Dioxide Solubility and Diffusivity in Aqueous Ethylene Glycol Solutions. *Journal of Chemical & Engineering Data*, 16(2), 143-146.
39. Won, Y. S., Chung, D. K., & Mills, A. F. (1981). Density, Viscosity, Surface Tension, and Carbon Dioxide Solubility and Diffusivity of Methanol, Ethanol, Aqueous Propanol, and Aqueous Ethylene Glycol at 25° C. *Journal of Chemical and Engineering Data*, 26(2), 140-141.
40. Garner, F. H., & Marchant, P. J. M. (1961). Diffusivities of Associated Compounds in Water. *Trans. Inst. Chem. Eng*, 39, 397-408.
41. Byers, C. H., & King, C. J. (1966). Liquid Diffusivities in the Glycol—Water System. *The Journal of Physical Chemistry*, 70(8), 2499-2503.
42. Ternström, G., Sjöstrand, A., Aly, G., & Jernqvist, Å. (1996). Mutual Diffusion Coefficients of Water+ Ethylene Glycol and Water+ Glycerol Mixtures. *Journal of Chemical & Engineering Data*, 41(4), 876-879.
43. Villamanan, M. A., Gonzalez, C., & Van Ness, H. C. (1984). Excess Thermodynamic Properties for Water/Ethylene Glycol. *Journal of Chemical and Engineering Data*, 29(4), 427-429.

44. Oyevaar, M. H., Morssinkhof, R. W., & Westerterp, K. R. (1989). Density, Viscosity, Solubility, and Diffusivity of Carbon Dioxide and Nitrous Oxide in Solutions of Diethanolamine in Aqueous Ethylene Glycol at 298K. *Journal of Chemical and Engineering Data*, 34(1), 77-82.
45. Serpa, F. S., Vidal, R. S., Filho, J. H. A., Nascimento, J. F. D., Ciambelli, J. R., Figueiredo, C. M., & Dariva, C. (2013). Solubility of Carbon Dioxide in Ethane-1, 2-diol–water mixtures. *Journal of Chemical & Engineering Data*, 58(12), pp 3464-3469.
46. Serpa, F. S., Vidal, R. S., Amaral Filho, J. H. B., Santos, A. F., do Nascimento, J. F., de Senna Figueiredo, C. M., & Franceschi, E. (2016). Experimental Study on the Solubility of Carbon Dioxide in Systems Containing Ethane-1, 2-diol+ Water+ Salt (Sodium Chloride or Calcium Carbonate). *Journal of Chemical & Engineering Data*, 62 (1), pp 62–68.
47. Mussini, P. R., Mussini, T., & Rondinini, S. A. N. D. R. A. (1997). Reference Value Standards and Primary Standards for pH Measurements in D₂O and Aqueous Organic Solvent Mixtures: New Accessions and Assessments (Technical Report). *Pure and Applied Chemistry*, 69(5), 1007-1014.
48. Covington, A. K., Bates, R. G., & Durst, R. A. (1985). Definition of pH Scales, Standard Reference Values, Measurement of pH and Related Terminology. *Pure and Applied Chemistry*, 57(3), 531-542.
49. Sandengen, K., Kaasa, B., & Østvold, T. (2007). pH Measurements in Monoethylene Glycol (MEG) + Water Solutions. *Industrial & Engineering Chemistry Research*, 46(14), 4734-4739.

50. Psarrou, M. N., Jøsang, L. O., Sandengen, K., & Østvold, T. (2011). Carbon Dioxide Solubility and Monoethylene Glycol (MEG) Degradation at MEG Reclaiming/Regeneration Conditions. *Journal of Chemical & Engineering Data*, 56(12), 4720-4724.
51. Trimble, H. M., & Potts, W. (1935). Glycol-Water Mixtures Vapor Pressure-Boiling Point-Composition Relations. *Industrial & Engineering Chemistry*, 27(1), 66-68.
52. Banerjee, S. K., Kundu, K. K., & Das, M. N. (1967). Autoprotolysis Constants of Ethylene Glycol-Water Mixtures at Different Temperatures and Related Thermodynamic Quantities. *Journal of the Chemical Society A: Inorganic, Physical, Theoretical*, 166-169.
53. Maples, R. E. (2000). *Petroleum Refinery Process Economics*. Pennwell Books. Pg. 379.
54. Study of Mass Transport Limited Corrosion with Rotating Cylinder Electrodes. (2016). Retrieved May 8, 2017, from <https://www.pineresearch.com/shop/wp-content/uploads/sites/2/2016/07/DRA10011-Study-of-Mass-Transport-Limited-Corrosion-with-Rotating-Cylinder-Electrodes-REV003.pdf>
55. Nestic, S., Thevenot, N., Crolet, J. L., & Drazic, D. M. (1996). Electrochemical Properties of Iron Dissolution in the Presence of CO₂ - Basics Revisited. *CORROSION/96*. Paper No. 3.
56. Nguyen, T. K. *Chemical Engineering Thermodynamics II*. 15 May 2017. CHE303 Course Notes - Chemical and Materials Engineering. Pomona, CA. Pg. 94. Example 4.2-2.

57. "Temperature and Pressure Dependence of Liquid Density," in *CRC Handbook of Chemistry and Physics, 97th Edition (Internet Version 2017)*, W. M. Haynes, ed., CRC Press/Taylor & Francis, Boca Raton, FL.
58. International Suppliers, LLC. (n.d.). Retrieved August 19, 2017, from <http://www.api5lx.com/api5lx-grades/>

APPENDIX A CHEMICAL COMPOSITION OF MATERIALS [WT. %]

Table 12. Chemical Composition of API 5L X65 steel (wt. %).⁵⁸

API 5L X65 mild steel (Balance Fe) [wt. %]							
C	Mn	Nb	P	S	Ti	V	Si
0.16	1.65	0.05	0.02	0.01	0.06	0.09	0.45

APPENDIX B COEFFICIENTS USED FOR MODELING THE ELECTROCHEMICAL REACTIONS

Table 13. Coefficients proposed in the literature^{21, 22} for the expression of the exchange current densities of electrochemical reactions.

	i_{oref} [A/m ²]	a1	$C_{\text{H}^+_{\text{ref}}}$ [Molar]	a2	$C_{\text{CO}_2_{\text{ref}}}$ [Molar]	a3	$C_{\text{H}_2\text{CO}_3_{\text{ref}}}$ [Molar]	ΔH [kJ/mol]	T_{ref} [°C]	E_{rev} [V vs. SHE]	b [V]
$2\text{H}^+ + 2\text{e}^- \rightarrow \text{H}_2$	0.05	0.5	10^{-4}	0	N/A	0	0	30	30	$-2.3 * R * T * \text{pH} / F$	$2.3 * R * T / 2 F$
$2\text{H}_2\text{C O}_3 + 2\text{e}^- \rightarrow \text{H}_2 + 2\text{HCO}_3^-$	0.06	-0.5	10^{-5}	0	N/A	1	1	50	50	$-2.3 * R * T * \text{pH} / F$	$2.3 * R * T / 2 F$
$\text{Fe} \rightarrow \text{Fe}^{+2} + 2\text{e}^-$	1	2 for pH < 4 1 for 4 < pH < 5 0 for pH > 5	10^{-4}	1 for $\text{pCO}_2 < 1 \text{ bar}$ 0 for $\text{pCO}_2 1 \text{ bar}$	0.0366	0	0	37.5	25	-0.488	0.03 for pH < 4 0.08 for 4 < pH < 5 0.12 for pH > 5
$2\text{H}_2\text{O} + 2\text{e}^- \rightarrow \text{H}_2 + 2\text{OH}^-$	$3 * 10^{-5}$	-0.5	10^{-4}	0	N/A	0	N/A	30	25	$-2.3 * R * T * \text{pH} / F$	$2.3 * R * T / 2 F$

APPENDIX C CHANGES IN SOLUTION PH DUE TO INCREASING MEG

CONTENT AT 30°C

Table 14. Changes in solution pH due to increasing MEG content at 30°C for a desired solution pH_{true} of 5.00.

MEG [wt. %]	pH_{rvs}	pH_{buffer}	$\Delta\text{pH}_{\text{MEG}}$	pH_{measured}
0	4.01	4.01	0.00	5.00
10	4.13	4.01	0.03	4.99
20	4.27	4.19	0.08	4.96
30	4.42	4.32	0.10	4.94
40	4.60	4.45	0.15	4.91
50	4.79	4.61	0.18	4.82
60	5.01	4.78	0.23	4.72
70	5.24	4.91	0.33	4.66
80	5.49	5.07	0.42	4.58
90	5.76	5.23	0.54	4.46

Table 15. Changes in solution pH due to increasing MEG content at 30°C for a desired solution pH_{true} of 6.00.

MEG [wt. %]	pH_{rvs}	pH_{buffer}	$\Delta\text{pH}_{\text{MEG}}$	pH_{measured}
0	4.01	4.01	0.00	6.00
10	4.13	4.01	0.03	5.99
20	4.27	4.19	0.08	5.96
30	4.42	4.32	0.10	5.94
40	4.60	4.45	0.15	5.91
50	4.79	4.61	0.18	5.82
60	5.01	4.78	0.23	5.72
70	5.24	4.91	0.33	5.66
80	5.49	5.07	0.42	5.58
90	5.76	5.23	0.54	5.46

APPENDIX D LIQUID DENSITY AND VISCOSITY INFORMATION FOR WATER
AND MONOETHYLENEGLYCOL

Table 16. Liquid properties for MEG and H₂O as a function of temperature and pressure.

Fluid Property	Species			
	Water ²¹			
Density, ρ [kg/m ³]	$753.596 + 1.87748 * T - 0.003564 * T^2$			
Dynamic viscosity, μ , [kg/m*s]	$0.001002 * 10^{(1.3277 * (293.15 - T) - 0.001053 * (298.15 - T)^2 / (T - 168.15))}$			
MEG⁵⁷				
Density, ρ [kg/m ³]	$\rho_{ref} / (1 - C(T) * \ln[(B(T) + P) / (B(T) + P_{ref})]); P = \text{Partial Pressure of MEG}$			
$B(T) = a_1 + a_2 * T + a_3 * T^2 + a_4 * T^3 + a_4 T^4$		$C(T) = a_1 + b_1 * T + c_1 * T^2$		
$a_1 = 0.095014; a_2 = -421.0600902; a_3 = 0.095014; a_4 = 0.0674427; b_1 = 0; c_1 = 0$				
Density, ρ_{ref} [kg/m ³]	$\rho(T, P)_{ref} = \rho_c * [1 + \sum(i - N_p) a_i * (a_i - T_r)^{i/3}]$, $i = 2$,			
$\rho_c = 333.7$	$T_c = 790$	$a_1 = 1.77482$	$a_2 = 1.11208$	
Dynamic viscosity, μ , [kg/m*s]	$e^{(C1 + C2/T + C3 * \ln(T) + C4 * T^C5)}$			
$C1 = -20.515$	$C2 = 2468.5$	$C3 = 1.2435$	$C4 = 2.5 * 10^{-12}$	$C5 = -5$

APPENDIX E EXPERIMENTAL LPR DATA

Table 17. Comparison between experimental LPR Data and FREECORP™ (FC) predictions for a solution at 30°C, pH 4.00, 5.00 and 6.00 at 0.5bar CO₂, 1wt. % NaCl and 0wt. % MEG.

30°C												
pH 4.00												
#	100RPM				1000RPM				2000RPM			
	Rp	I _{corr}	Exp.CR	FC™ CR	Rp	I _{corr}	Exp.CR	FC™ CR	Rp	I _{corr}	Exp.CR	FC™ CR
1	99.97	0.0002606	0.5391	1.1	65.88	0.0003954	0.8180	2.23	35.25	0.000739	1.529	2.72
2	25.61	0.001017	2.1040		17.12	0.001522	3.148		13.42	0.001942	4.018	
3	41.71	0.0006247	1.2924		13.42	0.0009759	2.019		26.7	0.001942	4.018	
pH 5.00												
1	142.2	0.0001832	0.3790	0.702	146.9	0.0001774	0.3670	0.826	148.3	0.0001757	0.3635	0.888
2	46.96	0.0005548	1.1478		45.41	0.0005738	1.1871		45.14	0.0005772	1.1941	
3	61.42	0.0004242	0.8776		60.62	0.0004298	0.892		61.11	0.0004263	0.882	
pH 6.00												
1	56.93	0.0004577	0.9469	0.662	48.65	0.0005355	1.1079	0.675	47.6	0.0005474	1.1325	0.682
2	80.46	0.0003238	0.6699		69.27	0.0003761	0.7781		70.76	0.0003782	0.7618	
3	108.3	0.0002405	0.4976		109.7	0.0002376	0.4916		81.22	0.0003208	0.6637	

Table 18. Comparison between experimental LPR Data and FREECORP™ (FC) predictions for a solution at 30°C, pH 3.91,4.91,5.91 at 0.5bar CO₂, 1wt. % NaCl and 40wt. % MEG.

30°C												
pH 3.91												
#	100RPM				1000RPM				2000RPM			
	Rp	I _{corr}	Exp.CR	FC™ CR	Rp	I _{corr}	Exp.CR	FC™ CR	Rp	I _{corr}	Exp.CR	FC™ CR
1	511.9	5.089e-5	0.1053	1.2	58.61	4.45e-4	0.9196	2.57	376.1	6.93e-5	0.1433	3.15
2	569.8	4.57e-5	0.0946		294.9	8.83e-5	0.1828		646.9	4.03e-5	0.0833	
3	609.9	4.27e-5	0.0884		351.2	7.41e-5	0.1535		589.4	4.42e-5	0.0915	
pH 4.91												
1	94.38	2.76e-4	0.571	0.712	101.1	0.0002577	0.533	0.864	226.4	0.000115	0.238	0.94
2	387.7	6.12e-5	0.139		109.9	0.000237	0.490		253.6	0.000103	0.216	
3	568.8	4.58e-5	0.0948		139.5	0.000186	0.386		424.4	6.14e-5	0.127	
pH 5.91												
1	203.8	0.000128	0.265	0.663	190.5	0.000137	0.283	0.679	200.2	0.000130	0.269	0.687
2	145.9	0.000179	0.369		119.3	0.000218	0.451		128.3	0.000203	0.420	
3	192.8	0.000135	0.280		175	0.000149	0.308		190.7	0.000137	0.283	

Table 19. Comparison between experimental LPR Data and FREECORP™ (FC) predictions for a solution at 30°C, pH 3.77, 4.77, 5.77 at 0.5bar CO₂, 1wt. % NaCl and 55wt. % MEG.

30°C												
pH 3.77												
#	100RPM				1000RPM				2000RPM			
	Rp	I _{corr}	Exp.CR	FC™ CR	Rp	I _{corr}	Exp.CR	FC™ CR	Rp	I _{corr}	Exp.CR	FC™ CR
1	1202	2.17e-5	0.04484	1.4	197.9	0.000132	0.2724	3.25	698.5	3.73e-5	0.0772	3.99
2	1204	2.16e-5	0.04477		729.3	3.57e-5	0.0739		1833	1.42e-5	0.0294	
3	1764	1.48e-5	0.03056		433.1	6.02e-5	0.1245		1537	1.70e-5	0.03507	
pH 4.77												
1	883.3	2.95e-5	0.0610	0.732	162.5	0.000160	0.3317	0.941	613.6	4.25e-5	0.0878	1.04
2	218.6	0.000119	0.24657		168	0.000155	0.3208		147.4	0.000177	0.367	
3	175.2	0.000149	0.30765		124.8	0.000209	0.4319		119.5	0.000218	0.451	
pH 5.77												
1	179.8	0.000145	0.299	0.666	154	0.0001692	0.350	0.687	170.6	0.000153	0.316	0.698
2	240.7	0.000108	0.224		239.7	0.0001087	0.225		253.7	0.000103	0.215	
3	207.8	0.000125	0.259		160.1	0.0001627	0.337		198.6	0.000131	0.271	

Table 20. Comparison between experimental LPR Data and FREECORP™ (FC) predictions for a solution at 30°C, pH 3.66, 4.66, 5.66 at 0.5bar CO₂, 1wt. % NaCl and 70wt. % MEG.

30°C												
pH 3.66												
#	100RPM				1000RPM				2000RPM			
	Rp	I _{corr}	Exp.CR	FC™ CR	Rp	I _{corr}	Exp.CR	FC™ CR	Rp	I _{corr}	Exp.CR	FC™ CR
1	1990	1.31e-5	0.0271	1.62	792.5	3.29e-5	0.0680	3.25	1581	1.65e-5	0.03409	3.99
2	1967	1.32e-5	0.027		900.4	2.89e-5	0.0589		2294	1.14e-5	0.0235	
3	1146	2.27e-5	0.047		361.4	7.21e-5	0.149		1969	1.32e-5	0.0274	
pH 4.66												
1	443.3	5.88e-5	0.122	0.732	443.3	8.87e-5	0.183	0.941	275.3	9.46e-5	0.196	1.04
2	423.7	6.15e-5	0.127		423.7	7.88e-5	0.163		288.6	9.03e-5	0.187	
3	773.5	3.37e-5	0.0697		773.5	2.33e-5	0.048		836.9	3.11e-5	0.064	
pH 5.66												
1	440.4	5.92e-5	0.122	0.668	373.4	6.97e-5	0.144	0.695	370.4	7.03e-5	0.146	0.709
2	366.6	7.11e-5	0.147		243.9	0.000107	0.221		329.5	7.91e-5	0.164	
3	440.4	5.91e-5	0.122		365.5	7.13e-5	0.148		397.4	6.55e-5	0.136	

Table 21. Comparison between experimental LPR Data and FREECORP™ (FC) predictions for a solution at 30°C, pH 3.54,4.54, 5.54 at 0.5bar CO₂, 1wt. % NaCl and 85wt. % MEG.

30°C												
pH 3.54												
#	100RPM				1000RPM				2000RPM			
	Rp	I _{corr}	Exp.CR	FC™ CR	Rp	I _{corr}	Exp.CR	FC™ CR	Rp	I _{corr}	Exp.CR	FC™ CR
1	3418	7.62e-5	0.0158	1.92	497.8	5.23e-5	0.1083	3.94	1256	2.07e-5	0.04291	4.85
2	2022	1.29e-5	0.0267		273.1	9.54e-5	0.1974		828.1	3.15e-5	0.06509	
3	3172	8.21e-5	0.0170		798.8	3.26e-5	0.0675		2262	1.15e-5	0.02383	
pH 4.54												
1	981.2	2.66e-5	0.05493	0.784	704.4	3.70e-5	0.07652	1.13	683.3	3.81e-5	0.07888	1.30
2	850.6	3.06e-5	0.06337		532.1	4.90e-5	0.1013		552.2	4.71e-5	0.09761	
3	683.5	3.81e-5	0.07886		438.1	5.95e-5	0.1230		553.2	4.70e-5	0.09738	
pH 5.54												
1	965.3	2.70e-5	0.05584	0.671	475.3	5.48e-5	0.1134	0.707	732.3	3.56e-5	0.0736	0.726
2	812.4	3.21e-5	0.06635		571.5	4.56e-5	0.09431		739.8	3.52e-5	0.07286	

Table 22. Comparison between experimental LPR Data and FREECORP™ (FC) predictions for a solution at 60°C, pH 3.44, 0.5bar CO₂, 1wt. % NaCl and 70wt. % MEG.

60°C												
pH 3.44												
#	100RPM				1000RPM				2000RPM			
	Rp	I _{corr}	Exp.CR	FC™ CR	Rp	I _{corr}	Exp.CR	FC™ CR	Rp	I _{corr}	Exp.CR	FC™ CR
1	224.5	0.000116	0.2401	4.33	58.25	0.0004473	0.9253	10.9	63.85	0.000408	0.8442	13
pH 4.44												
1	108.7	0.0002397	0.4959	1.18	58.25	0.0004473	0.9253	2.32	63.85	0.000408	0.8442	2.67
pH 5.44												
1	228.7	0.0001139	0.2357	1.21	195.6	0.000133	0.27556	1.29	209.3	0.0001245	0.2575	1.34

Table 23. Comparison between experimental LPR Data and FREECORP™ (FC) predictions for a solution at 80°C, pH 3.52, 4.52, 5.52 at 0.5bar CO₂, 1wt. % NaCl and 70wt. % MEG.

80°C												
pH 3.52												
#	100RPM				1000RPM				2000RPM			
	Rp	I _{corr}	Exp.CR	FC™ CR	Rp	I _{corr}	Exp.CR	FC™ CR	Rp	I _{corr}	Exp.CR	FC™ CR
1	35.19	0.000740	1.53	5.11	17.25	0.00151	3.13	12.8	14.97	0.00174	3.6	15.3
pH 4.52												
1	84.21	0.000309	0.6401	1.71	59.03	0.0004413	0.9131	2.69	51.29	0.0005080	1.05	3.11
pH 5.52												
1	53.11	0.0004906	1.01	1.37	47.7	0.000546	1.13	1.47	32.39	0.000804	1.66	1.52
2	79.11	0.0003293	0.681		52.39	0.000497	1.03		53.1	0.000491	1.02	

APPENDIX F VALIDATION OF CHEMISTRY MODEL USING LITERATURE

DATA

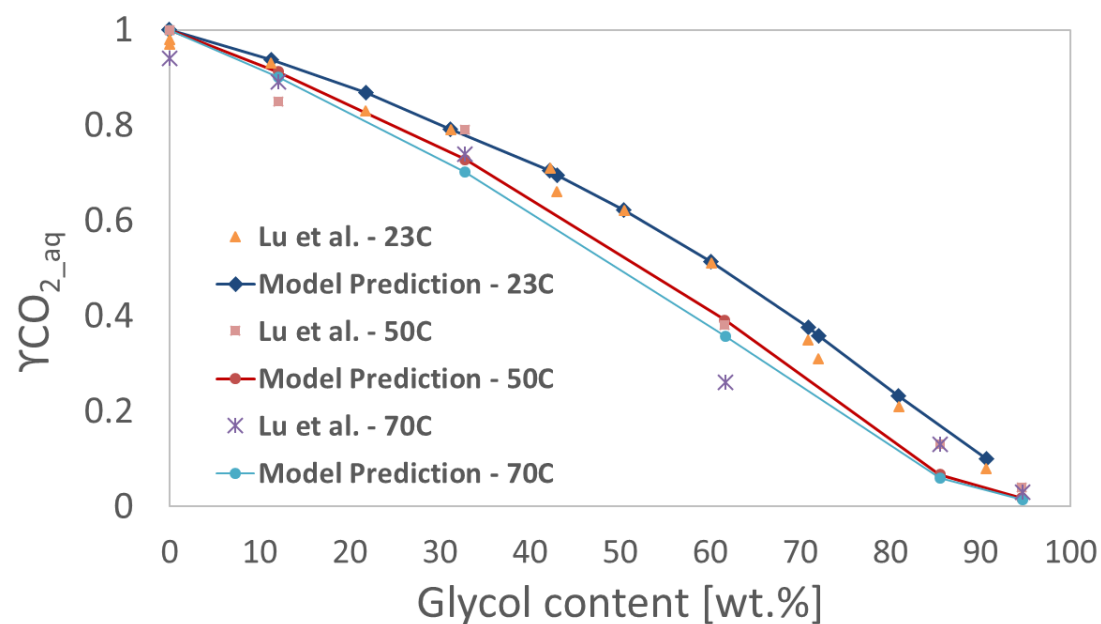


Figure 55. Comparison between model prediction (solid continuous lines) and literature data (dotted points in graph) for the activity coefficient of aqueous carbon dioxide as a function of ethylene glycol at different temperatures.

APPENDIX G MODEL VALIDATION – EFFECT OF FLOW

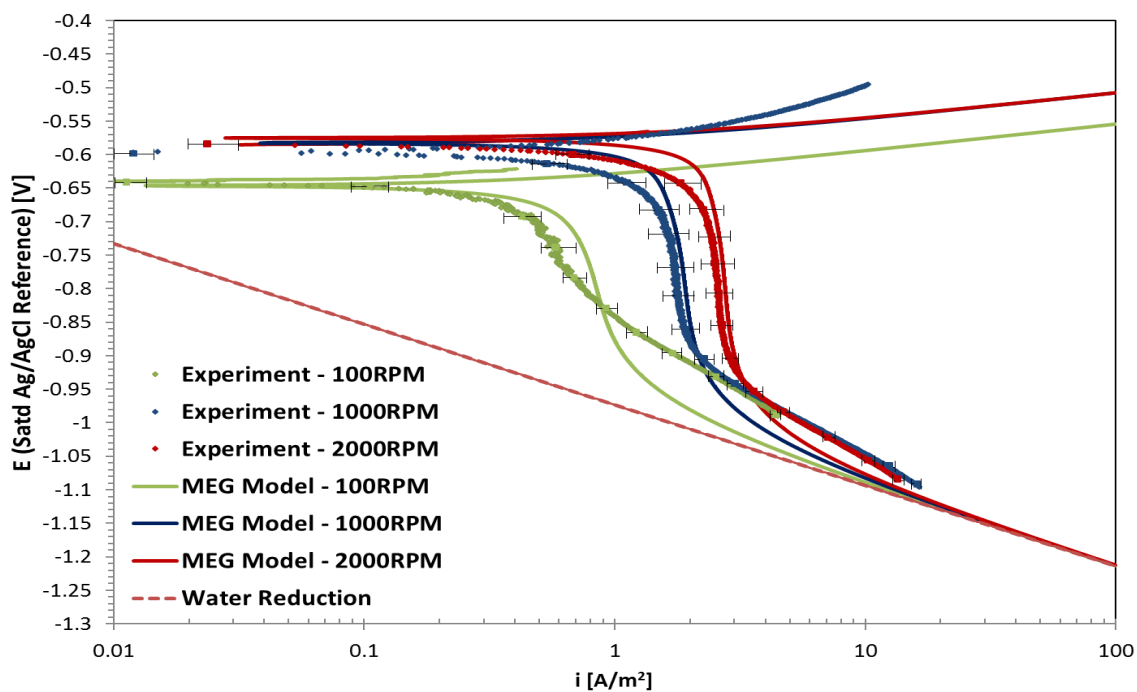


Figure 56. Comparisons between model predictions (solid continuous lines) and experimental results (dotted lines) for a solution at 30°C and pH 3.91 saturated with 0.5bar CO₂, 40vol. % MEG and 1wt. % NaCl.

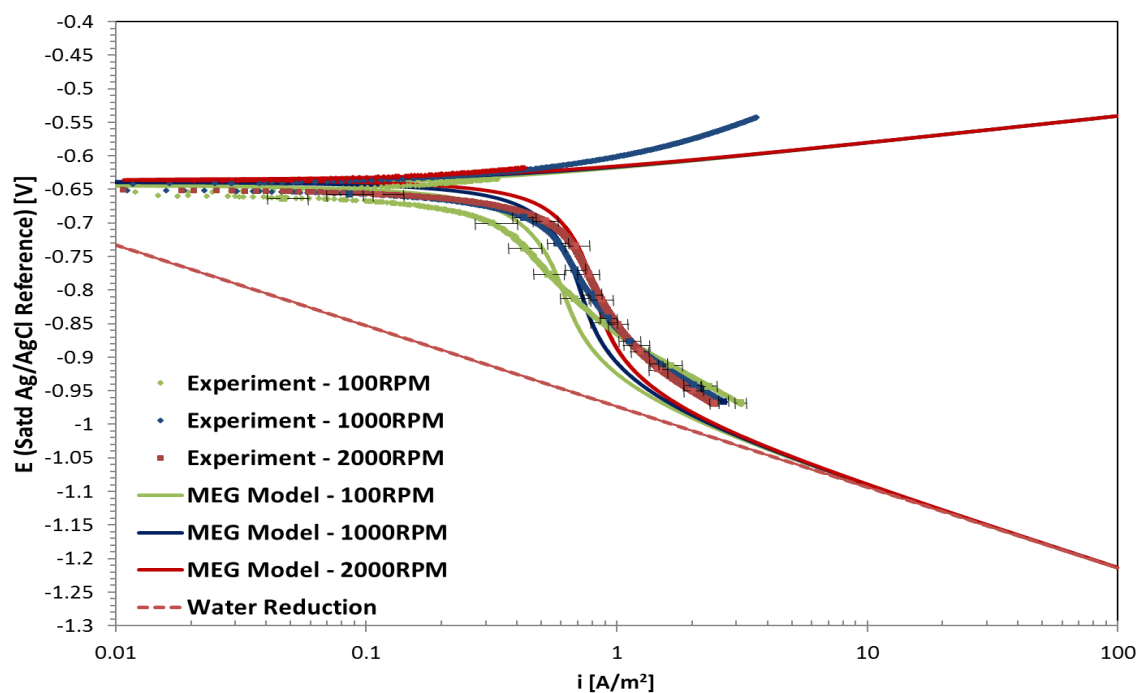


Figure 57. Comparisons between model predictions (solid continuous lines) and experimental results (dotted lines) for a solution at 30°C and pH 4.91 saturated with 0.5bar CO₂, 40vol. % MEG and 1wt. % NaCl.

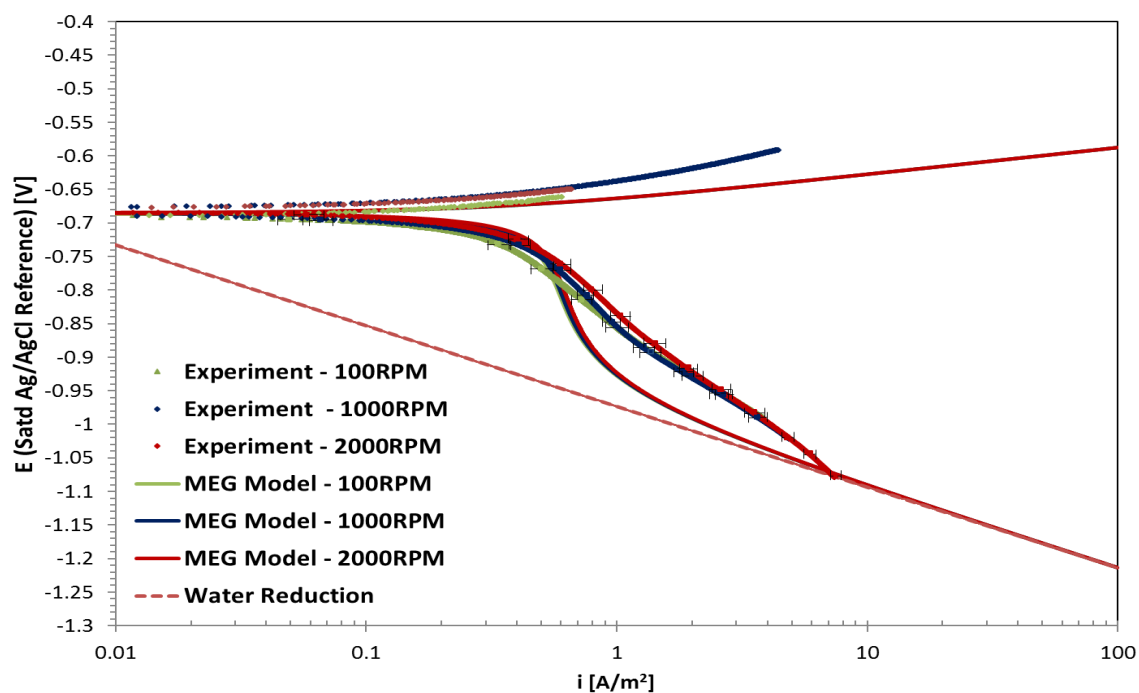


Figure 58. Comparisons between model predictions (solid continuous lines) and experimental results (dotted lines) for a solution at 30°C and pH 5.91 saturated with 0.5bar CO₂, 40vol. % MEG and 1wt. % NaCl.

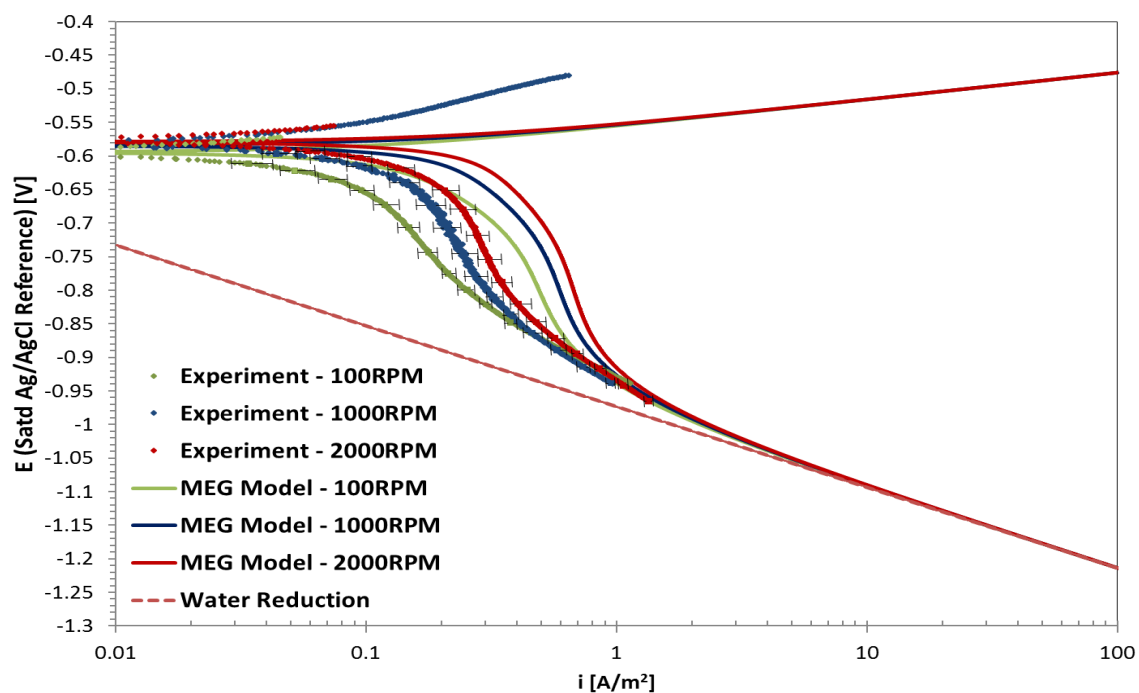


Figure 59. Comparisons between model predictions (solid continuous lines) and experimental results (dotted lines) for a solution at 30°C and pH 4.66 saturated with 0.5bar CO₂, 70vol. % MEG and 1wt. % NaCl.

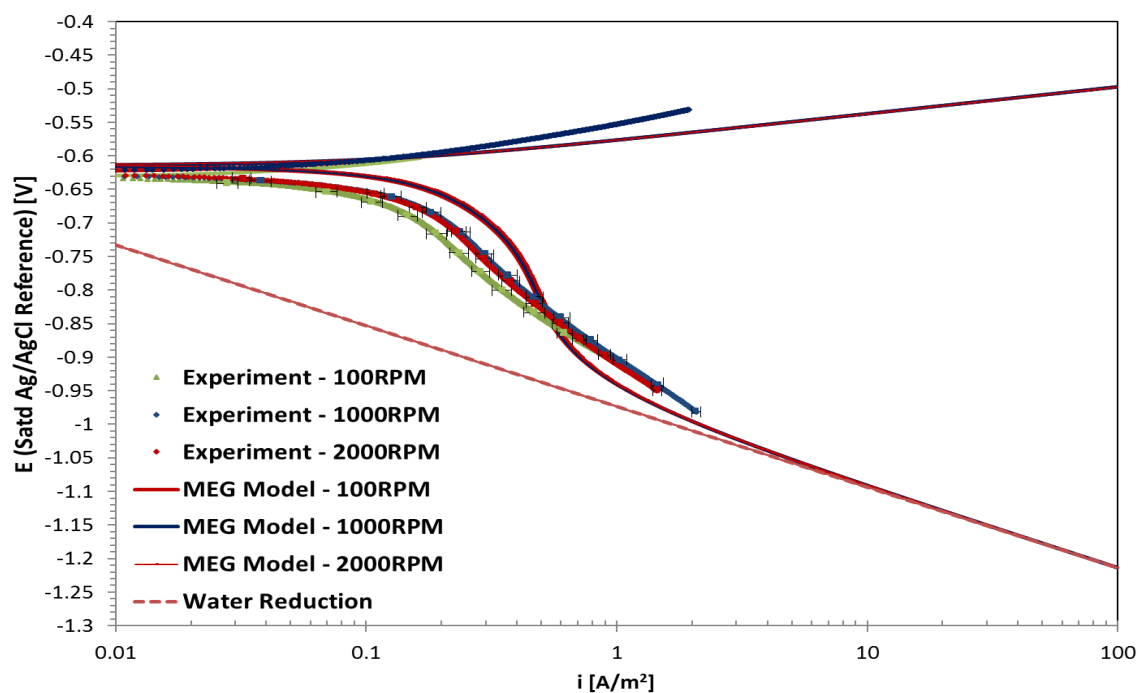


Figure 60. Comparisons between model predictions (solid continuous lines) and experimental results (dotted lines) for a solution at 30°C and pH 5.66 saturated with 0.5bar CO₂, 70vol. % MEG and 1wt. % NaCl.



OHIO
UNIVERSITY

Thesis and Dissertation Services